




Chair of Ferrous Metallurgy

Master's Thesis



Influence of Alkali Metal Oxides in  
Secondary Metallurgical Slags on the  
Behavior and Appearance of Non-Metallic  
Inclusions in Steel

Nikolaus Georg Anton Preißer, BSc

November 2022



Herrn **Nikolaus PREISSER** wird vom Lehrstuhl für Eisen- und Stahlmetallurgie folgendes Masterarbeitsthema S743 gestellt:

### **Einfluss von Alkalioxiden in sekundärmetallurgischen Schlacken auf das Verhalten und Aussehen von nichtmetallischen Einschlüssen im Stahl**

Der Reinheitsgrad von Stählen wird wesentlich in den sekundärmetallurgischen Prozessschritten bestimmt. Die Wechselwirkung Stahl-Schlacke ist hierbei von besonderer Bedeutung und beeinflusst neben dem Abscheideverhalten von Partikeln auch die finale Zusammensetzung und Morphologie von nichtmetallischen Einschlüssen. In letzter Zeit sind vermehrt Untersuchungen publiziert worden, die das Potential von Alkalioxiden (z.B.  $\text{Li}_2\text{O}$ ,  $\text{K}_2\text{O}$ ) zur verbesserten Abscheidung von Einschlüssen in der Sekundärmetallurgie beschreiben. Dies ist im Besonderen für hoch Reinheitsgrad sensitive Stähle (z.B. tire cord, saw wire) relevant. Im Rahmen der Masterarbeit soll der Einfluss definierter Alkalioxide auf das System Stahl-Schlacke-Einschluss im Detail im Labormaßstab untersucht werden. Ausgehend von einer definierten Stahlzusammensetzung und Einschlusspopulation sollen mittels verschiedener experimenteller Möglichkeiten (Tammannofen, HT-LSCM) die Veränderung der Einschlusseigenschaften durch Kontakt mit unterschiedlichen Schlackenzusammensetzungen untersucht und verglichen werden. Eine detaillierte Einschlusscharakterisierung (primär REM/EDX) soll die Basis für eine aussagekräftige Interpretation der Laborergebnisse bilden.

#### **Inhalte der Arbeit:**

- Literaturrecherche
- Thermodynamische Betrachtung des Systems Stahl-Schlacke-Einschluss für ausgewählte Zusammensetzungen unter spezieller Berücksichtigung der Alkalielemente
- Herstellung von definierten Schlackenzusammensetzungen im Labor unter Einbeziehung von Alkalioxiden
- Laborversuche zur Abbildung der Stahl/Schlacke Wechselwirkung am Tammannofen
- Untersuchung des Auflösungsverhaltens von ausgewählten nichtmetallischen Einschlüssen in den definierten Schlackenzusammensetzungen im HT-LSCM
- Metallographische Probenaufbereitung und anschließende Einschlusscharakterisierung im Stahl
- Diskussion, Vergleich und Zusammenfassung der Ergebnisse

#### **Industriepartner:**



Wir bedanken uns für die finanzielle Unterstützung durch das Bundesministerium für Digitalisierung und Wirtschaftsstandort und die Nationalstiftung für Forschung, Technologie und Entwicklung sowie die Christian Doppler Forschungsgesellschaft.

Leoben, Oktober 2021

Assoz. Prof. Dr. Susanne Michelic

## Abstract

With increasing demands on the mechanical properties of modern steels the role of non-metallic inclusions becomes more prominent. The control of their amount, size, morphology, and also chemical composition is the key to the production of highly advanced steel grades. An important factor influencing the steel cleanness are the slags used for ladle treatment in secondary metallurgy. In the course of this work commonly used low basicity pseudo-wollastonitic slags with additional contents of alkali metal oxides were studied. In particular, their capability to remove or affect non-metallic inclusions was analyzed. Thermodynamic calculations showed that the addition of  $R_2O$  ( $R=Li, Na, K$ ) to commonly used low basicity pseudo-wollastonitic slags, can lower the melting point drastically. As slag and non-metallic inclusions are interacting, the chemical composition of the particles is influenced. This can be used to decrease the liquidus temperature of the particles, which is often linked with lower hardness and better deformability. For a better understanding of the effects of alkali metal oxides on the non-metallic inclusions and therefore the steel cleanness, two sets of experiments were conducted. First dissolution of synthetic particles in alkali metal oxide containing slags was observed using HT-CSLM. Furthermore, steel samples were treated with the experimental slags at steelmaking temperatures. The inclusion populations before and after steel-slag interaction were compared using automated SEM/EDS-analysis. A clear impact of the alkali metal oxides on the dissolution behavior was shown. Particles modified with the added alkali elements could be observed as well as a shift in the overall composition of the inclusions.

## Kurzfassung

Mit steigenden Anforderungen an die mechanischen Eigenschaften moderner Stähle steigen auch die Bedeutung und der Einfluss nichtmetallischer Einschlüsse im Stahl. Die Kontrolle von Anzahl, Größe, Morphologie und auch der chemischen Zusammensetzung der Einschlüsse ist der Schlüssel, um hochqualitative Stähle zu erzeugen. Eine Haupteinflussgröße bezüglich des Reinheitsgrades ist dabei die in der Sekundärmetallurgie verwendete Schlacke. Im Zuge dieser Arbeit wurde der Einsatz von Alkalioxiden in diesen Schlacken und die daraus folgenden Auswirkungen auf die Aufnahme und Modifikation von Einschlüssen bewertet. Mittels thermodynamischen Berechnungen konnte gezeigt werden, dass durch den Zusatz von Alkalioxiden der Form  $R_2O$  ( $R = \text{Li, Na, K}$ ) der Schmelzpunkt niedrig basischer pseudo-wollastonitischer Schlacken maßgeblich absinkt. Da die chemische Zusammensetzung sekundärmetallurgischer Schlacken in starkem Zusammenhang mit jener der nichtmetallischen Einschlüsse steht, können diese gezielt modifiziert und damit ihre Eigenschaften verändert werden. Gerade die Liquidustemperatur der Partikel stellt dabei eine wichtige Zielgröße dar. Um den Einfluss von Alkalioxiden auf die nichtmetallischen Einschlüsse zu beleuchten, wurden zwei Experimentreihen durchgeführt. Zum einen wurde mittels Hochtemperatur-Konfokalmikroskop die Auflösung synthetischer Partikel in experimentellen Schlacken beobachtet. Zudem wurden Stahlproben mit den Schlacken in Kontakt gebracht, wobei die Einschlusspopulation vor und nach der Stahl-Schlacke Wechselwirkung mittels automatisierter REM/EDX-Messung analysiert wurde. Auswirkungen der Alkalioxide auf die Auflösung der Partikel, sowie die mittlere chemische Zusammensetzung der Einschlusslandschaft, wurden nachgewiesen.



**EIDESSTÄTTLICHE ERKLÄRUNG**

Ich erkläre an Eides statt, dass ich diese Arbeit selbständig verfasst, andere als die angegebenen Quellen und Hilfsmittel nicht benutzt, und mich auch sonst keiner unerlaubten Hilfsmittel bedient habe.

Ich erkläre, dass ich die Richtlinien des Senats der Montanuniversität Leoben zu "Gute wissenschaftliche Praxis" gelesen, verstanden und befolgt habe.

Weiters erkläre ich, dass die elektronische und gedruckte Version der eingereichten wissenschaftlichen Abschlussarbeit formal und inhaltlich identisch sind.

Datum 10.11.2022

---

Unterschrift Verfasser/in  
Nikolaus Georg Anton Preißer

# Table of contents

<b>Abstract</b> .....	<b>I</b>
<b>Kurzfassung</b> .....	<b>II</b>
<b>Affidavit</b> .....	<b>III</b>
<b>Table of contents</b> .....	<b>IV</b>
<b>Table of Figures</b> .....	<b>VI</b>
<b>List of Tables</b> .....	<b>IX</b>
<b>Acronyms</b> .....	<b>X</b>
<b>1 Introduction</b> .....	<b>1</b>
<b>2 Theoretical Background</b> .....	<b>3</b>
2.1 Effect of Non-Metallic Inclusions on the Mechanical Properties of Steel .....	3
2.2 Mechanisms of Inclusion Removal.....	5
2.3 Fundamentals of Inclusion Control.....	9
2.4 Usage of Alkali-Metals for Inclusion Removal and Control.....	15
2.5 Influence of Alkali-Metals on Slag Structure.....	17
<b>3 Preliminary Considerations and Thermodynamic Calculations</b> .....	<b>21</b>
<b>4 Experimental</b> .....	<b>28</b>
4.1 Preparation of experimental Slags .....	28
4.2 Dissolution Experiments .....	30
4.2.1 Manual Analysis of Dissolution Behavior .....	32
4.2.2 Automated Analysis of Dissolution Behavior .....	33

---

4.3	Steel-Slag Interaction Experiments .....	33
4.4	SEM/EDS-Analysis .....	36
<b>5</b>	<b>Results .....</b>	<b>38</b>
5.1	Composition of Experimental Slags .....	38
5.2	Results of HT-CSLM Analysis of Particle Dissolution .....	39
5.2.1	Dissolution of Al <sub>2</sub> O <sub>3</sub> in Slag REF .....	40
5.2.2	Dissolution of Al <sub>2</sub> O <sub>3</sub> in Slag L1 .....	41
5.2.3	Dissolution of Al <sub>2</sub> O <sub>3</sub> in Slag L2 .....	42
5.2.4	Dissolution of Al <sub>2</sub> O <sub>3</sub> in Slag L3 .....	42
5.2.5	Overview: Results of HT-CSLM Dissolution Experiments .....	43
5.3	Results of Automated SEM/EDS-Analysis .....	47
5.3.1	Amount of Detected Non-Metallic Inclusions.....	47
5.3.2	Size of Detected Non-Metallic Inclusions .....	48
5.3.3	Size Distribution of Detected O- and OS-Particles.....	51
5.3.4	Morphology and Chemical Composition of Detected Non-Metallic Inclusions .....	52
5.3.5	Chemical Composition of Detected O- and OS-Particles.....	57
<b>6</b>	<b>Discussion.....</b>	<b>65</b>
6.1	Influence on the Liquidus Temperature and Viscosity of the Slag .....	65
6.2	Influence on the Dissolution of Non-Metallic Inclusions.....	66
6.3	Influence on the Inclusion Population.....	68
<b>7</b>	<b>Summary .....</b>	<b>71</b>
	<b>Bibliography .....</b>	<b>73</b>
	<b>Appendix A: Synthetic Particles Datasheets .....</b>	<b>79</b>
	<b>Appendix B: Dissolution Data.....</b>	<b>85</b>

## Table of Figures

<b>Figure 2-1:</b> Origin of fatigue cracks in fatigue testing samples.[29] .....	4
<b>Figure 2-2:</b> Schematic of different dissolution mechanisms and the respective driving force. [33].....	7
<b>Figure 2-3:</b> Concentration profile in case of inclusion dissolution controlled by mass transport in a boundary layer.[40] .....	8
<b>Figure 2-4:</b> Concentration profile in case of inclusion dissolution controlled by diffusion in a stagnant fluid. [40] .....	8
<b>Figure 2-5:</b> Ternary slag system $\text{SiO}_2\text{-CaO-Al}_2\text{O}_3$ with areas of industrially used low melting slag compositions. [21] .....	11
<b>Figure 2-6:</b> Influence of Basicity R ( $R=\text{SiO}_2/\text{CaO}$ ) on a) total oxygen content in the melt, b) number of inclusions per area, c) average size and largest size of NMI. [45] .....	12
<b>Figure 2-7:</b> Influence of $\text{Al}_2\text{O}_3$ content in wt% on a) total oxygen content in the melt, b) number of inclusions per area, c) average size and largest size of NMI. [45] .....	12
<b>Figure 2-8:</b> Quasi quaternary System $\text{SiO}_2\text{-CaO-Al}_2\text{O}_3\text{-7wt% MgO}$ . [19] .....	13
<b>Figure 2-9:</b> Chemical composition of NMI detected in different tire cord steel samples. [11] .....	14
<b>Figure 2-10:</b> Young's modulus depending on chemical composition the ternary system $\text{SiO}_2\text{-CaO-Al}_2\text{O}_3$ . [11].....	15
<b>Figure 2-11:</b> Depolymerization of silicate structures by additional $\text{O}^{2-}$ anions. [13] .....	18
<b>Figure 2-12:</b> Schematic of the formation of tetrahedral aluminate units. [9] .....	19



<b>Figure 2-13:</b> Schematic of polymerizing and depolymerizing effects of a) $\text{Li}_2\text{O}$ and $\text{Na}_2\text{O}$ or b) $\text{K}_2\text{O}$ , $\text{Rb}_2\text{O}$ , and $\text{Cs}_2\text{O}$ . [14].....	19
<b>Figure 2-14:</b> Schematic of effects of alkali metal oxides on slag structures. [11] .....	20
<b>Figure 3-1:</b> Liquidus projection of Slag system $\text{SiO}_2\text{-CaO-Al}_2\text{O}_3$ .....	22
<b>Figure 3-2:</b> Quasi-quaternary liquidus projections of slag systems with 5wt% a) $\text{Li}_2\text{O}$ , b) $\text{Na}_2\text{O}$ , and c) $\text{K}_2\text{O}$ . .....	23
<b>Figure 3-3:</b> Comparison of area of low melting slag of base system and after addition of 5 wt% of $\text{Li}_2\text{O}$ .....	24
<b>Figure 3-4:</b> Comparison of area of low melting slag ( $1400^\circ\text{C}$ ) with the addition of 5 wt% of $\text{Li}_2\text{O}$ , $\text{Na}_2\text{O}$ , or $\text{K}_2\text{O}$ respectively.....	24
<b>Figure 3-5:</b> Influence of $\text{Li}_2\text{O}$ addition on liquidus temperature of low basicity refining-slag. [51].....	25
<b>Figure 3-6:</b> Influence of $\text{K}_2\text{O}$ addition on liquidus temperature of low basicity refining-slag. [51].....	26
<b>Figure 4-1:</b> Setup for conducted HT-CSLM dissolution experiments. ....	30
<b>Figure 4-2:</b> Heating cycle of HT-LSCM experiments. ....	31
<b>Figure 4-3:</b> Dissolution of a synthetic particle in an experimental slag.....	32
<b>Figure 4-4:</b> Experimental setup of steel-slag sample in so-called “Tammann Furnace”....	36
<b>Figure 5-1:</b> Dissolution data $\text{Al}_2\text{O}_3$ in slag REF.....	41
<b>Figure 5-2:</b> Dissolution data $\text{Al}_2\text{O}_3$ in slag L1.....	41
<b>Figure 5-3:</b> Dissolution data $\text{Al}_2\text{O}_3$ in slag L2.....	42
<b>Figure 5-4:</b> Dissolution data $\text{Al}_2\text{O}_3$ in slag L3.....	43
<b>Figure 5-5:</b> Results of HT-LSCM dissolution experiments. ....	45
<b>Figure 5-6:</b> Average ECD of detected NMI.....	50
<b>Figure 5-7:</b> Relative average ECD of detected NMI. ....	50
<b>Figure 5-8:</b> Average ECD over experimental time.....	51
<b>Figure 5-9:</b> Size distribution of detected NMI in steel-slag interaction experiments. ....	52
<b>Figure 5-10:</b> MnS inclusion detected in cast and hot-rolled spring steel sample.....	53
<b>Figure 5-11:</b> $\text{SiO}_2$ inclusion detected in cast and hot-rolled spring steel sample.....	53

---

<b>Figure 5-12:</b> SiO <sub>2</sub> -Al <sub>2</sub> O <sub>3</sub> inclusion detected in cast and hot-rolled spring steel sample. ....	54
<b>Figure 5-13:</b> CaO inclusion detected in cast and hot-rolled spring steel sample.....	54
<b>Figure 5-14:</b> Alumina oxide surrounded by MnS inclusion detected in cast and hot-rolled spring steel sample. ....	55
<b>Figure 5-15:</b> Complex heterogeneous oxide inclusion accompanied by MnS detected in cast and hot-rolled spring steel sample.....	55
<b>Figure 5-16:</b> Homogeneous complex oxide inclusion containing Na detected in steel sample after contact with slag N3 for 30 min.....	56
<b>Figure 5-17:</b> Homogeneous complex oxide inclusion containing K detected in steel sample after contact with slag K3 for 30 min.....	56
<b>Figure 5-18:</b> Chemical composition of NMI after contact with reference slag for 30 min...57	
<b>Figure 5-19:</b> Chemical composition of NMI after contact with reference slag for a) 10 min, b) 20 min, c) 25 min and d) 30 min. ....	59
<b>Figure 5-20:</b> Chemical composition of NMI after contact with slag N3 for a) 10 min, b) 20 min, c) 25 min and d) 30 min. ....	59
<b>Figure 5-21:</b> Chemical composition of NMI after contact with slag K3 for a) 10 min, b) 20 min, c) 25 min and d) 30 min. ....	60
<b>Figure 5-22:</b> Chemical composition of NMI after contact with slag L2 for a) 10 min, c) 25 min and d) 30 min. ....	60
<b>Figure 5-23:</b> Chemical composition of O and OS particles after contact for 30 min with slags a) – c) N1, d) – f) N2, and g) – i) N3. ....	62
<b>Figure 5-24:</b> Chemical composition of O and OS particles after contact for 30 min with slags a) – c) K1, d) – f) K2, and g) – i) K3. ....	63
<b>Figure 5-25:</b> Chemical composition of O and OS particles after contact for 20 min with slag K2, Particles contain a) below 0.2 wt%, b) above 0.2 wt%, c) above 1.0 wt% of potassium..63	
<b>Figure 6-1:</b> Attack on Al <sub>2</sub> O <sub>3</sub> crucible (white) from interaction with slag N3. ....	70

## List of Tables

<b>Table 2-I:</b> Summary of effects of alkali oxides in slags on NMI.....	17
<b>Table 3-I:</b> Calculated and measured values of viscosity at 1600°C (*1500°C) for selected slag compositions.....	26
<b>Table 4-I:</b> Target chemical composition of experimental slags.....	29
<b>Table 4-II:</b> Chemical composition of steel sample as received.....	34
<b>Table 4-III:</b> Sampling Plan of steel-slag interaction experiments.....	34
<b>Table 4-IV:</b> Settings for SEM/EDS analysis.....	37
<b>Table 5-I:</b> Chemical composition of experimental slags.....	38
<b>Table 5-II:</b> Parameters and average results of dissolution experiments.....	46
<b>Table 5-III:</b> Amounts of O-, S-, and OS-NMI.....	48
<b>Table 5-IV:</b> Calculated liquidus temperatures of particles containing high amounts of Na <sub>2</sub> O. .....	64
<b>Table 6-I:</b> Chemical compositions of experimental slags after interaction with crucibles...	69

## Acronyms

DOP	...	Degree of Polymerization
ECD	...	Equivalent Circle Diameter
EDS	...	Energy Dispersive Spectroscopy
HT-CSLM	...	High Temperature Confocal Scanning Laser Microscope/Microscopy
ICP	...	Inductively Coupled Plasma
NMI	...	Non-Metallic Inclusion
O	...	Oxide
OS	...	Oxide-Sulfide
S	...	Sulfide
SEM	...	Scanning Electron Microscope/Microscopy
XRF	...	X-Ray Fluorescence

# 1 Introduction

The need for steel to accommodate the needs of a great variety of different fields of applications has led to a tremendous progress regarding the decisive properties of steels in the last few decades. Steels with superb mechanical properties such as yield strengths over 1500 MPa are produced as well as steels with values for elongation to fracture of over 50%. [1,2] This is why steel will continue to be of outstanding importance to modern society. While optimizing steel grades regarding their chemical composition and fine tuning production parameters to ensure best possible properties of the finished products, the importance of the control of non-metallic inclusions (NMI) has been often overlooked in the past. But as requirements on the properties of the material continue to increase, the effect of NMI in the steel matrix becomes more and more prominent. Especially in applications where high dynamic loads have to be endured like in springs or tirecord, lowest contents of NMI must be reached, as to avoid failure due to fracture inducing particles. [3] A single particle could lead to devastating failure when present in saw wire steels with diameters as low as 50  $\mu\text{m}$  (approximately the thickness of a human hair), used to precisely cut monolithic silicon crystals. [4] Also regarding the corrosion resistance, the presence of NMI on the materials surface can have detrimental effects especially concerning pitting corrosion resistance. [5-7] In contrary, NMI could also positively influence certain aspects of the steels behavior during production and in the finished product. Such effects could be for example the improvement of the machinability of the steel or the formation of a certain microstructure. Although, this is only possible when amount, size, morphology, composition, and position of the NMI is perfectly controlled. So knowledge about NMI and ways to influence the mentioned parameters are the keys to successful modern steelmaking. [8] All parameters regarding NMI can be summed up as the so-called steel cleanness. This can refer to the amount of particles, their size or size

distribution, as well as the chemical composition. Further a distinction between the macro-, meso-, and micro-cleanliness of the steel can be made. Where macro usually refers to particles larger than 100  $\mu\text{m}$ , whereas micro refers to particles with sizes below 15  $\mu\text{m}$ . Mesoscopic particles are those in between those two thresholds. As this categorization is not standardized in any way, threshold values can vary depending on steel grade and application. In modern clean steels macro-inclusions are usually controlled very well, as the removal of particles is generally favored by their size. The mechanisms behind this are explained in the literature part of this thesis. But with smaller diameters removal and control of NMI becomes increasingly difficult. Therefore, research is conducted on multiple approaches to increase inclusion removal rates or to modify the chemical composition of NMI to configurations which are less harmful to the products mechanical properties. In this work the influence of changing the composition of ladle slag used in secondary metallurgy on the steel cleanliness is examined. Especially the effects of the addition of alkali metal oxides to the slag is in the focus of the following considerations as some research implies the possible advantageous usage of such components. [9-15]

In the following the theoretical background regarding the effect of NMI on the steels properties as well as means for inclusion removal and control are presented. Based on the literature review thermodynamic calculations were performed for further insight in the influence of alkali metal oxide addition to secondary metallurgical slags. Experiments concerning the dissolution behavior of various particles in experimental slags were conducted using HT-CSLM. Additionally, experiments where the same experimental slags could interact with steel at steelmaking temperatures were carried out to study the modification of the pre-existing inclusion population.

## 2 Theoretical Background

### 2.1 Effect of Non-Metallic Inclusions on the Mechanical Properties of Steel

The formation of non-metallic inclusions is inevitable even in modern steelmaking, but the effects on production processes and the finished products can be detrimental, as for example breakage of the wire during drawing, fatigue failure of parts like valve springs under cyclic loads or degradation of the surface quality. [16-22] There are multiple ways in which NMI can influence the mechanical properties of the steel, but the most prominent mechanisms are:

- a) Amplification of the stress field of the steel matrix around the NMI, in which case the particle is considered a notching element
- b) Generation of residual stresses or voids around the NMI due to different thermal expansion coefficients of particle and steel matrix.

Generally, nearly all oxides, except CaO and MgO, have a lower thermal expansion coefficient than steel. This would lead to residual stresses after cooling, or the formation of voids around the NMI while heating of the material. These effects are stronger with bigger size particles so limitation of the inclusion size is among the highest priorities. Higher stresses in the material around NMI can cause crack formation along the interface between the particle and the steel. Voids can be treated as an early stage of a crack, but even if the void does not develop further to the point of crack formation the overall effect of high numbers of voids around multiple NMI can lead to a detrimental decrease of the mechanical properties of the material. Regarding the coalescence of nucleated voids which can lead to large cracks, elongated strips

of NMI which can form during rolling or other forming operations are the most problematic. [23] The effects different inclusions can have on the properties of the steel are different owing to different plasticities of the particles, where hard and non-deformable inclusions can have detrimental effects as stated above, while deformable particles may have little to no damaging effect on the production process or the finished product. Prominent examples for hard, non-deformable inclusions are  $\text{Al}_2\text{O}_3$ ,  $\text{MgAl}_2\text{O}_4$ , mullite and other particles with high contents of alumina. To meet highest demands regarding product quality NMI should be small in numbers and remaining particles should be controlled to spherical shapes, good plasticity and low melting temperatures. [3,21,24,25]

One example of the damaging effects hard, non-deformable inclusion can have on finished products is the decrease of the fatigue life cycle of valve springs used in modern combustion engines. Here the product is required to withstand far over  $10^8$  load cycles over the lifetime of the engine, while maintaining constant controlling forces. Breakage of the spring in this part of the engine could lead to devastating damages to the vehicle, so the fatigue properties are of utmost importance. [26] As there is an increasing need for smaller engines to reduce emissions and lower the fuel consumption, parts like valve springs are reduced in size. This leads to an even higher importance of clean steels, as the detrimental effect of hard NMI on the fatigue life increases with smaller size parts. [27,28] In **Figure 2-14** it is shown that fatigue failure due to influence of NMI (dashed marks) can occur after millions of load cycles even at low stresses, whereas crack initiation due to surface defects (non-dashed marks) tend to occur after much lower numbers of cycles. [29]

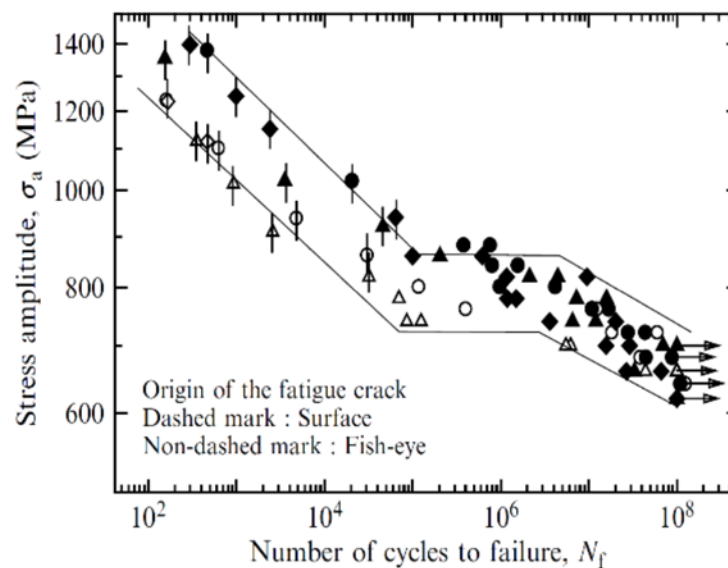


**Figure 2-1:** Origin of fatigue cracks in fatigue testing samples.[29]



## 2.2 Mechanisms of Inclusion Removal

The most effective way of avoiding problems correlated with the presence of NMI is to hinder the formation of inclusions or to remove all NMI from the steel during production. As formation of NMI cannot be suppressed completely due to the need of deoxidation of the steel in some way or another it is very important to understand the mechanisms involved in the removal of NMI. Inclusions originating either from oxidation processes of the melt or differences in solubility due to changes in the temperature of the steel are considered endogenous. Impurities due to breakage of refractory lining or entrapment of slag are considered exogenous NMI. [16,23,30] In any case, refining of the steel with top slag is one of the available methods to remove NMI. Generally, the mechanism of inclusion removal is divided in three stages, namely:

- a) Flotation
- b) Separation
- c) Dissolution

NMI can be considered only fully removed from the steel if all three of these stages have been completed and the particle is fully dissolved in the slag. Otherwise it could come to re-entrapment of the particle in the steel. To achieve proper conditions for all of the three stages to complete, the slag has to have sufficient wettability regarding the particle and show high rates of dissolution once the inclusion is fully entrained in the slag phase. [16,31-33] The first step for inclusion removal is the transport of the particle to the steel-slag interface. This is usually considered by flotation mechanisms, where the transport of the NMI to the steel-slag interface is performed by fluid dynamics and flow control and can be enhanced by finely dispersed gas bubbles in the melt which collect the NMI by collision. This process is discussed in great detail in other work and will not be considered further. [34-37]

The second stage in the removal of inclusions is the separation of the particle at the steel-slag interface. Here the particle leaves the steel melt and should be fully entrained by the liquid slag. For this to be possible the overall surface energy has to be lower once the particle is in contact with the slag phase. Thermodynamically all inclusions show lower surface energy when covered by slag instead of the liquid steel, but for separation to start the inclusion has to overcome the interfacial tension that separates the steel melt and the liquid slag. This mechanism is dependent on the buoyancy force, drag force, capillary forces, but also size and shape of the inclusion. [16,32] There are several models trying to predict this separation process during inclusion removal, as there are many factors involved. The most important

parameters for successful passing of the particle to the slag phase is according to Strandh et al. [38] the overall wettability of the system which is calculated by **Equation (2-1)**, where  $\cos\theta_{IMS}$  is the overall wettability, and  $\sigma_{IM}$ ,  $\sigma_{IS}$ , and  $\sigma_{MS}$  are the interfacial tensions between the inclusion and the metal, the inclusion and slag, or the metal and the slag respectively.

$$\cos\theta_{IMS} = \frac{\sigma_{IM} - \sigma_{IS}}{\sigma_{MS}} \quad (2-1)$$

If the overall wettability is below 0 the metal wets the inclusion, at values of overall wettability above 0 the inclusion should be wet by the slag phase. For NMI to pass to the slag phase it is necessary in almost all cases for the overall wettability to show values above 0. A second very influential parameter for the separation mechanism is the viscosity of the slag. For optimal separation the overall wettability should be high, while slag viscosity is low. This is especially true for small NMI as the influence of particle and slag densities decrease with decreasing size of the NMI. Therefore, the driving force of particle separation is reduced and the effect of overall wettability increases. When conditions for passing of the particle to the slag are not optimal inclusions can either start to oscillate at the interface or remain in the metal phase at all. If this is the case re-entrainment of the particle to the steel phase is likely and the removal of the inclusion failed. [38] Particles oscillating or remaining at the steel-slag interface could also be subject to agglomeration. This leads to a higher buoyancy force of the particle, which in effect could finally lead to a sufficient driving force for removal of the NMI.

The last step of inclusion removal is the dissolution of the particle in the liquid slag. This step is crucial as NMI can only be considered fully removed and bear no potential harm to the product if they are fully dissolved by the slag phase. The dissolution of solid particles in the slag is generally controlled by mass transfer mechanisms but may be limited by diffusion of the species in the bulk slag or reaction kinetics. If a mass-transfer controlled mechanism is proposed, the factors influencing the dissolution rate are the density of the slag and inclusion as well as the difference in wt% of the saturated slag at the interface between particle and slag and the wt% of the species (for example  $Al_2O_3$ ) in the bulk slag. The difference in wt% is in this case referred to as the driving force of the dissolution. The model for mass transfer controlled dissolution is given in Equation (2-2) where  $(dr/dt)$  is the dissolution rate,  $k$  the mass transfer coefficient,  $\rho_i$  and  $\rho_s$  the density of the inclusion and slag respectively, and wt% NMI and wt% Slag the wt% of the dissolving species respectively at the interface and in the bulk slag as proposed by Choi et al.. [39]

$$-\frac{dr}{dt} = k \left( \frac{\rho_s}{100\rho_i} \right) [wt\% NMI - wt\% Slag] \quad (2-2)$$

If dissolution is controlled by the diffusion of a species in the bulk slag instead of the mass transfer, it can be described as a variation of the shrinking core model where also the initial radius of the particle as well as the diffusivity of the species with the slowest diffusion in the respective slag are considered. The driving force in this model is again the difference in concentration of the observed species as with the mass-transfer controlled model. **Equation (2-3)** shows the dependency of the total dissolution time on the mentioned parameters. The terms of **Equation (2-3)** are:  $\tau$  the total dissolution time,  $\rho$  the density of the particle,  $R$  the initial radius of the particle,  $D$  the diffusion coefficient of the species,  $C_i$  and  $C_s$  the concentration of the species at the interface and the slag respectively.

$$\tau = \frac{\rho R^2}{2D[C_i - C_s]} \quad (2-3)$$

The third option of describing the dissolution of solid particles in liquid slag is the model controlled by reaction kinetics, also based on the assumption of a shrinking core model. Here the dissolution is limited only by the speed of the dissolution reaction at the interface of the particle and the slag. This can be described by **Equation (2-4)**. Here  $k_R$  is the constant dissolution reaction rate, all other variables are the same as in **Equation (2-3)**. In **Figure 2-2** a schematic of kinetic- and diffusion-controlled dissolution processes is shown. In the case of purely kinetic controlled dissolution, there is a distinct difference in concentration of the dissolving species in the bulk slag and on the interface of the particle. For the case of diffusion controlled dissolution it is shown that a concentration gradient is established, the so called boundary layer. [16,33]

$$\tau = \frac{\rho R}{k_R[C_i - C_s]} \quad (2-4)$$

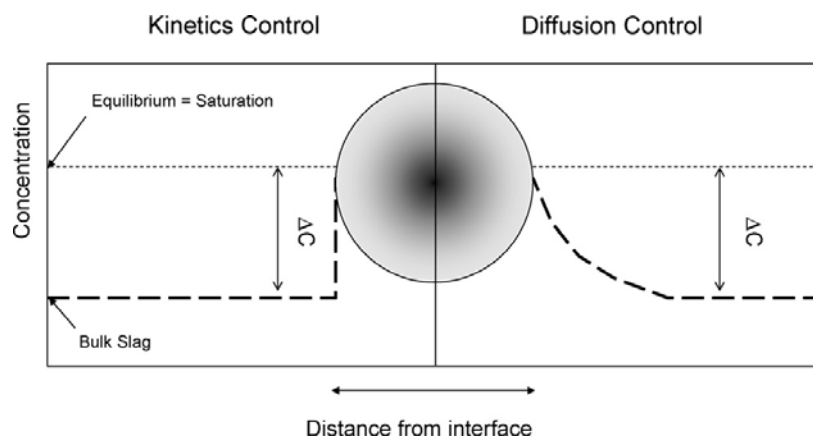


**Figure 2-2:** Schematic of different dissolution mechanisms and the respective driving force. [33]

According to Feichtinger [40] the different dissolution mechanisms can be identified when the diameter of the particle is plotted over the dissolution time. This plot shows a parabolic

shape if the dissolution is governed by mass transfer in the boundary layer. The concentration profile between the interface and the bulk slag stays in this case constant over the whole dissolution. Therefore, the only parameter affecting the dissolution rate is the ratio of surface to volume of the particle, which increases with decreasing diameter of the particle. The concentration profile for this case is shown on in **Figure 2-3** for dissolution of an  $\text{SiO}_2$  particle.

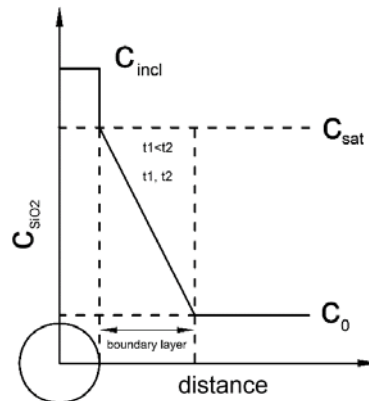


**Figure 2-3:** Concentration profile in case of inclusion dissolution controlled by mass transport in a boundary layer.[40]

If the controlling mechanism of dissolution is the diffusivity in the stagnant bulk slag the concentration profile between interface and bulk slag changes over time. At the beginning of the dissolution there is a steep gradient, providing fast dissolution, but as time passes, the gradient flattens and the dissolution slows down. At the end of the dissolution process, when particle diameters reach small values the dissolution is likely to speed up again due to the higher ratios of surface area to volume of the particle. This change of the concentration gradient over time is shown in **Figure 2-4**. This dissolution mechanism leads to a S-shaped dissolution graph when the diameter is plotted over dissolution time.

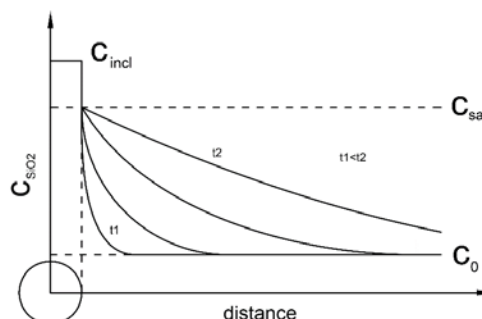


**Figure 2-4:** Concentration profile in case of inclusion dissolution controlled by diffusion in a stagnant fluid. [40]

Furthermore, Feichtinger [40] found that most dissolution processes cannot be explained to full extent by one model or another and proposed a mixed model based on shrinking core models of dissolution controlled by mass transfer in the boundary layer as well as dissolution controlled by diffusion in a stagnant fluid. This consideration leads to an adapted dissolution model as stated in **Equation (2-5)**. A parameter  $f$  with possible values between 0 and 1 is introduced to describe mixed dissolution where diffusion in a stagnant fluid as well as mass transfer in the boundary layer must be considered. When  $f$  equals 0 the dissolution is controlled by mass transfer in the boundary layer. When  $f$  reaches a value of 1 the dissolution is fully controlled by diffusion in a stagnant fluid. In **Equation (2-5)**  $R$  is the radius of the particle,  $t$  is the dissolution time,  $D$  is the diffusion coefficient of the dissolving species in the slag,  $f$  is the above introduced fitting parameter, and  $k$  is the so called dimensionless saturation as calculated by **Equation (2-6)**. Here  $c_{sat}$  describes the concentration of the dissolving species in the saturated slag at the interface,  $c_0$  is the concentration of the dissolving species in the bulk slag, and  $c_{inc}$  is the concentration of the dissolving species in the particle. [40,41]

$$\frac{dR}{dt} = -\frac{kD}{R} - fk\sqrt{\frac{D}{\pi t}} \quad (2-5)$$

$$k = \frac{c_{sat} - c_0}{c_{inc} - c_{sat}} \quad (2-6)$$

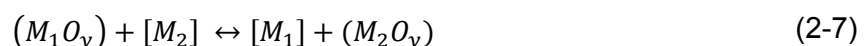
## 2.3 Fundamentals of Inclusion Control

As described in the previous chapter the removal of NMI consists of a complex series of different mechanisms and provides multiple chances for particles to avoid removal from the steel. Therefore, it is neither feasible nor possible with current experimental and industrial methods to produce steel completely free from inclusions. A way to counteracted the influence of these particles is the so called inclusion control. The aim is to control non-removable inclusions regarding their size, shape and chemical composition to a relatively harmless configuration, which does not interfere with the products quality or the production processes. This has the goal to either prevent nozzle clogging during production, improve the processing for example due to less risk of wire breakage during drawing or to improve the mechanical properties of the finished products as in the case of fatigue behavior of spring steels. This can be done on the one hand by the selection of appropriate deoxidizing agents, for example choosing Si/Mn-deoxidation over primary deoxidation with Al to avoid excessive formation of alumina-rich particles in the first place. Especially for cleanliness-sensitive steels like spring steel, this is already a common and widely used practice. [17-21,42]

Top slag treatment or slag deoxidation is another method which is used to influence the chemical composition and therefore the physical properties of NMI. This can be done due to the similarities in composition of NMI and selected slags, as changes in slag composition are thermodynamically linked to changes in the composition of NMI. Even if complete thermodynamic equilibrium cannot be achieved, the composition of the top slag influences the chemical composition of the NMI to great extent. [23,42,43] When Al is not used for primary deoxidation of the melt, alumina-rich particles can still be found in the steel, owing to the fact that to reach lowest contents of oxygen in the melt, sometimes a second deoxidation step is necessary. This can be done using Al-deoxidation after primary Si/Mn-deoxidation or as described above through slag deoxidation. In both cases primary deoxidation products like manganese silicates react with Al, either dissolved in the melt from secondary Al-deoxidation or originating from the slag when secondary deoxidation is performed using slag deoxidation method. In the case of slag deoxidation Alumina particles tend to be less in quantity and appear more homogeneous. [11,42]

Main components of slags for this refining step, usually carried out in the ladle furnace, are  $\text{SiO}_2$ ,  $\text{CaO}$ , and  $\text{Al}_2\text{O}_3$ . These are the same components commonly found in oxidic NMI which are sought to be controlled in their chemical composition. [19] For cleanliness sensitive steel grades like spring steels there are two different slag compositions commonly used in industry, depending on the primary deoxidation method. When the melt is deoxidized by Al-addition a slag with high basicity and relatively high alumina content is used. For steel grades deoxidized by Si- and Mn-addition a low basicity slag with lowest possible amounts of  $\text{Al}_2\text{O}_3$  is preferred. The ternary system  $\text{SiO}_2$ - $\text{CaO}$ - $\text{Al}_2\text{O}_3$  is shown in **Figure 2-5**. Area A marks the compositional range of the latter, low basicity slag for Si/Mn-deoxidized steel grades, whereas area B shows the composition of the former high basicity slags commonly used for Al-deoxidized melts. In general, particles should be controlled to chemical compositions of low melting point, as this is correlated to good hot-formability and therefore less problems regarding crack formation. Both, slags of composition A as well as composition B as mentioned before represent such a low melting configuration. [20,21,44]

The general thermodynamic principle for inclusion control via top slag refinement is shown in **Equation (2-7)** where  $[M]$  describes components in liquid steel, whereas  $(M_xO_y)$  stands for components of the slag phase. Owing to the strong affinity of Al to O, it should be possible to lower the amounts of Al dissolved in the steel melt. But without proper management of inclusion removal mechanisms as described in **Chapter 2.2** this could possibly lead to higher numbers of alumina inclusions. [19]



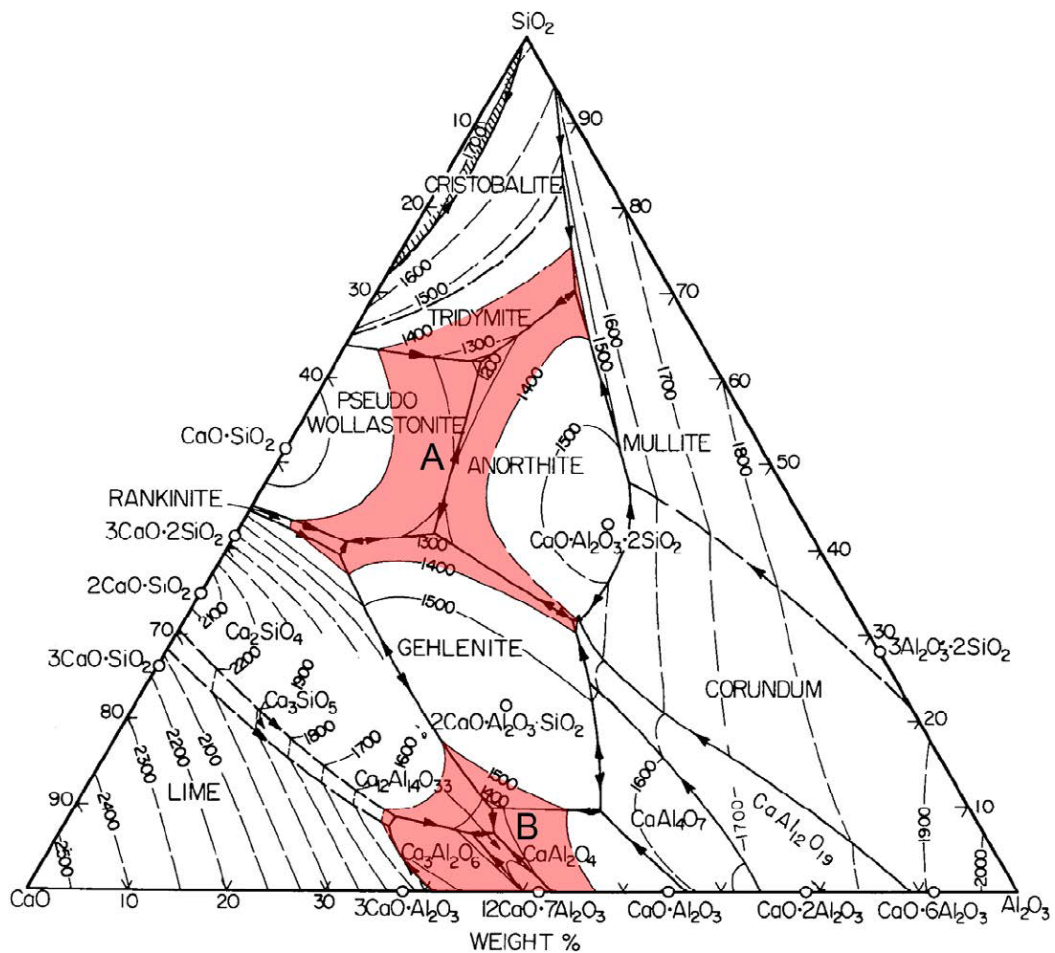


**Figure 2-5:** Ternary slag system  $\text{SiO}_2\text{-CaO-Al}_2\text{O}_3$  with areas of industrially used low melting slag compositions. [21]

There are several parameters that greatly influence the slags capability of inclusion removal and control. One of the most important factors is the slags basicity. It has been observed that increasing slag basicity is beneficial to the cleanness of steel, as the activities of  $\text{SiO}_2$  and  $\text{Al}_2\text{O}_3$  decrease. This leads on the one hand to less formation of alumina particles through reaction of  $\text{SiO}_2$  from the slag with dissolved Al in the melt, as well as increased adsorption of  $\text{Al}_2\text{O}_3$  to the slag phase. These effects are shown in **Figure 2-6**, where with increasing slag basicity ( $R = \text{SiO}_2/\text{CaO}$ ) the total oxygen content of the melt, as well as the number and size of remaining particles decreases. Additionally, the chemical composition of remaining particles shifted to lower contents of  $\text{Al}_2\text{O}_3$  with increasing basicity.

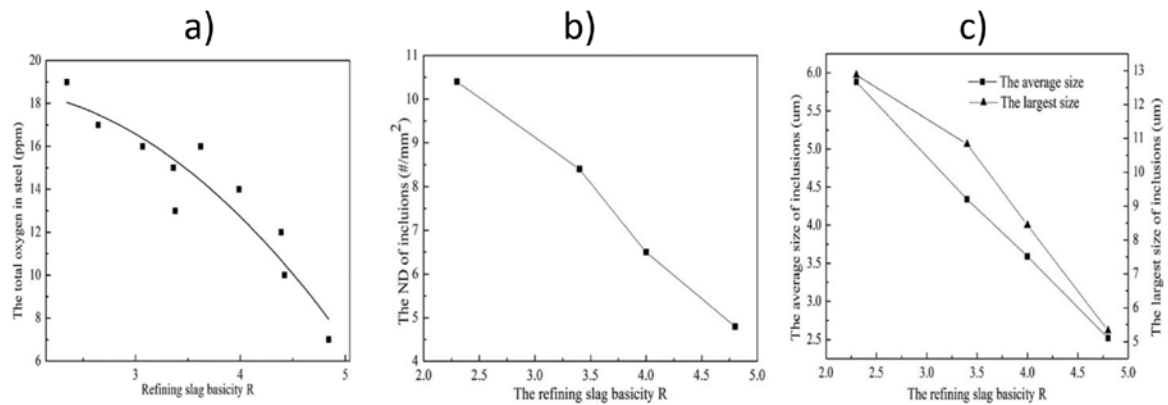


**Figure 2-6:** Influence of Basicity R ( $R=SiO_2/CaO$ ) on a) total oxygen content in the melt, b) number of inclusions per area, c) average size and largest size of NMI. [45]

A second parameter that is very influential on the slags capabilities to absorb NMI or change their chemical composition is the content of  $Al_2O_3$ . Higher contents of  $Al_2O_3$  in the refining slag lead to higher amounts of total oxygen in the melt, as well as an increase in number and size of NMI. Not surprisingly also the content of  $Al_2O_3$  in inclusions increases with higher contents of  $Al_2O_3$  in the slag. The effects of increased amounts of  $Al_2O_3$  in refining slag is shown in **Figure 2-7**. [45]

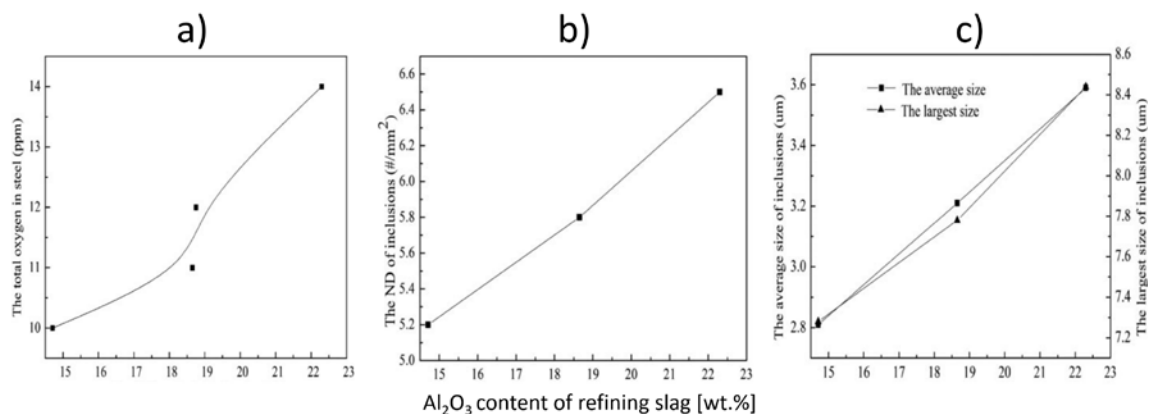


**Figure 2-7:** Influence of  $Al_2O_3$  content in wt% on a) total oxygen content in the melt, b) number of inclusions per area, c) average size and largest size of NMI. [45]

Some thermodynamic calculations as well as industrial trials have been conducted by Yang et al. [20] to evaluate the ideal composition of low basicity refining slag in the system  $SiO_2-CaO-Al_2O_3-MgO$  regarding steel cleanliness and control of NMI to low melting compositions. The premise of their calculations is to achieve the biggest area of low melting slag (below 1400°C) in the ternary system of  $SiO_2-CaO-Al_2O_3$  by variation of MgO content



with special constraints to the slags composition. Slags basicity should be above a value of 1 and ratio of CaO to  $\text{Al}_2\text{O}_3$  (by wt%) must be above 9. These restraints are based on before mentioned effects of slag basicity and content of  $\text{Al}_2\text{O}_3$ , where higher basicities and lower contents of Alumina lead to overall better steel cleanness, as well as on the premise that steels deoxidized by Si- and Mn-addition need refinement by low basicity slags. At MgO content of 7 wt% the area of low melting slag with the mentioned restrictions is the biggest. Therefore, the range of so-called optimum composition is largest at this point. The quasi quaternary phase diagram of this system is shown in **Figure 2-8**. [19,20,45]

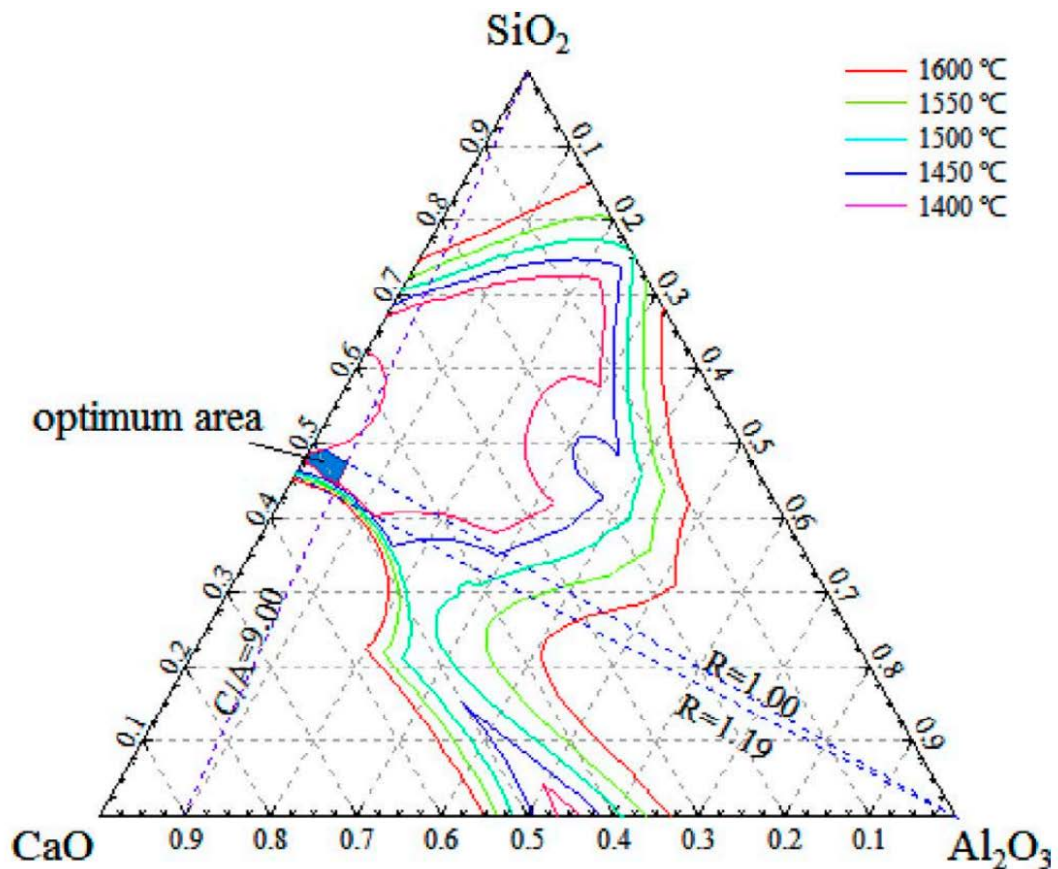


**Figure 2-8:** Quasi quaternary System  $\text{SiO}_2$ - $\text{CaO}$ - $\text{Al}_2\text{O}_3$ -7wt% MgO. [19]

In other research it is stated that the melting point of NMI alone is not sufficient in describing the effect of the particles on the mechanical properties of the steel. The low melting temperature can only be correlated with good hot-formability which is beneficial for example to good deformability of inclusions during hot-rolling processes. But as temperatures for cold-drawing operations of wire, or the working conditions of spring steels are much below melting temperatures of NMI it is proposed that control of particles to chemical compositions of low melting areas is not sufficient to ensure good performance of the steel in production or

the finished product. This is shown by a study performed by a tire manufacturer, where different samples of tire-cord steel have been analyzed regarding the composition of NMI as well as frequency of wire breakage during cold-drawing operations. Samples where most inclusions concentrated in the low melting area of the  $\text{SiO}_2\text{-CaO-Al}_2\text{O}_3$  ternary system performed significantly worse than samples containing mostly  $\text{SiO}_2$ -rich particles with higher melting temperatures. The results of this study are shown in **Figure 2-9**, where samples c) showed wire breakage during cold drawing about once per 750 km, whereas samples a) and b) broke about once every 30 km during drawing operation.

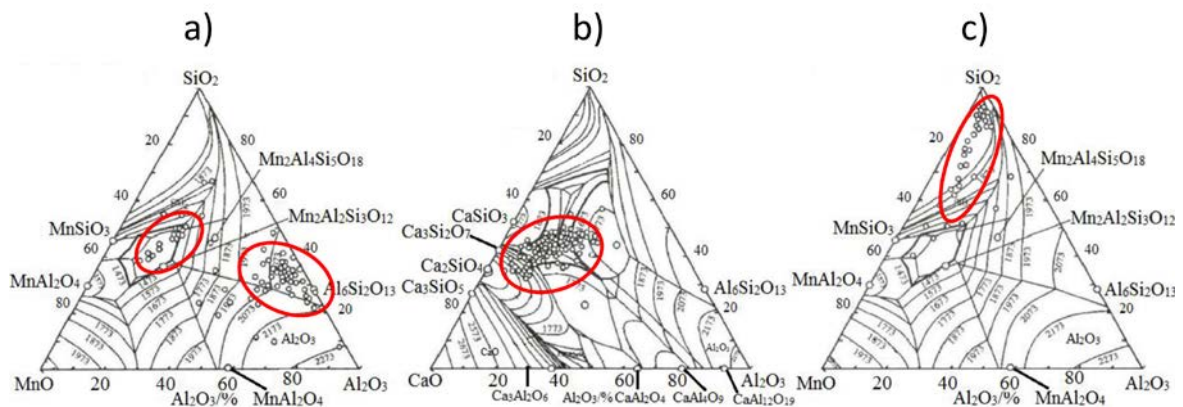


**Figure 2-9:** Chemical composition of NMI detected in different tire cord steel samples. [11]

It is proposed that using the hardness of NMI or the Young's modulus of the inclusion is a better way of determining the steels aptitude for deformation at lower temperatures, as the control of inclusions to low melting temperatures could only be correlated to good hot-deformability of the steel. As Young's modulus shows good linear correlation with Vickers hardness for low temperatures researchers decided to use Young's modulus of the inclusions to express capability of deformation and cold-drawability. It is proposed that inclusion with lower values of Young's modulus and therefore lower levels of hardness are less harmful to the steels mechanical properties. **Figure 2-10** shows values of Young's modulus in the ternary system of  $\text{SiO}_2\text{-CaO-Al}_2\text{O}_3$ . Areas of smallest Young's moduli are that with lowest amounts of  $\text{Al}_2\text{O}_3$  but high amounts of  $\text{SiO}_2$ . Comparing this region with areas of low melting points it is obvious that there is a big difference in chemical composition and therefore it is not possible to achieve low melting temperatures as well as lowest values for Young's modulus in NMI. Researchers are not sure whether or not to use this information to adapt currently used refining slag compositions to control NMI to these areas of low Young's moduli to improve steel performance. Further studies regarding this have to be conducted. [11,24]

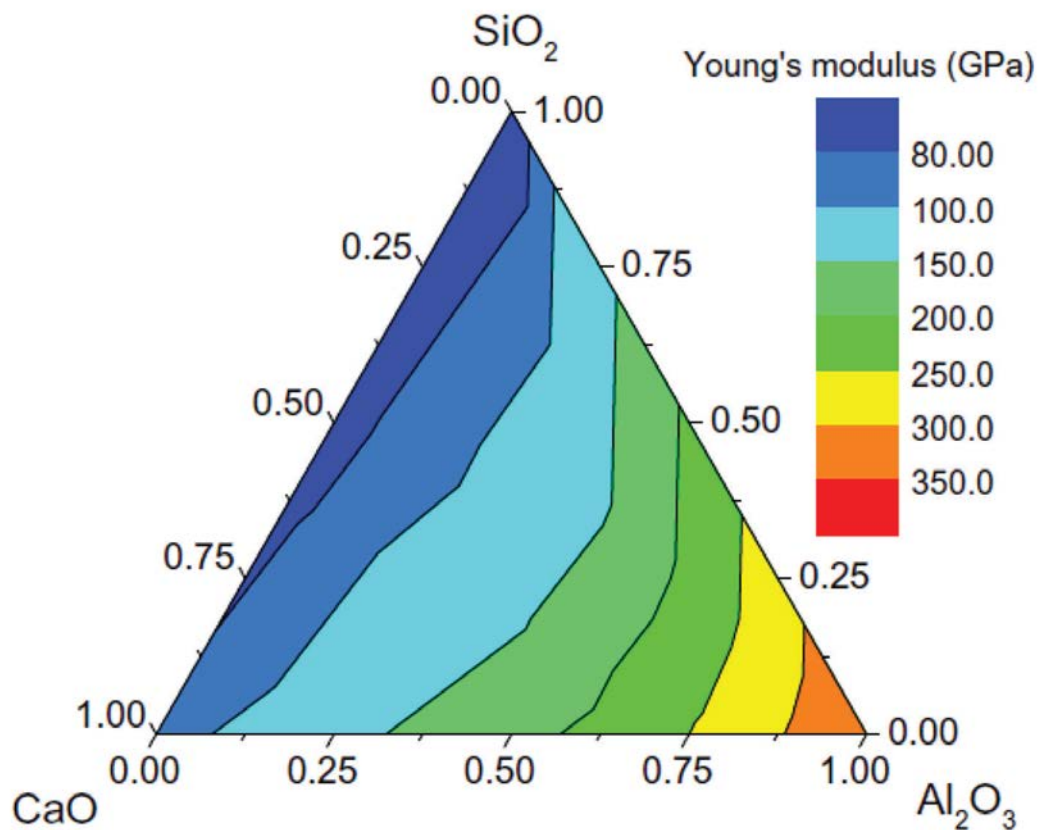


**Figure 2-10:** Young's modulus depending on chemical composition the ternary system  $\text{SiO}_2\text{-CaO-Al}_2\text{O}_3$ . [11]

## 2.4 Usage of Alkali-Metals for Inclusion Removal and Control

Alkali metal oxides have been successfully used in the industry for steelmaking slags such as mold powders to influence the slags properties like viscosity, fluidity and melting temperature. Especially the viscosity is of interest in the case of mold powders regarding proper lubrication of the mold, thus providing good surface quality of the strand and smooth operation during continuous casting. Traditionally, low viscosity in mold fluxes is achieved by addition of fluorine containing species but as concerns regarding environmental impact of fluorine gets stronger new ways of viscosity control are of interest. [46-49]

Taking on from the usage in mold powders alkali metal oxides found their way upstream and research regarding improving NMI absorption of tundish slags was conducted. In addition with various methods of flow control of the melt, slags with best capabilities of inclusion removal

should ensure highest levels of cleanness before casting. As shown before high basicity and preferably low amounts of  $\text{Al}_2\text{O}_3$  are used to enhance inclusion removal. Assumed  $\text{Al}_2\text{O}_3$  appears in the slag phase in a tetrahedral configuration similar to silicates, where  $\text{Al}^{3+}$  cations are surrounded by 4 shared  $\text{O}^{2-}$  anions, this tetrahedral unit lacks a positive charge. In theory, this charge could be provided by single Alkali cations. Due to this charge compensation effect addition of alkali metal oxides could help to attract alumina containing NMI and therefore enhance removal of hard and non-deformable inclusions. This mechanism is described in more detail in **Chapter 2.5**. [12,14] Yu et al. [14] found that addition of  $\text{K}_2\text{O}$  to synthetic tundish slags could enhance steel cleanness of stainless steel grades in laboratory scale experiments significantly, whereas additions of  $\text{Li}_2\text{O}$  and  $\text{Na}_2\text{O}$  could not improve cleanness but sometimes even hindered inclusion removal. Choi et al. [12] report similar results regarding  $\text{Li}_2\text{O}$ ,  $\text{Na}_2\text{O}$ , and  $\text{K}_2\text{O}$  and suggest that the addition of  $\text{Rb}_2\text{O}$  and  $\text{Cs}_2\text{O}$  would also improve steel cleanness in the same manner as  $\text{K}_2\text{O}$ . However, they indicate that due to economics the usage of  $\text{Rb}_2\text{O}$  and  $\text{Cs}_2\text{O}$  is not feasible for industrial scale, but the use of  $\text{K}_2\text{O}$  in the carbonatic form of  $\text{K}_2\text{CO}_3$  could be economically feasible while providing means of improving steel cleanness. In respect to this work presented results have to be treated carefully, as tundish slag compositions of the mentioned research does not resemble the composition of refining slags for Si/Mn-deoxidized steels regarding basicity and  $\text{Al}_2\text{O}_3$  content. Additionally, the main inclusion type subject to removal in the presented research was TiN as stainless-steel samples have been used to conduct the experimental work.

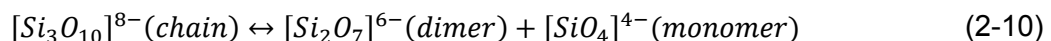
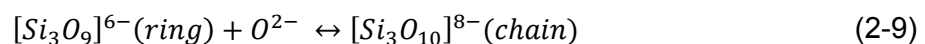
As research results regarding tundish slags were quite promising, it is not surprising that further experiments were conducted to use alkali metal oxides in ladle furnace refining slags for enhanced inclusion removal. Li et al. [13] report that again  $\text{K}_2\text{O}$  could improve inclusion removal and that remaining particles are not only smaller in size but concentrated in the low melting areas of the systems  $\text{SiO}_2\text{-CaO-Al}_2\text{O}_3$  and  $\text{SiO}_2\text{-MnO-Al}_2\text{O}_3$ . This effect was observed up to contents of 10 wt% of  $\text{K}_2\text{O}$  in the slag.  $\text{Li}_2\text{O}$  on the other hand seems to slightly hinder inclusion removal. Jiang et al. [15] report similar results for the addition of  $\text{K}_2\text{O}$  but only up to contents of 7.5 wt%. Chen et al. [9] found that  $\text{Na}_2\text{O}$  could not improve inclusion removal and in fact both the number and size of NMI increased when  $\text{Na}_2\text{O}$  was added to the refining slag. With the addition of  $\text{Rb}_2\text{O}$  inclusion count and size decreased with refining time and remaining particles mainly concentrated in the low melting areas of the systems  $\text{SiO}_2\text{-CaO-Al}_2\text{O}_3$  and  $\text{SiO}_2\text{-MnO-Al}_2\text{O}_3$ . [10] All results regarding addition of alkali metal oxides to refining slags were conducted with low basicity slags with low contents of  $\text{Al}_2\text{O}_3$  and saw wire steel samples. **Table 2-I** summarizes the above presented results of usage of alkali metal oxides in secondary metallurgical slags and the influence on number, size, and chemical composition of NMI.

**Table 2-I:** Summary of effects of alkali oxides in slags on NMI.

Species	Slag	Steel	Effect on			Source
			Number	ECD	Chemical comp.	
Li <sub>2</sub> O	Tundish	Stainless	↑	↓	/	[14]
Na <sub>2</sub> O	Tundish	Stainless	↑	↓↑	/	[14]
K <sub>2</sub> O	Tundish	Stainless	↓	↓	Spinel-rich	[14]
Rb <sub>2</sub> O	Tundish	Stainless	↓	↓	TiN removed	[12]
Cs <sub>2</sub> O	Tundish	Stainless	↓	↓	TiN removed	[12]
Li <sub>2</sub> O	Refining	Saw wire	↑	↑	SiO <sub>2</sub> -rich	[13]
Na <sub>2</sub> O	Refining	Saw wire	↑	↑	SiO <sub>2</sub> -rich	[9]
K <sub>2</sub> O	Refining	Saw wire	↓	↓	Low melting	[13,15]
Rb <sub>2</sub> O	Refining	Saw wire	↓	↓	Low melting	[9,10]

## 2.5 Influence of Alkali-Metals on Slag Structure

As established in the previous chapter alkali metals can alter slag properties in such a way as to influence the slags capability of inclusion removal and their effect on the overall steel cleanliness. This can be traced mainly to two effects of alkali metals on the slag structure. The first mechanism is the depolymerization of silicate structures like rings, chains, and complex networks. This is due to alkali metal oxides providing O<sup>2-</sup> which can break down complex silicates to simpler structures as expressed in **Equations (2-8), (2-9), and (2-10)**, as well as in **Figure 2-11**. R<sup>+</sup> represents the cation of the alkali element, for example Li<sup>+</sup>, Na<sup>+</sup>, or K<sup>+</sup>. [13,50]



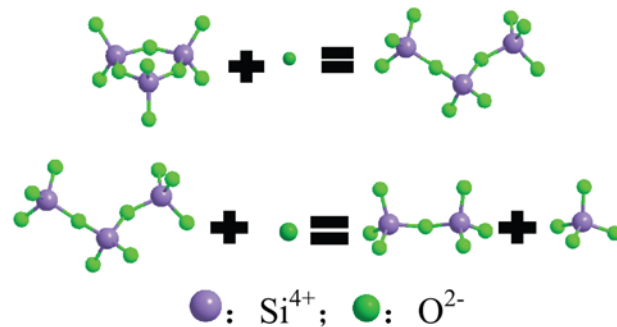


**Figure 2-11:** Depolymerization of silicate structures by additional  $\text{O}^{2-}$  anions. [13]

Additionally,  $\text{Li}^+$  and  $\text{Na}^+$  are reported to have a similar effect on aluminate structures which will also be depolymerized by provided  $\text{O}^{2-}$ . This decrease in degree of polymerization (DOP) of the slag leads to a decrease in surface tension and viscosity of the slag phase. Which in theory should promote inclusion removal as discussed in **Chapter 2.2** [9,50]

The second effect alkali elements can have on the slag structure is as mentioned before that in theory the single positive charge of alkali cations could balance the charge of tetrahedral units of  $[\text{AlO}_4]^{5-}$  and promote the formation of such units. The mechanism of formation of tetrahedral aluminate units is shown in **Equation (2-11)** and **Figure 2-12**. These tetrahedral  $[\text{AlO}_4]^{5-}$  units act as network-formers in the slag structure. This could lead to polymerization of the slag and formation of complex aluminate structures, which would increase the surface tension and viscosity of the slag. Several researchers propose that this helps in avoiding slag entrapment into the melt as well as ensuring that particles do not return to the melt once separated into the slag phase. However, the second step of inclusion removal, the separation of the particle from the steel to the slag phase is hindered by these effects. Therefore, excessive addition of alkali oxides to the slag could decrease the ability of the slag to adsorb NMI properly and be detrimental to steel cleanness. According to research this behavior of increasing the DOP is only true for  $\text{K}_2\text{O}$  and heavier alkali metal oxides like  $\text{Rb}_2\text{O}$  and  $\text{Cs}_2\text{O}$ .

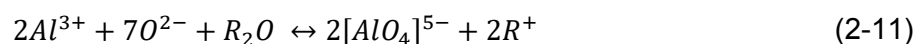




**Figure 2-12:** Schematic of the formation of tetrahedral aluminate units. [9]

Further  $K_2O$ ,  $Rb_2O$ , and  $Cs_2O$  could polymerize aluminate and silicate units in the slag even more and promote the formation of complex alumino-silicate structures, enhancing the effect of increasing surface tension and viscosity even more. So effectively light alkali metal oxides like  $Li_2O$  and  $Na_2O$  were found to depolymerize the slag phase through providing  $O^{2-}$  anions leading to decreased viscosity and surface tension. This enhances separation forces and would lead to increased separation of NMI to the slag phase. On the other hand, this same effect increases the risk of slag entrapment to the melt and inclusions returning from the slag to the melt. Heavier alkali metal oxides like  $K_2O$ ,  $Rb_2O$ , and  $Cs_2O$  show the same mechanism of decreasing the DOP due to providing additional  $O^{2-}$  but polymerizing effects due to balancing of ionic charge and promoting the formation of tetrahedral aluminate units as well as formation of complex alumino-silicate networks seem to outweigh depolymerization of silicate structures. This results in overall increase of viscosity and surface tension, hindering separation of NMI to the slag phase but decreasing the risk of re-entrainment of particles due to binding of NMI to polymerized slag networks. The two counteracting mechanisms are visualized in **Figure 2-13** and **Figure 2-14**. [12,13,15]

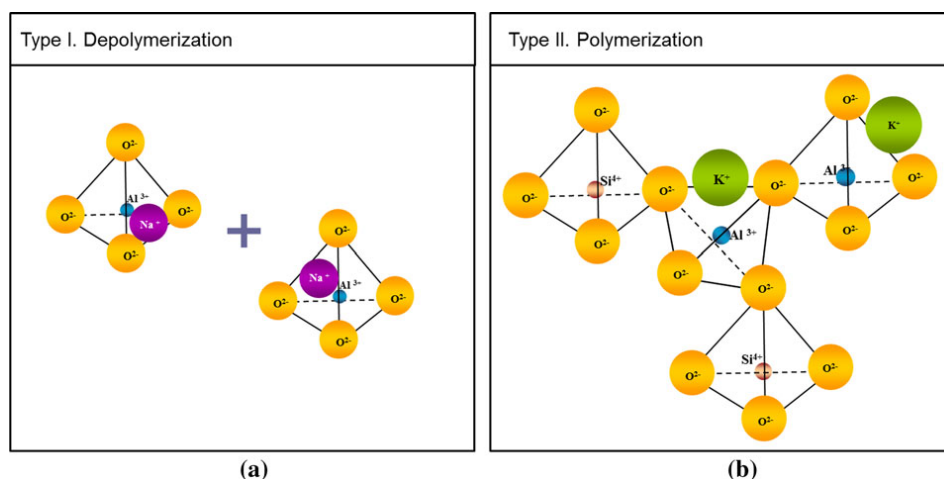


**Figure 2-13:** Schematic of polymerizing and depolymerizing effects of a)  $Li_2O$  and  $Na_2O$  or b)  $K_2O$ ,  $Rb_2O$ , and  $Cs_2O$ . [14]

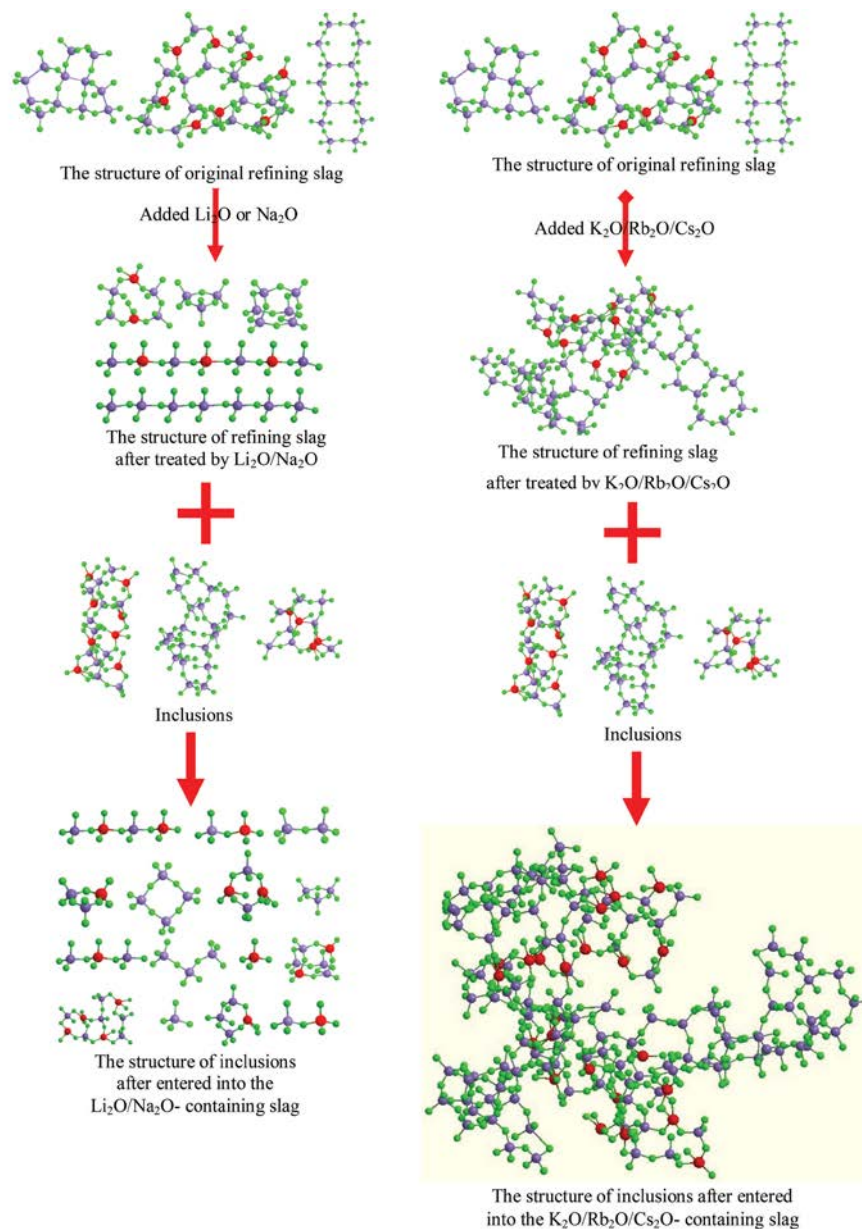


**Figure 2-14:** Schematic of effects of alkali metal oxides on slag structures. [11]

In conclusion not all alkali metal oxides influence the slags structure and therefore the properties regarding inclusion removal in the same way. Mechanisms to increase or decrease the DOP are counteracting each other and dependent on the ionic radius of the alkali metal cations different mechanisms overweigh and influence the overall effect on the slag. Generally,  $\text{K}_2\text{O}$ ,  $\text{Rb}_2\text{O}$ , and  $\text{Cs}_2\text{O}$  are reported to positively affect the removal of inclusions from the melt and improve steel cleanness, while  $\text{Li}_2\text{O}$  and  $\text{Na}_2\text{O}$  seem to have the opposite effect, namely decreasing steel cleanness due to slag entrapment and disability to hinder inclusion from returning to the melt. This is based on the observation that  $\text{K}_2\text{O}$  and heavier alkali metal oxides tend to increase slag viscosity while lighter species decrease the viscosity.



### 3 Preliminary Considerations and Thermodynamic Calculations

In previous chapters the theoretical influence of alkali metal oxides on the properties of slags in secondary metallurgy has been described. For a better understanding of the slag system and potential changes in properties and behavior due to addition of alkali metal oxides thermodynamic calculations are performed before planning and conducting of experiments. Especially the influence on the liquidus temperature and viscosity of the slag is of interest, as these are the parameters that have the most effect on NMI removal and control regarding to research presented earlier. All calculations for this work have been done using FactSage Version 8.2 with Database FToxid. The first parameter which was observed regarding its change due to addition of alkali metal oxides to the slag was the liquidus temperature. For this, so-called liquidus projections can be performed using the Phasediagram module of FactSage. For comparison the first calculated system is that of the base slag system  $\text{SiO}_2\text{-CaO-Al}_2\text{O}_3$  without addition of alkali metal oxides. As the first step the involved components are defined in the software. Further the appropriate database must be selected. For these slag calculations the database FToxid is sufficient as it describes all the involved components up to and above steelmaking temperatures. The calculations are performed at atmospheric pressure. All solution phases are selected to be considered for calculation but only the phase of liquid slag (FToxid-SLAGA) should be plotted. This is indicated by the setting O in Fact sage (only plot this single Phase). The plot should be in the form of a ternary diagram, each corner representing one of the three base components of the slag. When choosing the temperature for the calculation the option 'projection' is used with a temperature range of 1200 – 1400°C and steps of 100°C. For faster calculation only isotherms are plotted as phase boundary lines

can be found in literature to great extent as shown in **Figure 2-5**. In **Figure 3-1** the calculated ternary liquidus projection of the base slag system is shown. The area of lowest liquidus temperatures, where liquid slag forms at about 1200 °C is at the phase boundary between tridemite, pseudo-wollastonite, and anorthite. This area expands at higher temperatures to lower SiO<sub>2</sub> contents until it reaches the phase boundary of gehlenite. A second area of lower melting slag lies at very low SiO<sub>2</sub> contents in the area of CaAl<sub>2</sub>O<sub>4</sub>. Near the CaO or Al<sub>2</sub>O<sub>3</sub> corners of the ternary diagram phases like C<sub>2</sub>S with very high liquidus temperatures are stable. It should be avoided at all times to achieve slag compositions in these areas to prevent formation of solid slags.

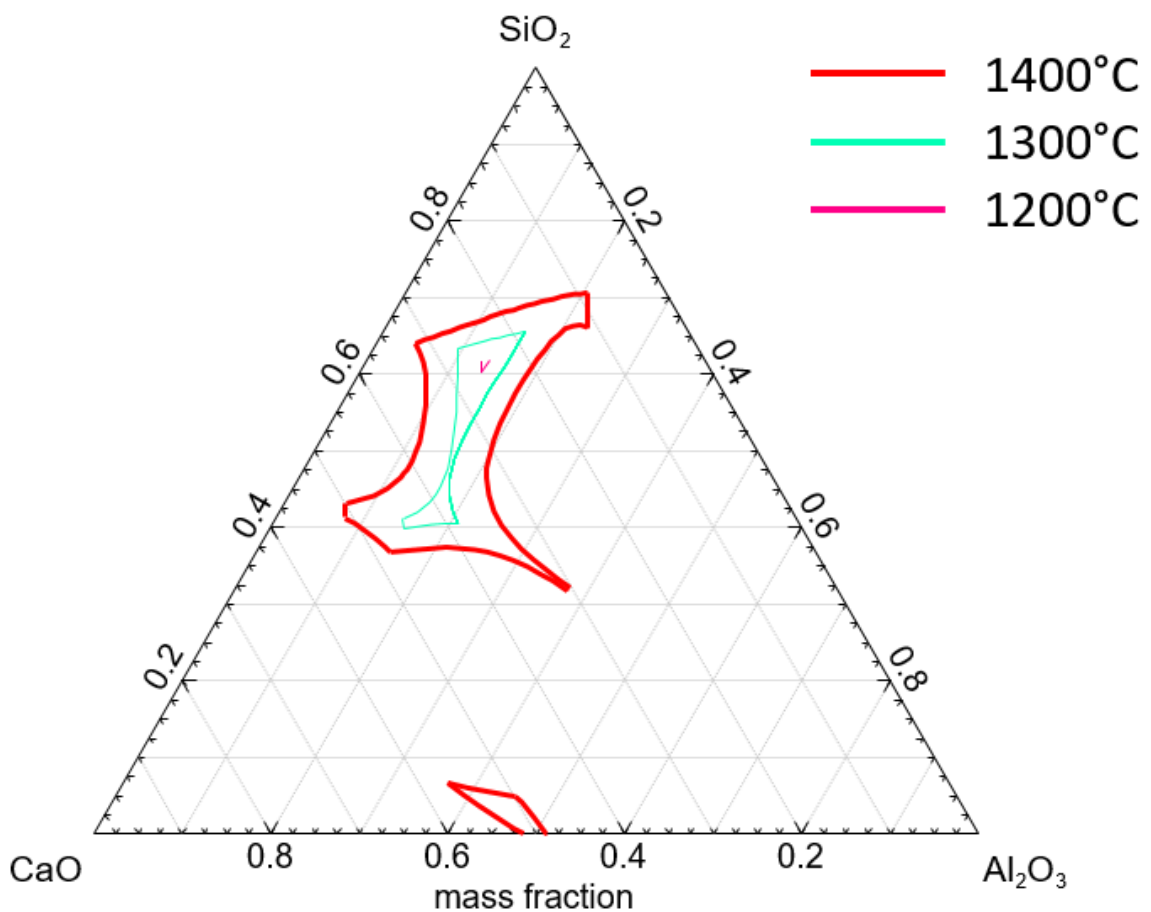


**Figure 3-1:** Liquidus projection of Slag system SiO<sub>2</sub>-CaO-Al<sub>2</sub>O<sub>3</sub>.

When calculating systems containing alkali metal oxides alongside the three base components of the slag system the content of alkali metal oxide is fixed to a specific value, thus creating a quasi-quaternary diagram. With this method a specific point in the ternary diagram can be directly related to the same point in the quasi-quaternary diagram as the ratio of the base components is constant. In this work this is done for all three selected alkali oxides

with varying contents. In **Figure 3-2** three quasi-quaternary liquidus projections for 5% of a)  $\text{Li}_2\text{O}$ , b)  $\text{Na}_2\text{O}$ , and c)  $\text{K}_2\text{O}$  respectively are shown between 1200 and 1400°C. It is clear that for all three added components the area of liquid phase at specific temperatures increases. The strongest effect can be observed for addition of  $\text{Li}_2\text{O}$ . Here the area of slag melting above at 1400°C increases drastically. Low melting areas of low and high basicity are even joined, so slags with any basicity could theoretically be used without risk of producing solid slags. With higher atomic weight of the alkali element the effect on the liquidus temperature seems to decrease. With addition of  $\text{Na}_2\text{O}$  the low melting area of high basicity slag disappears according to calculations. Low melting area of low basicity slag increases drastically. Especially the region of industrially used low basicity refining slags expands towards lower  $\text{Al}_2\text{O}_3$  contents which should allow to decrease  $\text{Al}_2\text{O}_3$  contents and therefore enhance steel cleanliness regarding alumina-rich non-deformable NMI. The addition of  $\text{K}_2\text{O}$  shifts the position of low melting area of high basicity slags to higher contents of  $\text{SiO}_2$ . Low basicity low melting area also expands, but not to the extent as in the case of the addition of  $\text{Na}_2\text{O}$  or even  $\text{Li}_2\text{O}$ .

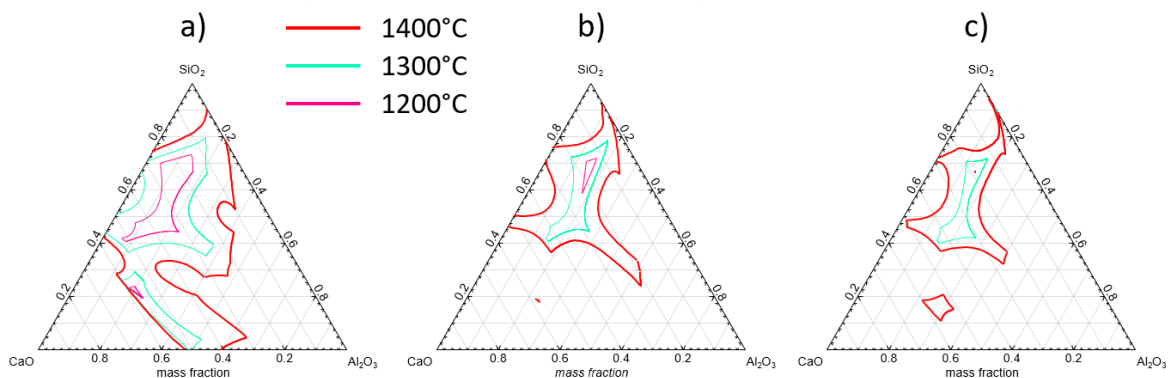


**Figure 3-2:** Quasi-quaternary liquidus projections of slag systems with 5wt% a)  $\text{Li}_2\text{O}$ , b)  $\text{Na}_2\text{O}$ , and c)  $\text{K}_2\text{O}$ .

To stress the effect of  $\text{Li}_2\text{O}$  addition to the slag system **Figure 3-3** compares the area of the base slag system melting above 1400°C (solid black line) with the area of slag melting above 1200°C after addition of 5 wt%  $\text{Li}_2\text{O}$  (solid red line). It is obvious that due to the addition of  $\text{Li}_2\text{O}$  liquidus temperatures in a big area drops over 200°C. For better comparison of the effects of different alkali metal oxides on the liquidus temperature of the slag system **Figure 3-4** shows the areas of slag liquid above 1400°C with additions of 5 wt% of alkali metal oxide respectively. Additionally lines for a basicity ( $B_2 = \text{SiO}_2/\text{CaO}$ ) of 1 and ratio of  $\text{CaO}/\text{Al}_2\text{O}_3 = 9$  are shown in **Figure 3-4** to compare areas of “ideal” slag composition as described in **Chapter 2.3** and **Figure 2-8**.

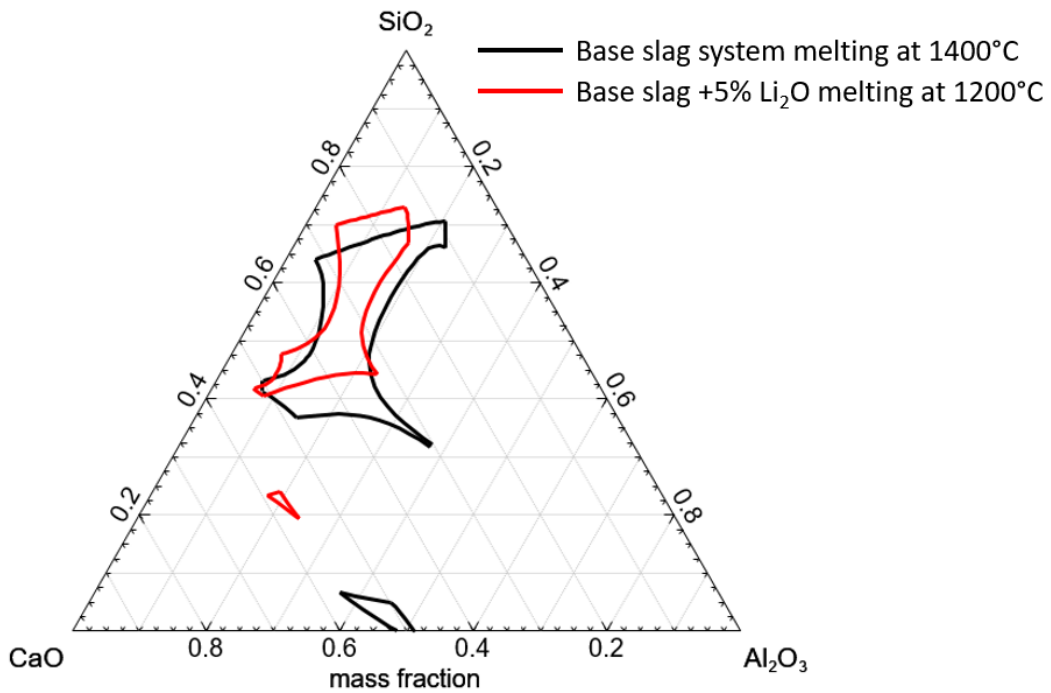


**Figure 3-3:** Comparison of area of low melting slag of base system and after addition of 5 wt% of Li<sub>2</sub>O.

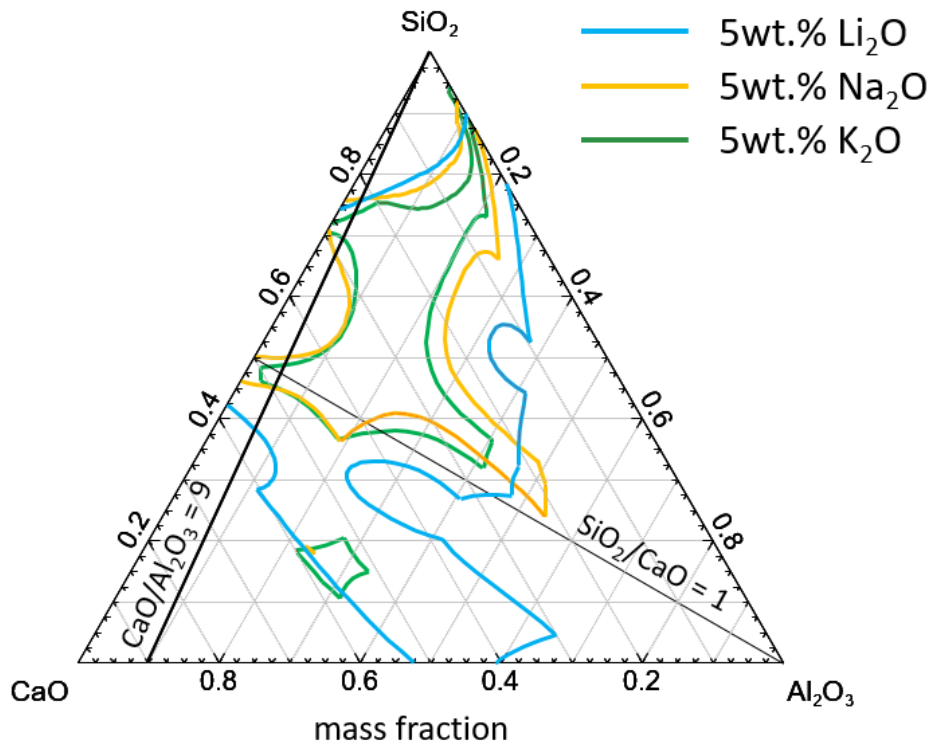


**Figure 3-4:** Comparison of area of low melting slag (1400°C) with the addition of 5 wt% of Li<sub>2</sub>O, Na<sub>2</sub>O, or K<sub>2</sub>O respectively.

The effect of alkali metal oxides on the liquidus temperature of the slag system has been further studied regarding the influence of amount of addition. Liquidus temperatures have been calculated for a slag with composition of 50 wt%  $\text{SiO}_2$ , 45 wt%  $\text{CaO}$ , and 5 wt%  $\text{Al}_2\text{O}_3$  which resembles the chemical composition of a low basicity refining slag for the production of Si/Mn deoxidized steel. Further the effect on this temperature with continuous addition of alkali metal oxides has been calculated. The liquidus temperature of the base slag without addition of alkali metal oxides was calculated to be  $1492.2^\circ\text{C}$ . The addition of  $\text{Li}_2\text{O}$  to the slag leads to a drastic decrease in liquidus temperature even at low amounts as shown in **Figure 3-5**. At a content of 7.5 wt%  $\text{Li}_2\text{O}$  the liquidus temperature of the slag is decreased to  $1147.2^\circ\text{C}$ . This corresponds to a decrease of  $345^\circ\text{C}$ .

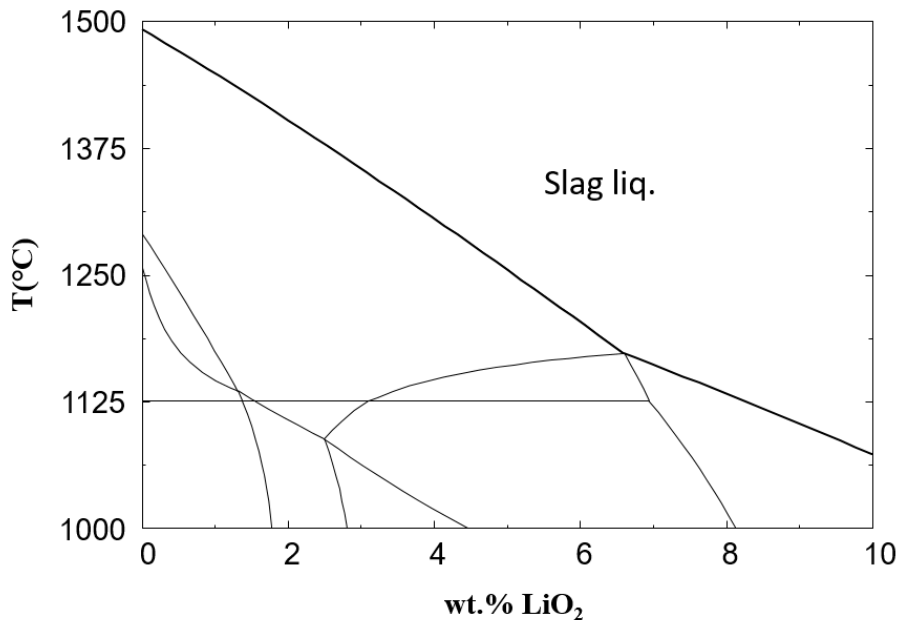


**Figure 3-5:** Influence of  $\text{Li}_2\text{O}$  addition on liquidus temperature of low basicity refining-slag. [51]

With additions of  $\text{K}_2\text{O}$  the effect is not as pronounced as with  $\text{Li}_2\text{O}$  but liquidus temperature still decreases significantly with higher contents of the alkali metal oxide. **Figure 3-6** shows the influence of increasing the content of  $\text{K}_2\text{O}$  in the slag. Once a content of 7.5 wt% of  $\text{K}_2\text{O}$  in the slag is reached, the calculated liquidus temperature is  $1362.6^\circ\text{C}$  which represents a decrease of about  $130^\circ\text{C}$ . The calculated effect of  $\text{Na}_2\text{O}$  addition to the slag is as expected in between the effects of the other two alkali metal oxides. At a content of 7.5 wt% the calculated decrease in liquidus temperature is about  $152^\circ\text{C}$  which corresponds to a temperature of  $1340.5^\circ\text{C}$ . This leads to the conclusion that the effect of alkali metal oxide addition to a low basicity refining slag with the base composition of 50 wt%  $\text{SiO}_2$ , 45 wt%  $\text{CaO}$ , and 5 wt%  $\text{Al}_2\text{O}_3$  is most

pronounced with  $\text{Li}_2\text{O}$ , but also  $\text{Na}_2\text{O}$  and  $\text{K}_2\text{O}$  lead to a significant decrease in liquidus temperature.

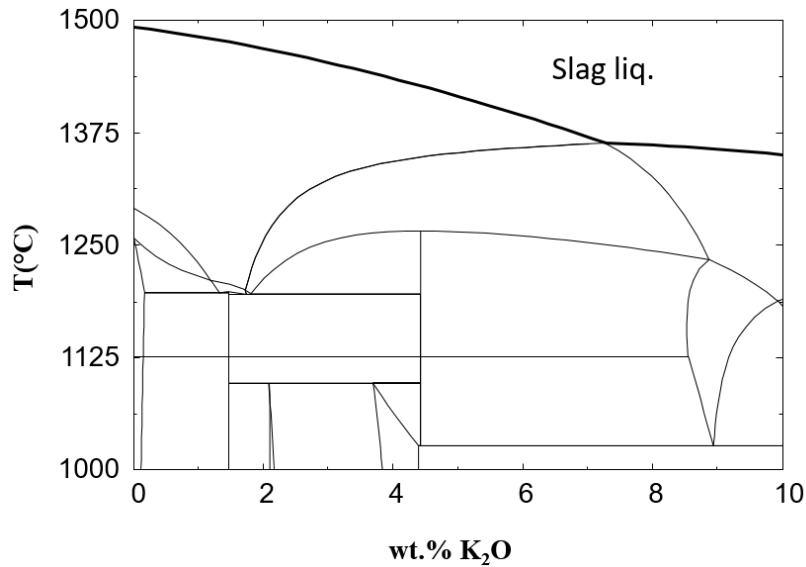


**Figure 3-6:** Influence of  $\text{K}_2\text{O}$  addition on liquidus temperature of low basicity refining-slag. [51]

Other than liquidus temperatures of the slag system the effect of alkali metal oxides on the viscosity of the slag is of interest. Using FactSage Viscosity module as well as Riboud-Model viscosities of selected slag compositions have been calculated at  $1600^\circ\text{C}$ . Additionally the viscosities have been measured by FRS 1800 shear rheometer at the Chair of Ceramics. The results of the calculations as well as measurements are presented in **Table 3-I**.

**Table 3-I:** Calculated and measured values of viscosity at  $1600^\circ\text{C}$  ( $*1500^\circ\text{C}$ ) for selected slag compositions.

Slag	$\text{SiO}_2$	$\text{CaO}$	$\text{Al}_2\text{O}_3$	$\text{R}_2\text{O}$	Viscosity FactSage	Viscosity Riboud	Viscosity measured
/	[wt%]	[wt%]	[wt%]	[wt%]	[Pas]	[Pas]	[Pas]
REF	50.0	45.0	5.0	/	0.260	0.416	0.478*
L2	48.4	43.1	4.9	3.0 ( $\text{Li}_2\text{O}$ )	0.179	0.259	0.160
N2	47.7	42.1	4.8	5.0 ( $\text{Na}_2\text{O}$ )	0.246	0.290	0.272
K1	47.3	43.2	5.8	3.1 ( $\text{K}_2\text{O}$ )	0.267	0.351	0.351
K2	46.2	42.1	5.7	5.6 ( $\text{K}_2\text{O}$ )	0.267	0.305	0.321
K3	45.1	40.9	5.5	7.8 ( $\text{K}_2\text{O}$ )	0.271	0.271	0.309

These results show some differences in the values of viscosities for example as calculations of  $\text{Li}_2\text{O}$  containing slag L2 by Riboud-model are about 45% higher than calculated by FactSage. Nevertheless, a general trend of impact of addition of alkali metal oxides to the slag system can be shown. Addition of  $\text{Li}_2\text{O}$  results in lower viscosity compared to the base slag system (REF), especially when calculated by FactSage and by measurement. With addition of  $\text{Na}_2\text{O}$  FactSage predicts a slight decrease in viscosity, while Riboud-model and measurement show a significantly larger impact regarding viscosity reduction. Additions of  $\text{K}_2\text{O}$  increase the viscosity of the slag regarding the FactSage calculation, but Riboud-model and measurements show a decrease in viscosity compared to the reference slag. Higher contents of  $\text{K}_2\text{O}$  seem to further decrease the viscosity following the results of measurements and Riboud-model calculations, while FactSage predicts a slight increase with higher additions. As viscosity-measurements of slags L2 and N2 were slightly corrupted by slag spillage these results have to be treated with care and re-measurement of these values in future work is advised. Generally, the calculations seem to confirm theoretical considerations regarding the viscosity decreasing capabilities of  $\text{Li}_2\text{O}$  and  $\text{Na}_2\text{O}$ . However, the decrease in viscosity of the slag with increasing contents of  $\text{K}_2\text{O}$  regarding to measurements and Riboud-model calculations does not match with slag structural models presented in **Chapter 2.5**.

The following conclusions can be drawn from the presented thermodynamic observations:

- a) Addition of alkali metal oxides such as  $\text{Li}_2\text{O}$ ,  $\text{Na}_2\text{O}$ , and  $\text{K}_2\text{O}$  lead to a significant decrease of the liquidus temperature of slags in the  $\text{SiO}_2\text{-CaO-Al}_2\text{O}_3$  system
- b) The area of low melting slag with basicities  $B_2$  ( $B_2=\text{CaO/SiO}_2$ ) greater than 1 and ratio of  $\text{CaO/Al}_2\text{O}_3$  greater than 9 increases with all additions of these alkali metal oxides
- c) The biggest effect on the above mentioned properties can be expected with the addition of  $\text{Li}_2\text{O}$ . The least effect can be expected with addition of  $\text{K}_2\text{O}$ .
- d) The effect of alkali metal oxides on slag viscosities and the underlying principles have to be studied in more detail in further work.

Based on the literature review and the performed thermodynamic calculations a series of experiments are conducted. The first set of experiments should gather data on the influence of added alkali metal oxides to  $\text{SiO}_2\text{-CaO-Al}_2\text{O}_3$  system slags regarding their capabilities of particle dissolution. The second set of experiments shall show if alkali metal oxides can be used to modify NMI effectively in a way that reduces the potential harm of the particles during further production steps or the finished product.

## 4 Experimental

In the following chapter the procedures of conducted experimental work are described in detail. The theoretical basics are discussed in **Chapter 2**. The main aim of the experimental work is to gain insight into the interaction of non-metallic particles with alkali metal oxide containing experimental slags. Two different sets of experiments have been conducted. Slags with 10 different chemical compositions are prepared. In the first set of experiments dissolution of synthetic particles in these experimental slags is observed using HT-CSLM. During the second set of experiments steel samples collected at a steel plant of industrial partners are treated with the experimental slags at steelmaking temperatures. The NMI landscape in these steel samples and detailed information about NMI composition are acquired during and after slag treatment using automated SEM/EDS measurements.

### 4.1 Preparation of experimental Slags

To study the influence of alkali metal oxides in low basicity slags for refining in secondary metallurgy of steelmaking, the production of slags with defined contents is necessary. All experimental slags are produced at the Chair of Ferrous Metallurgy from base components. In total 10 different compositions of slag are prepared. For each of the alkali metal oxides  $\text{Li}_2\text{O}$ ,  $\text{Na}_2\text{O}$ , and  $\text{K}_2\text{O}$  slags with 3 different contents of these species are produced. Additionally, a slag without any content of alkali metal oxide is prepared to gather reference results. The target compositions of all 10 slags are shown in **Table 4-I**. Slag preparation is conducted as follows:

1. Base substances in powdered or granulated form are weighed
2. Powders are thoroughly mixed



3. 50 g of powder is filled into Pt crucible
4. Powder is heated in a laboratory scale top-loading furnace to 1600°C
5. Slag is cooled by pouring onto a steel plate at room temperature
6. Grinding of solid slag to a fine homogeneous powder

The composition of the produced slags is analyzed using XRA at the Chair of General and Analytical Chemistry as well as at the industry partner. The result of this analysis is presented in **Chapter 5.1**.

Slags with contents of 2.5%, 5.0%, and 7.5% of each alkali metal oxide respectively are the goal. These values are chosen as several experiments have been described already in this range of composition. [9,12,14,15] Further some experiments describe negative influences with higher additions. [10,13] The ratio of SiO<sub>2</sub> : CaO : Al<sub>2</sub>O<sub>3</sub> is 50:45:5 and is constant for all slags as this is a rather typical slag composition for the low basicity refining slag in the production of ultra clean steel grades like spring, tire-cord or saw-wire steels deoxidized by addition of Si and Mn. Carbonatic substances are used for slag preparation as alkali metals cannot easily be purchased in their oxidic form. During heating carbonates are decomposed to oxides and CO<sub>2</sub> via **Equation 4-1** where M represents Li, Na, or K respectively. This must be considered before weighing of the base materials, to achieve target target compositions.



**Table 4-I:** Target chemical composition of experimental slags.

Name [-]	SiO <sub>2</sub> [wt%]	CaO [wt%]	Al <sub>2</sub> O <sub>3</sub> [wt%]	Li <sub>2</sub> O [wt%]	Na <sub>2</sub> O [wt%]	K <sub>2</sub> O [wt%]
Ref	50.00	45.00	5.00	/	/	/
L1	48.72	43.88	4.90	2.50	/	/
L2	47.50	42.75	4.75	5.00	/	/
L3	46.22	41.62	4.65	7.50	/	/
N1	48.72	43.88	4.90	/	2.50	/
N2	47.50	42.75	4.75	/	5.00	/
N3	46.22	41.62	4.65	/	7.50	/
K1	48.72	43.88	4.90	/	/	2.50

K2	47.50	42.75	4.75	/	/	5.00
K3	46.22	41.62	4.65	/	/	7.50

## 4.2 Dissolution Experiments

For better insight into the dissolution mechanisms of non-metallic particles in alkali metal oxide containing slags, experiments using High Temperature Confocal Scanning Laser Microscopy (HT-CSLM) are conducted. During these experiments the dissolution of synthetic particles in the premelted slags can be observed in-situ. Detailed information about the particle composition and chemical, mechanical, and physical properties is shown in **Appendix A**. For each slag described in **Table 4-1** the dissolution of particles with three different compositions are observed. Pure Alumina, Magnesia-Alumina-Spinel, and pure Silicon-oxide particles are used. The particles are synthetically produced by Sandoz Fils SA, have a perfectly spherical geometry and an initial diameter of 500  $\mu\text{m}$ . Each combination of experimental slag and synthetic particle is observed two times. This leads to 60 conducted experiments. The basic working principles of HT-CSLM are presented already to great extend in other work and will not be discussed further. [52,53] The experimental setup is shown in **Figure 4-1**.

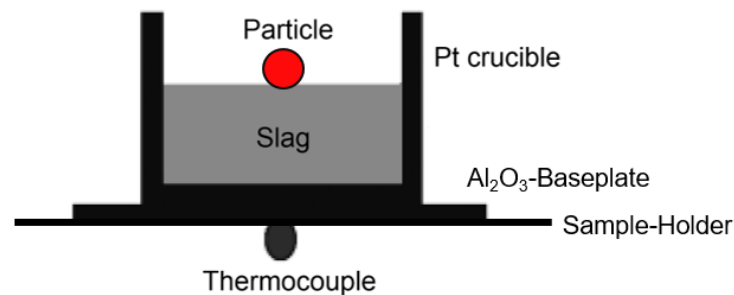


**Figure 4-1:** Setup for conducted HT-CSLM dissolution experiments.

The steps for conducting the experiments are as follows:

1. Calibration of the thermocouple in the heating chamber of the microscope
2. Premelting of grinded experimental slags in Pt-crucible
3. Cooling of premelted slag
4. Insertion of synthetic particle on top of solid slag
5. Heating of synthetic particle and slag to 1600°C
6. Observation of dissolution of the particle
7. Cooling of the slag

Calibration of the thermocouple, which is located on the bottom of the sample holder inside the heating chamber, is done via a second thermocouple embedded in slag in a crucible, similar to the experimental setup. This ensures experimental temperatures are reached and correctly measured. The Pt-crucibles for this experimental setup have diameters of approximately 8 mm and a height of about 4 mm. For each experiment approximately 0.25 g of slag are used. Premelting is performed to minimize the amount of gas bubbles entrapped in the slag, as these bubbles can cause problems during analysis of the experimental data, and therefore should be avoided. The temperature and heating rates used during all dissolution experiments are shown in **Figure 4-2**. As 1600°C is the desired experimental temperature, once this temperature is reached the heating cycle is paused to hold the temperature until total dissolution of the particle is achieved. After that, cooling of the heating chamber can begin. During the observation of the dissolution the operator must pay close attention to the particle, as gradients in concentration and temperature of the slag can cause rapid movement of the particle, especially for SiO<sub>2</sub>-particles as they are dissolving at much higher rates compared to spinel- and alumina-type particles. Once a particle has left the field of view of the microscope it can be very challenging to locate it again for further observation, and repetition of the experiment may be needed. Over the whole duration of the experiment video data of the dissolving particle as well as corresponding time and temperature are captured. This data is later used for analysis of the dissolution behavior of the particles.

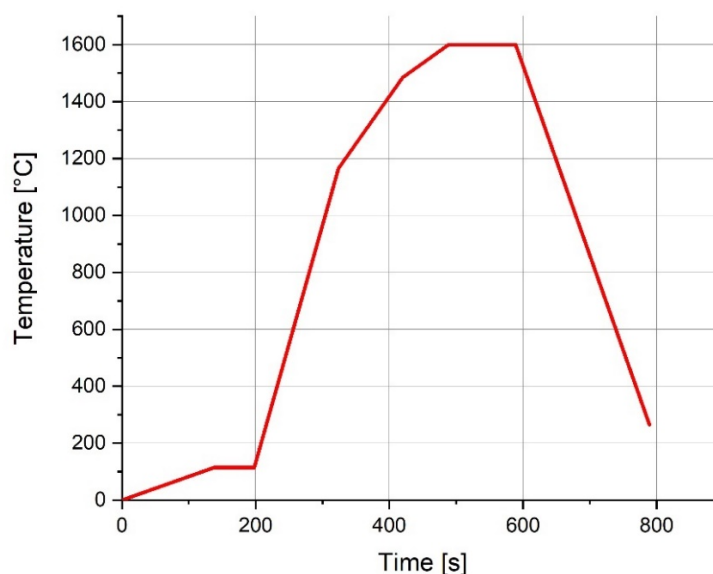


**Figure 4-2:** Heating cycle of HT-LSCM experiments.

### 4.2.1 Manual Analysis of Dissolution Behavior

To analyze the dissolution behavior of the particles in the experimental slags it is necessary to convert the obtained video data to actual particle size over dissolution time. The first step for this is to determine the so-called time zero of the dissolution. In earlier experiments at the Chair of Ferrous Metallurgy time zero was set as the first time the pre-defined experimental temperature was reached. This is also the case for the majority of experiments in this work, but for some slag-particle combinations this had to be altered, as the particle was already completely dissolved once the experimental temperature has been reached. In practice time zero is chosen at the time where dissolution visibly begins but the particle diameter is still above 400  $\mu\text{m}$ . The video data is then cut from chosen time zero until complete dissolution of the particle. In this work this is done using the software VirtualDub 1.10.4 but can be achieved by any other video editing software. For evaluation of particle diameters frames of the video data at a defined rate are exported to .bmp format. As following methods of analysis are done manually, the number of exported images should be between 40-100 to ensure sufficient amounts of data for satisfying results while maintaining manageable amounts of manual work. In **Figure 4-3** one of the exported image files is shown. The particle can be seen in the center of the image, whereas on the left-hand side a gas bubble of similar size as the particle is visible. Especially for evaluation of  $\text{SiO}_2$  dissolution these bubbles can lead to difficulties during analysis as they resemble  $\text{SiO}_2$  particles closely.

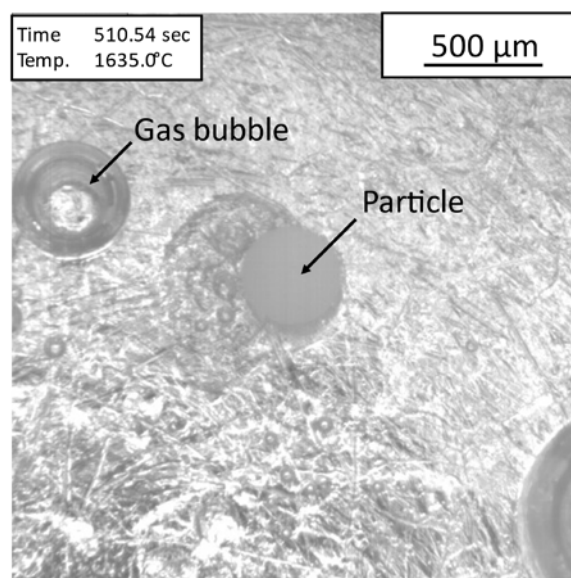


**Figure 4-3:** Dissolution of a synthetic particle in an experimental slag.

The exported images are processed using the software JensRüdigsMakroaufmaßprogramm 0.9.2. With this software the area of the dissolving particle on the micrograph can be measured by manually tracing the borders of the particle. For reference the scale contained in the micrograph is used. Assuming perfectly spherical particles the equivalent circle diameter (ECD) can be calculated from the measured area using **Equation 4-2**.

$$ECD = \sqrt{\frac{4 * Area}{\pi}} \quad (4-2)$$

Measured area as well as corresponding time and temperature are noted. ECD, total dissolution time (from time zero) as well as relative values for time and Diameter can be calculated and used for further evaluation of the gathered data.

#### 4.2.2 Automated Analysis of Dissolution Behavior

As the previously described method for manual analysis of the HT-CSLM Data is very work intensive and time consuming, ways of automating this step are favorable. For this a custom program using the MATLAB Image Processing Toolbox was developed to standardize the analysis of CSLM-Data. This ensures minimal influence of the operator on the results of the analysis and brings great benefits regarding the necessary time for individual evaluation of gathered data. To have enough data for comparison of the results obtained via this new automated method, all experiments have been analyzed manually. Further experiments can be evaluated using the new automated method of image processing.

The main challenge for the automated analysis is the inconsistent image quality, as contrast and brightness can change drastically over the course of the experiments or in between experiments. Additionally, the gas bubbles and other artifacts in the images as scratches on the bottom of the crucible or motion blur from particle movements can have negative effects on the reliability of the results from automated analysis. [54]

### 4.3 Steel-Slag Interaction Experiments

To gain information about the influence of the experimental slags on number, size and chemical composition of NMI in a steel sample, steel-slag interaction experiments are conducted. A sample of steel produced at the industrial partner with high levels of cleanness is used in these experiments. The objective of the conducted experiments is to observe the

interaction of the steel and slag and the change in composition and appearance of the NMI in the steel sample after the treatment. The composition of the steel sample as provided by the industry partner is shown in **Table 4-II**.

**Table 4-II:** Chemical composition of steel sample as received.

<b>C</b> [wt%]	<b>Si</b> [wt%]	<b>Mn</b> [wt%]	<b>P</b> [wt%]	<b>S</b> [wt%]	<b>Cr</b> [wt%]	<b>Ni</b> [wt%]	<b>Cu</b> [wt%]
0.543	1.423	0.67	0.009	0.009	0.66	0.02	0.01
<b>Al</b> [wt%]	<b>Ti</b> [wt%]	<b>Ca</b> [wt%]	<b>H</b> [ppm]	<b>O</b> [wt%]	<b>Mo</b> [wt%]	<b>V</b> [wt%]	<b>N</b> [wt%]
0.0014	0.0007	0	1.8	0.0014	0.005	0.001	0.0055

The experiments are conducted as follows:

1. Cutting of the steel to samples of approximately 280 g
2. Weighing of experimental slag (5% of the mass of the steel sample)
3. Filling steel sample and slag into alumina-crucible
4. Heating crucible in so-called Tammann Furnace (top loading high-temperature electrical resistance type furnace) until slag and steel are liquid
5. First sampling
6. Further heating to 1530°C and sampling according to **Table 4-III**
7. Cooling to 1300°C
8. Removing crucible from furnace
9. Quenching in water

**Table 4-III:** Sampling Plan of steel-slag interaction experiments.

<b>Sample</b> [-]	<b>Time</b> [min]	<b>Temperature</b> [°C]
1	0	Liq. Melt
2	10	1530
3	20	1530
4	25	1530
5	30	1530

The steel sample is cut from a part of a cast billet of approximately 10 kg. The samples must be cut to fit the dimensions of the alumina crucible which measures 46 mm in diameter and 80 mm in height. The amount of slag relative to the weight of the melt used for these experiments is approximately 5%. This value is chosen to ensure sufficient interaction between the slag and the steel, as there is no external stirring or bubbling of the melt with this specific experimental setup, which is depicted in **Figure 4-4**. In industrial application the relative amount of slag is usually much lower.

Before heating, the furnace is flushed with argon to remove the oxygen. Additionally, a constant argon flow to the furnace is used to prevent excessive oxidation of the steel-slag system during heating and sampling. Samples are taken using a low alloyed steel tube with a pipetting ball. The steel tube has a length of approximately 50-75 cm, the pipetting ball used has a volume of 100 ml. With this setup small amounts of liquid steel can be gathered in the low alloyed steel tube. After cooling of the sample and the tube in water, the sample can be extracted by carefully cutting and peeling the tube. Due to the high temperatures of the system, it cannot be avoided that parts of the tube used for sampling melt. This results in introducing additional steel to the system. As the same tubes are used for each experiment the change in steel composition should be similar for each sample and therefore not relevant for analysis of the results. The samples are weighed before melting, as well as the remaining melt after the experiment. Using differences in weight one can assume the amount of introduced steel from the sampling tubes, as the weight of the actual samples is negligible. In earlier experiments at the Chair of Ferrous Metallurgy using the same method the gathered samples had to be pressed before further analysis as a lot of gas had been entrapped in the sample which could lead to problems during evacuation for SEM. The samples taken for this work did not show a lot of pores, and therefore were not further processed before preparation for SEM-analysis.

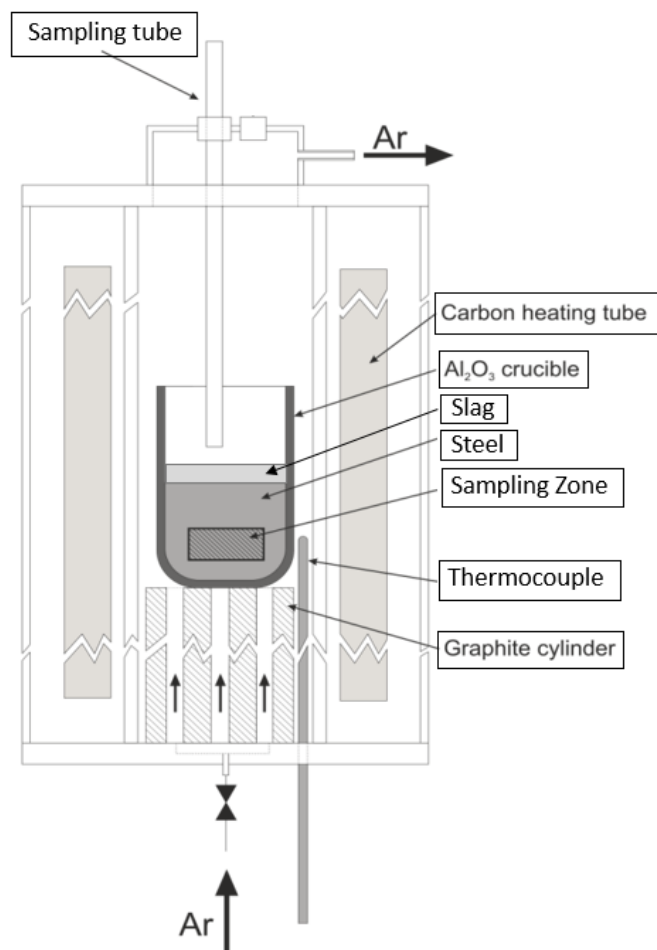


**Figure 4-4:** Experimental setup of steel-slag sample in so-called “Tammann Furnace”.

#### 4.4 SEM/EDS-Analysis

Analysis via SEM/EDS is state of the art for steel cleanliness characterization, especially regarding the micro cleanliness which considers particles with equivalent diameters of below 15  $\mu\text{m}$ . At the Chair of Ferrous Metallurgy this is usually done using the JEOL 7200F field emitting SEM with so-called AztecFeature Analysis provided by the AZTEC Software used to operate the SEM. This uses differences in the greyscale value of the micrograph to differentiate between matrix and NMI to perform EDS measurements on each detected particle. The greyscale range and contrast are to be defined by the operator. The specific settings and parameters of the SEM for this kind of analysis is shown in **Table 4-IV**.



**Table 4-IV:** Settings for SEM/EDS analysis.

Acceleration voltage	15	kV
Probe current	13	PC
Deadtime	32	%
Counts In	100000	cps
Counts Out	70000	cps
Resolution	1024	pxl
ECD Range	1-max	$\mu\text{m}$
Pixel/Feature	9	pxl
Magnification	400	-
Time of Measurement	1	s

For best comparison of the samples gathered during the steel-slag interaction experiments all five samples which were in contact with one specific slag were embedded together. This enables measurements in the SEM without the need of changing the sample, thus similar measurement properties are ensured during the observation. Samples were embedded in bakelite at 180°C and 218 bar. After embedding the samples were grinded with 180, 360, 600, and 1200 grit SiC-sandingpaper. Additionally, a 1200 grit sanding was performed using diamond grinding. This is done to minimize the amount of Si-containing particles from the sample preparation influencing the results of SEM/EDS analysis. After grinding the samples were polished using 9 and 3  $\mu\text{m}$  diamond particles. Before SEM/EDS measurements are performed, it has to be ensured that samples are completely dry and free from dust. This is achieved by cleaning with ethanol, warm blow drying and subjecting the sample to a mild vacuum for multiple minutes.

## 5 Results

### 5.1 Composition of Experimental Slags

The compositions of all produced experimental slags, except slag N1, have been analyzed at the Chair of General and Analytical Chemistry using XRF methods. The composition of slag N1 was measured at the industry partner also using XRF method for the contents of SiO<sub>2</sub>, CaO, and Al<sub>2</sub>O<sub>3</sub> and ICP for the contents of Li<sub>2</sub>O, Na<sub>2</sub>O, and K<sub>2</sub>O. The results are presented in **Table 5-I**.

**Table 5-I:** Chemical composition of experimental slags.

Name	SiO <sub>2</sub>	CaO	Al <sub>2</sub> O <sub>3</sub>	Li <sub>2</sub> O	Na <sub>2</sub> O	K <sub>2</sub> O	Balance
[-]	[wt%]	[wt%]	[wt%]	[wt%]	[wt%]	[wt%]	[wt%]
L1	48.9	43.0	5.0	2.2	0.0	0.0	0.9
L2	48.4	43.1	4.9	3.0	0.0	0.0	0.6
L3	47.2	41.8	4.8	5.0	0.0	0.0	1.2
N1	43.5	45.9	6.8	/	2.5	0.0	1.3
N2	47.7	42.1	4.8	/	5.0	0.0	0.4
N3	46.5	40.7	4.7	/	7.4	0.0	0.7
K1	47.3	43.2	5.8	/	0.1	3.1	0.5
K2	46.2	42.1	5.7	/	0.1	5.6	0.3
K3	45.1	40.9	5.5	/	0.1	7.8	0.6

For slags L1, L2, and L3 content of  $\text{Li}_2\text{O}$  has been determined as the balance to 100 wt% as there is no available method for correct measurement of Li due to the low atomic weight of the element. The measured chemical composition of N1 seems not to fit, as the most prominent component is CaO instead of  $\text{SiO}_2$  as for all other samples, which leads to an apparent basicity  $B_2 (= \text{SiO}_2/\text{CaO})$  of 1.06 as opposed to a mean basicity of 0.89 for the 8 other slags. This is probably due to the change of laboratory and operator of measurement for this specific slag. Especially target contents of  $\text{Na}_2\text{O}$  have been reached with good accuracy. Also, for  $\text{K}_2\text{O}$  the contents in the produced slags are near the desired values but only a little bit too high with deviations of about 0.6 wt% in slags K1 and K2, or 0.3 wt% in slag K3. Contents of  $\text{Li}_2\text{O}$  are overall a little lower as planned in the achieved slag compositions. In Slag L1 the content of  $\text{Li}_2\text{O}$  is about 0.3 wt% lower than desired, and slags L2 and L3 lack approximately 2.0 and 2.5 wt% of  $\text{Li}_2\text{O}$  respectively. Other components of the experimental slags found during measurements are mainly Mg-, Ti-, and Fe- Oxides and labeled as *Balance* in **Table 5-I**. The deviations in contents of alkali metal oxides should be considered for the production of experimental slags for further experiments. Especially the volatility of  $\text{Li}_2\text{O}$  should be given special consideration in further melting regarding  $\text{Li}_2\text{CO}_3$  contents of the primary mix. Also, the maximum melting temperature of  $\text{Li}_2\text{O}$  containing slags could be reduced as the liquidus temperature is much lower than the temperature used for production of the slags for this work.

## 5.2 Results of HT-CSLM Analysis of Particle Dissolution

Spherical particles of three different compositions ( $\text{Al}_2\text{O}_3$ , MA-spinel,  $\text{SiO}_2$ ) were observed during dissolution in multiple experimental slags at steelmaking temperatures. The obtained video data was further analyzed, the area of the particles in specific frames of the video data was measured, and the measured area was converted to equivalent circle diameters. Every combination of the three types of particles and 10 different compositions of slags has been conducted two times. This leads to a total of 60 sets of dissolution data. The data is presented in the following. Two datasets of the same combination of particle and experimental slag are presented together as well as the mean value. The time referred to as *total dissolution time* is the timeframe starting from chosen time zero to the time of the last frame where a particle could be distinguished from the bulk slag. For most datasets the last measured ECD is between 20 – 100  $\mu\text{m}$ . If not otherwise stated, the temperature of time zero of the two datasets is identical. To get an approximation of the time needed for complete dissolution of a particle, the initial diameter can be divided by the average dissolution rate. This is especially helpful if the last measured ECD is high due to problems during the observation or due to fast dissolution

rates. For calculation of the average dissolution rate the difference in observed ECD at the start and end of the experiment is divided by the absolute experimental time which has passed between these two events. This is shown in **Equation (5-1)**. If the theoretical initial diameter of the particle is divided by this calculated dissolution rate, the time for complete dissolution of a particle can be calculated as presented in **Equation (5-2)**. As dissolution usually speeds up with smaller particle dimensions, due to an increase of the ratio of surface to volume of the particle, this time can be seen as a maximum amount of time that is needed for complete dissolution.

$$\text{Diss. rate} = \frac{ECD_{start} - ECD_{end}}{\text{experimental time}} \quad (5-1)$$

$$t_D = \frac{D_{initial}}{\text{mean Diss. rate}} \quad (5-2)$$

### 5.2.1 Dissolution of Al<sub>2</sub>O<sub>3</sub> in Slag REF

To get a value of expected dissolution times in slag systems that are currently used, reference experiments were conducted using a slag which contains no alkali oxides but just SiO<sub>2</sub>, CaO, and Al<sub>2</sub>O<sub>3</sub>. This composition is similar to low basicity refining slags for the production of Si/Mn-deoxidized ultra-clean steels. As seen in **Figure 5-1** the two conducted experiments are very consistent in their results as the dissolution curves are nearly identical. The temperature at time zero was 1600°C. Total dissolution times are 753 s and 781 s with last measured ECD of 62 µm and 37 µm respectively.

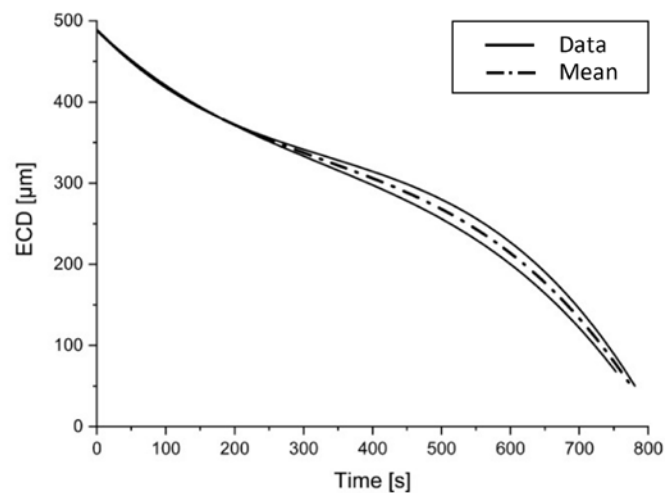


**Figure 5-1:** Dissolution data Al<sub>2</sub>O<sub>3</sub> in slag REF.

## 5.2.2 Dissolution of Al<sub>2</sub>O<sub>3</sub> in Slag L1

The two datasets of this experiments are quite different, both regarding shape of the curve as well as total dissolution time. The temperature of time zero is 1600°C. Last measured ECD are 30 µm and 39 µm. Total dissolution times are 384 s and 527 s respectively. This results in a difference of total dissolution time of about 37%. The mean value of dissolution time for complete dissolution of the particle is slightly less than 500 s. But as the data of the two conducted trials is rather inconsistent the mean values are not ideal for further considerations. The data of ECD of alumina particle over dissolution time in slag L1 is presented in **Figure 5-2**.

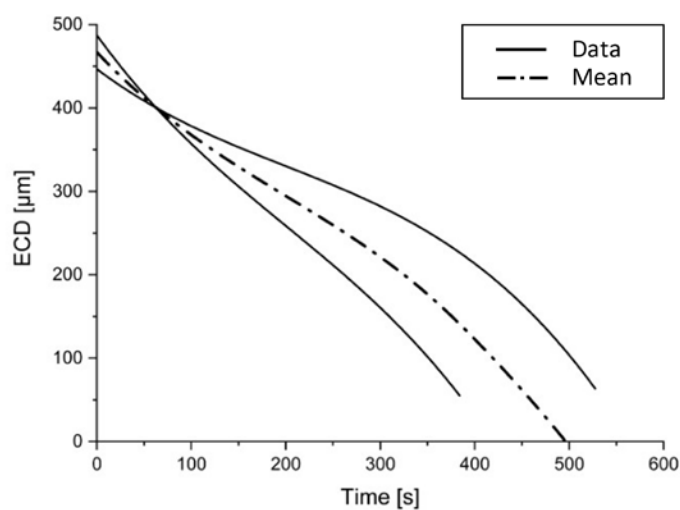


**Figure 5-2:** Dissolution data Al<sub>2</sub>O<sub>3</sub> in slag L1.

### 5.2.3 Dissolution of Al<sub>2</sub>O<sub>3</sub> in Slag L2

The data of dissolution of alumina in slag L2 is consistent with only very little deviation between the two datasets. The temperature of time zero is 1515°C as particles are visibly dissolved already once the planned experimental temperature of 1600°C is reached. Last measured ECD are 87 μm and 96 μm. Total experimental time is 130 s for both datasets. The data of ECD of alumina particle over dissolution time in slag L2 is presented in **Figure 5-3**. Using **Equations (5-1)** and **(5-2)**, the maximum time for complete dissolution of an alumina particle in slag L2 can be assumed with 183 s. The relatively high values for last measured ECD imply that the rate of dissolution drastically increased towards the end of the dissolution experiment. This leads to the assumption that the real time for complete dissolution will be much lower than the calculated value.

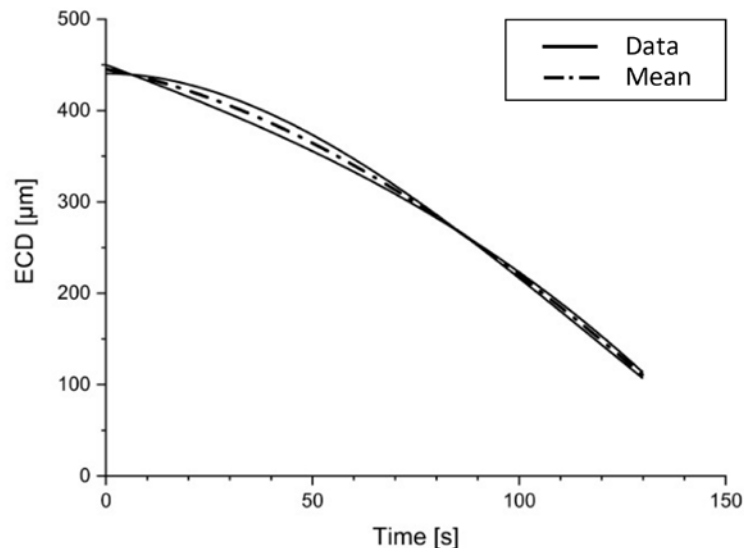


**Figure 5-3:** Dissolution data Al<sub>2</sub>O<sub>3</sub> in slag L2.

### 5.2.4 Dissolution of Al<sub>2</sub>O<sub>3</sub> in Slag L3

The data of dissolution of alumina in sag L3 is also very consistent with only slight deviations in later stages of dissolution as shown in **Figure 5-4**. The temperature of time zero is 1465°C as dissolution of the particles started at much lower temperatures than with slags L1 and L2. Last measured ECD are 50 μm and 156 μm. Total dissolution times are 101 s and 93 s respectively. The calculated value for the time of complete dissolution is 126 s which again should be seen as the maximum time of dissolution for the same reasons as described in **Chapter 5.2.3**.

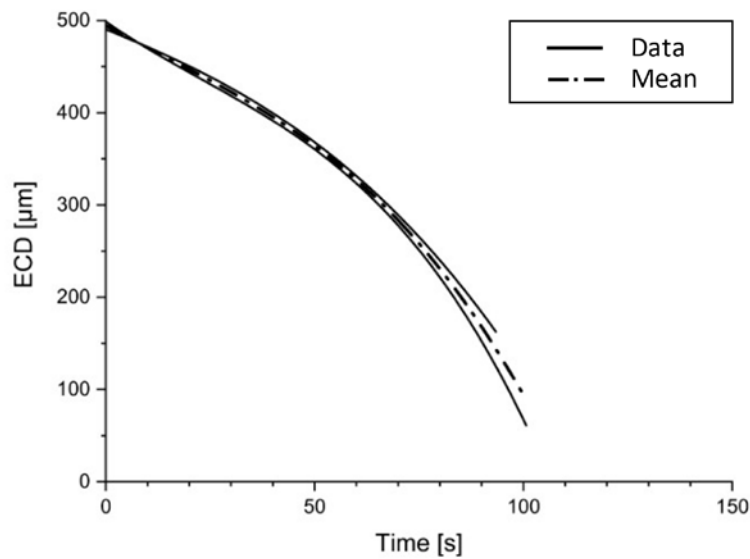


**Figure 5-4:** Dissolution data  $\text{Al}_2\text{O}_3$  in slag L3.

### 5.2.5 Overview: Results of HT-CSLM Dissolution Experiments

The analysis of all dissolution experiments has been done following the schematic as presented in **Chapters 5.2.1** through **5.2.4**. An overview of the results of all 60 conducted experiments is shown in **Figure 5-5**. Each subfigure shows the mean dissolution data of one type of particle in 3 different slags, compared to the dissolution of that same type of particle in the reference slag. The solid, dashed, and dotted black lines represents dissolution in slags containing 2.5, 5.0, and 7.5 wt% of alkali metal oxide, whereas the solid red line indicates the dissolution in the reference slag. Subfigures a) – c) show the dissolution data of the three types of particles in  $\text{Li}_2\text{O}$  containing slags, d) – f) show the data for  $\text{Na}_2\text{O}$  containing slags, and g) – i) for  $\text{K}_2\text{O}$  containing slags respectively. In general, dissolution times are much shorter for the dissolution of  $\text{SiO}_2$  particles compared to spinel- and alumina-particles as indicated by subfigures c), f), and i). For alumina particles nearly all experimental slags except one could increase the dissolution rate. Spinel particles show a similar trend but not as prominent. For silica particles slags containing  $\text{Li}_2\text{O}$  decreased dissolution times with higher additions,  $\text{K}_2\text{O}$  increased the dissolution time, whereas addition of  $\text{Na}_2\text{O}$  show only improvement of the dissolution rate at 5.0 wt%. Following the results of all dissolution experiments shown in **Figure 5-5** are summarized:

- a) The addition of  $\text{Li}_2\text{O}$  decreases the dissolution time of alumina particles. Higher contents of  $\text{Li}_2\text{O}$  have a stronger effect, where addition of 7.5 wt% of  $\text{Li}_2\text{O}$  lead to almost 8-times faster dissolution of the particle.

- b) A similar effect of  $\text{Li}_2\text{O}$  addition on the dissolution of spinel-particles is shown. Here only additions of 5 wt% and above have positive effects on the dissolution rate whereas addition of 2.5 wt% of  $\text{Li}_2\text{O}$  seem to have a slight negative effect on dissolution rate if any effect at all.
- c) The same is true for the influence of  $\text{Li}_2\text{O}$  on the dissolution rate of silica-particles.
- d) Addition of  $\text{Na}_2\text{O}$  decrease the dissolution time of alumina particles to approximately half the time compared to dissolution in the reference slag, but there is little to no influence on this effect with higher contents of  $\text{Na}_2\text{O}$ .
- e) Spinel type particles also dissolve faster with additions of  $\text{Na}_2\text{O}$  but the effect is not as strong as for alumina particles. Nevertheless, with contents of 7.5 wt% of  $\text{Na}_2\text{O}$  a nearly twice as fast dissolution of spinel particles can be observed.
- f) There is no clear effect of  $\text{Na}_2\text{O}$  additions on the dissolution of silica particles. With contents of 2.5 wt% an increase in dissolution time is observed whereas 5 wt% lead to a faster dissolution. With 7.5 wt% of  $\text{Na}_2\text{O}$  the observed dissolution time is nearly identical to the dissolution in the reference slag.
- g) Additions of  $\text{K}_2\text{O}$  up to a content of 5 wt% can significantly improve the dissolution of alumina particles, but higher contents lead to lower dissolution rates.
- h) Disregarding the content, all additions of  $\text{K}_2\text{O}$  have a decreasing effect on the dissolution time of spinel particles with the highest effect with 2.5 wt% of  $\text{K}_2\text{O}$ .
- i) Silica particles dissolved slower in all slags containing  $\text{K}_2\text{O}$ .



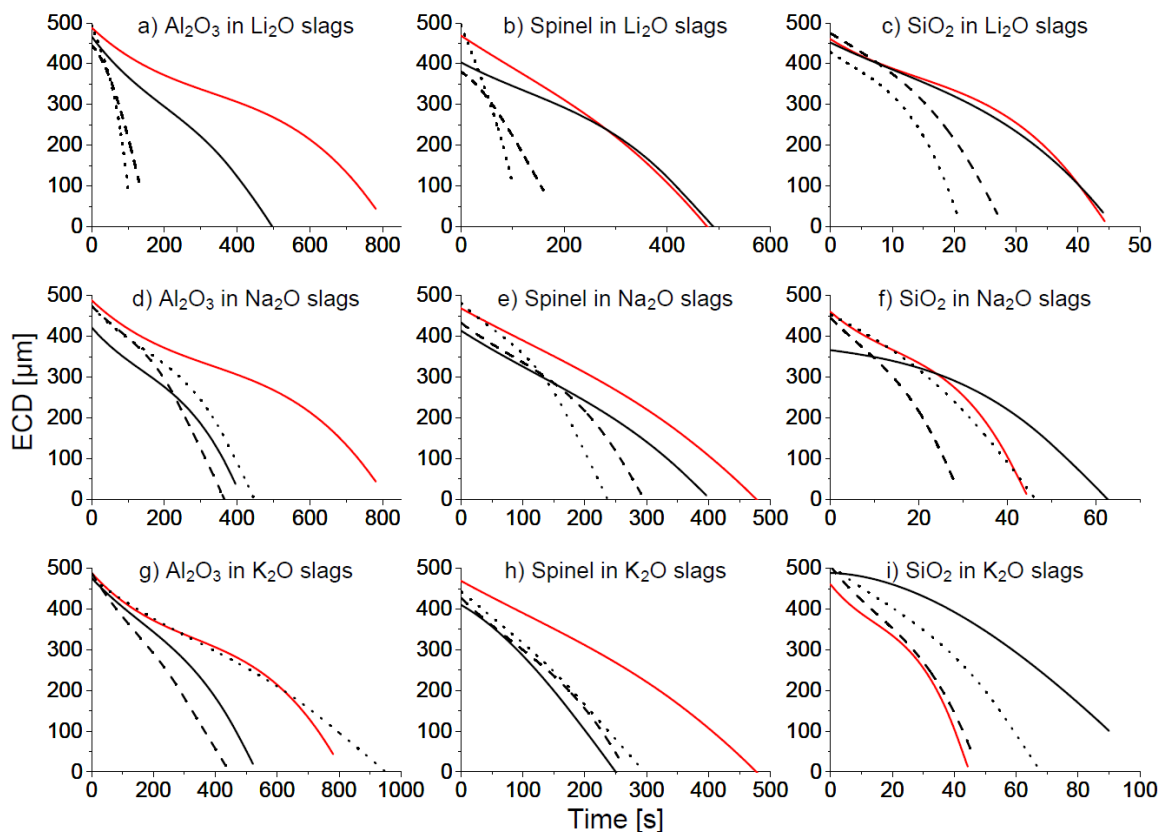


**Figure 5-5:** Results of HT-LSCM dissolution experiments.

An overview of gathered data from all dissolution experiments regarding temperature of experimental time-zero as well as average dissolution rates and observed dissolution time are shown in **Table 5-II**. *Temp.-0* refers in this table to the temperature detected at chosen time-zero. It has to be acknowledged that this temperature was not constant over the duration of the experiment, as the heating-curve was the same for all experiments, and therefore a maximum temperature of 1600°C was reached during all experimental combinations of slag and particle. *Diss.rate* refers to the average dissolution rate as described by **Equation (5-1)**. *Diss.t* is the measured time between chosen time-zero and the last detectable diameter of the respective particle. Further discussion and conclusion of these effects follows in **Chapter 6.2**. Detailed figures for all dissolution experiments as well as information regarding measured ECD at experimental time-zero, last measured ECD, and calculated maximum dissolution time are listed in **Appendix B**.

**Table 5-II:** Parameters and average results of dissolution experiments.

<b>Particle</b> [-]	<b>Slag</b> [-]	<b>Temp.-0</b> [°C]	<b>Diss.rate</b> [μm/s]	<b>Diss.t</b> [s]
Al <sub>2</sub> O <sub>3</sub>	REF	1600	0.6	767
Al <sub>2</sub> O <sub>3</sub>	L1	1600	1.0	456
Al <sub>2</sub> O <sub>3</sub>	L2	1515	2.7	130
Al <sub>2</sub> O <sub>3</sub>	L3	1465	4.0	97
Al <sub>2</sub> O <sub>3</sub>	N1	1600	1.0	392
Al <sub>2</sub> O <sub>3</sub>	N2	1600	2.0	198
Al <sub>2</sub> O <sub>3</sub>	N3	1600	0.9	443
Al <sub>2</sub> O <sub>3</sub>	K1	1600	0.9	493
Al <sub>2</sub> O <sub>3</sub>	K2	1600	1.0	289
Al <sub>2</sub> O <sub>3</sub>	K3	1600	0.5	935
Spinel	REF	1600	1.0	422
Spinel	L1	1600	0.8	486
Spinel	L2	1600	1.8	158
Spinel	L3	1465	4.1	90
Spinel	N1	1600	1.0	378
Spinel	N2	1600	1.4	273
Spinel	N3	1600	1.6	267
Spinel	K1	1600	1.6	229
Spinel	K2	1600	1.6	249
Spinel	K3	1600	1.4	302
SiO <sub>2</sub>	REF	1600	9.6	43
SiO <sub>2</sub>	L1	1600	9.6	44
SiO <sub>2</sub>	L2	1465	15.9	25
SiO <sub>2</sub>	L3	1465	19.0	20
SiO <sub>2</sub>	N1	1515	5.4	58

SiO <sub>2</sub>	N2	1600	13.5	25
SiO <sub>2</sub>	N3	1465	9.1	32
SiO <sub>2</sub>	K1	1515	4.4	88
SiO <sub>2</sub>	K2	1565	9.8	45
SiO <sub>2</sub>	K3	1515	6.6	67

### 5.3 Results of Automated SEM/EDS-Analysis

In the following the results of the automated SEM/EDS measurements are presented. Analysis was performed for a steel sample taken after billet rolling mill, samples of the same steel after interaction with the reference slag and experimental alkali metal oxides containing slags as well as a sample of a similar steel grade taken from the tundish. All samples except the material taken from the tundish were analyzed at the Chair of Ferrous Metallurgy following the method described in **Chapter 4.4**. The tundish sample was analyzed following a comparable method at the industry partner. All samples are characterized by various values regarding steel cleanliness. One important factor is the amount of NMI per mm<sup>2</sup> on polished sample surface. This can be stated as number of detected NMI per mm<sup>2</sup> or area of detected NMI in μm<sup>2</sup> per mm<sup>2</sup>. The average size of the NMI is also relevant information when discussing differences in steel cleanliness. Additionally, the chemical composition of detected NMI regarding the nonmetallic bonding partners (O, S, N) and metallic components of NMI (Al, Ca, Si, ...) is of high importance when comparing analyzed steel samples.

#### 5.3.1 Amount of Detected Non-Metallic Inclusions

In **Table 5-III** the detected amounts of NMI of each steel sample are shown both as measured area of inclusions per measured sample area and number of inclusions per sample area. Only values of the last available samples of steel-slag interaction experiments are used for this comparison. Longer interaction times between steel and experimental slags should emphasize differences in the influence of the observed alkali metal oxides. Results are shown for overall amounts of NMI as well as amounts of certain inclusion classes like oxides (O), sulfides (S) or multiphase inclusions (OS) containing both oxides and sulfides. It is obvious that the overall detected amounts of NMI are much higher after steel-slag interaction experiments. This is due to the conditions of the experiment, like influence of the crucible material, sampling and stirring of the melt via low-alloyed steel rods or influence of the

atmosphere, even though the furnace is flushed with argon continuously. This is discussed further in **Chapter 6.3**. Not surprisingly, the amounts of NMI are lowest in the sample taken after the billet rolling mill with less than 50 detected inclusions per mm<sup>2</sup>, as these results represent steel cleanliness levels of the finished product. This is a drastic improvement compared to the sample taken from the tundish which contains over 200 NMI per mm<sup>2</sup>, which demonstrates the importance of steel cleanliness relevant processes in the tundish and during casting.

**Table 5-III:** Amounts of O-, S-, and OS-NMI.

Name [-]	Total [Nr/mm <sup>2</sup> ]	Total [μm <sup>2</sup> /mm <sup>2</sup> ]	O [Nr/mm <sup>2</sup> ]	O [μm <sup>2</sup> /mm <sup>2</sup> ]	S [Nr/mm <sup>2</sup> ]	S [μm <sup>2</sup> /mm <sup>2</sup> ]	OS [Nr/mm <sup>2</sup> ]	OS [μm <sup>2</sup> /mm <sup>2</sup> ]
Tundish	215	398	4	9	191	333	20	56
Billet	47	362	16	53	17	108	13	201
Ref	500	1371	87	352	282	578	131	441
L1	453	1612	112	339	1	1	340	1273
L2	551	1540	148	503	42	68	362	968
L3	359	1264	83	328	24	43	251	893
N1	255	823	50	111	0	0	205	712
N2	383	1729	329	1443	0	0	55	286
N3	801	3736	635	2730	4	5	162	1001
K1	327	899	45	138	5	7	277	754
K2	249	1287	127	562	4	8	118	718
K3	403	1152	346	965	0	0	57	187

### 5.3.2 Size of Detected Non-Metallic Inclusions

The size of detected NMI is also an important factor considering steel cleanliness. As particles can have various shapes, comparability of sizes can be difficult. To achieve a common factor by which NMI size and its distribution can be characterized the equivalent circle diameter (ECD) is calculated. This represents the diameter of a circle with the same area as the respective detected NMI. The absolute and normalized average ECD of measured NMI of all samples are shown in **Figure 5-6** and **Figure 5-7**. Again, data of the last available samples of steel-slag interaction experiments is used for the same reasons as stated in the previous

chapter. The average ECD for all samples is quite low with values between 1.4 and 2.5  $\mu\text{m}$ . There is no clear trend visible comparing the results for samples of steel-slag interaction experiments. Nevertheless, there is again a significant difference in the results of steel samples before and after casting (sample from tundish and sample after billet rolling mill). NMI appear to be about 30% larger after billet rolling as the average ECD exceeds 2  $\mu\text{m}$ , compared to an average ECD of about 1.6  $\mu\text{m}$  for the tundish sample. This could be due to differences in cooling rates, as it is expected that the material experiences much faster cooling when sampling from the tundish as opposed to cooling conditions during continuous casting. Also deformation of some particles during hot-rolling could lead to an increased ECD due to particles being less spherical in shape. Average ECD for all steel-slag interaction experiments do not seem to follow a specific trend, but all are higher than that of the tundish sample.

The influence of the contact time during steel-slag interaction experiments can be shown by comparing the average ECD over the course of the experiment. This is done in **Figure 5-8** for the spring steel sample in combination with all experimental slags. The change in ECD from the reference experiment can be used as a baseline to describe the influence of the refining process as carried out in this work. As the ECD seems rather stable over the course of the refining time, changes of ECD in further experiments are expected to arise from interaction with the added alkali metal oxides. The black lines on the top and bottom of **Figure 5-8** represent the average ECD from samples taken after billet rolling and from the tundish respectively. The red line indicates the ECD values for samples in interaction with reference slag. It is shown that all experimental slags lead to average inclusion sizes between that of the samples taken during the industrial steelmaking process. Only one sample exceeds the average inclusion size of the sample taken after billet rolling. This is from interaction with slag K1 after 20 minutes and corresponds to an average ECD of over 5  $\mu\text{m}$ . As the average diameter in the samples taken 10 minutes earlier and 5 minutes later are only about 1.7  $\mu\text{m}$ , it can be assumed that these unusually high values stem from problems during sampling or analysis. Overall, this treatment using the reference slag without addition of any alkali metal oxides leads to smallest average particle diameters, but there seems to be no drastic influence of the contact time with any of the experimental slags.

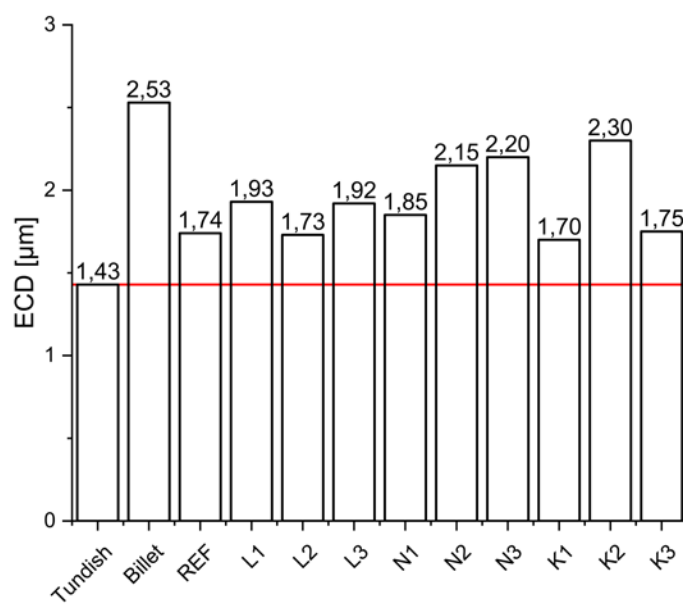


Figure 5-6: Average ECD of detected NMI.

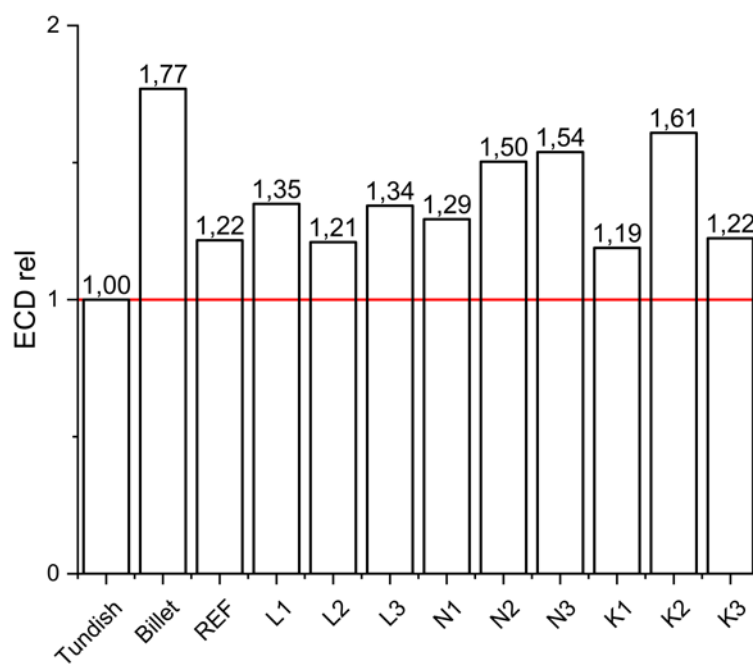
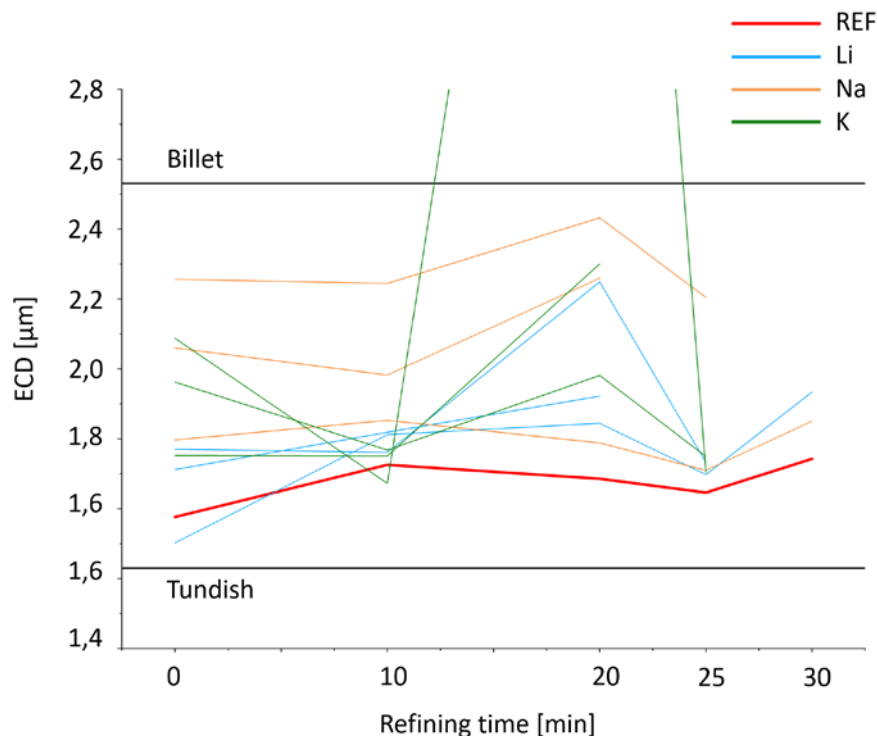


Figure 5-7: Relative average ECD of detected NMI.



**Figure 5-8:** Average ECD over experimental time.

### 5.3.3 Size Distribution of Detected O- and OS-Particles

In addition to comparing just the average ECD of analyzed steel samples from steel-slag interaction experiments, also the size distribution can lead to a better understanding of the influence of alkali metal oxides on steel cleanliness. In **Figure 5-9** the size distribution of O- and OS-particles is shown for each steel-slag combination. The gray distribution indicates particles detected after contact with the reference slag. As the smallest detectable particles are limited with 1 μm with the available SEM/EDS-setup the distribution is cut at this value. Most of the detected particles are within a size range of 1-4 μm. For all samples in contact with alkali metal oxide containing slags the peak of the distribution is located at smaller ECD as the reference sample. But as much bigger particles were detected additionally to this peak of small NMI the calculated average ECD is still bigger compared to the reference sample as indicated in the previous chapter. In **Figure 5-9** subfigures a) – c) represent samples treated with 2.5, 5.0, and 7.5 wt% Li<sub>2</sub>O-containing slag. Subfigures d) – f) show results for Na<sub>2</sub>O, and g) – i) for K<sub>2</sub>O treated samples.

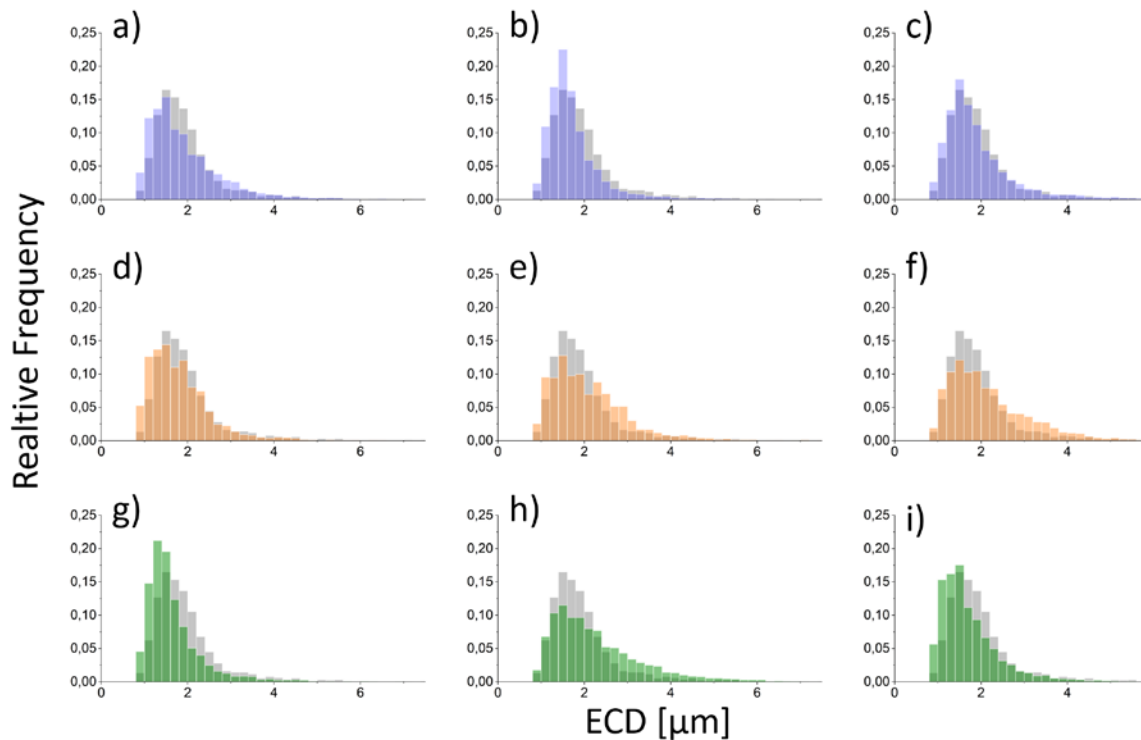


**Figure 5-9:** Size distribution of detected NMI in steel-slag interaction experiments.

### 5.3.4 Morphology and Chemical Composition of Detected Non-Metallic Inclusions

Detected particles in the steel samples have been analyzed by manual SEM/EDS-method after automated feature analysis regarding their morphology and chemical composition. This is necessary as automated measurements alone without respective information about the morphology and appearance of selected particles, the mechanisms of inclusion modification and control cannot be fully explained. Specific particles have been selected from the data of automated feature analysis for further manual investigation. As expected for this steel grade most detected NMI were of two main types. MnS inclusions were commonly found in the as received sample alongside with particles from the ternary system  $\text{SiO}_2\text{-CaO-Al}_2\text{O}_3$  with varying contents. Additionally, a lot of the detected inclusions were heterogeneous particles consisting of the before mentioned types. Most of the oxidic particles were pure silica or silica rich inclusions but there are also alumina and calcium rich particles to be found in the steel samples. **Figure 5-10** shows a homogeneous MnS particle detected in the cast and hot rolled steel sample. The particle features a typical rounded form which together with relatively low hardness leads to good formability and low risk of decreasing mechanical properties of the steel. The dark area around the light grey particle could originate from sample preparation.



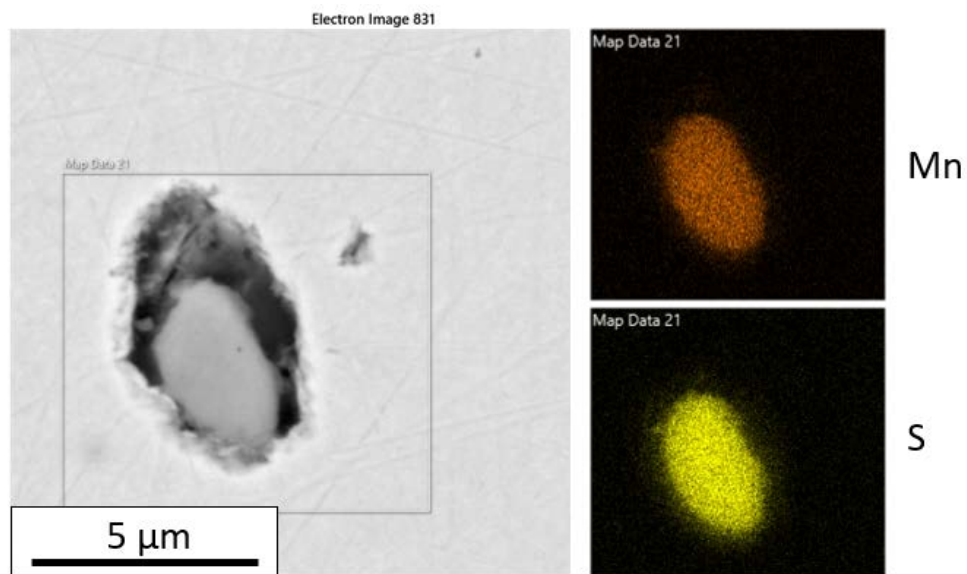


**Figure 5-10:** MnS inclusion detected in cast and hot-rolled spring steel sample.

**Figure 5-11** shows a homogeneous pure silica inclusion with quite large dimensions compared to the vast majority of the detected particles in the samples. These types of inclusions represent the largest quantity of oxidic particles detected in all measured samples. As mentioned before oxidic particles of different compositions of the ternary system  $\text{SiO}_2\text{-CaO-Al}_2\text{O}_3$  could be detected. **Figure 5-12** shows for example an alumina-silica inclusion whereas **Figure 5-13** shows an oxidic particle containing only calcium.

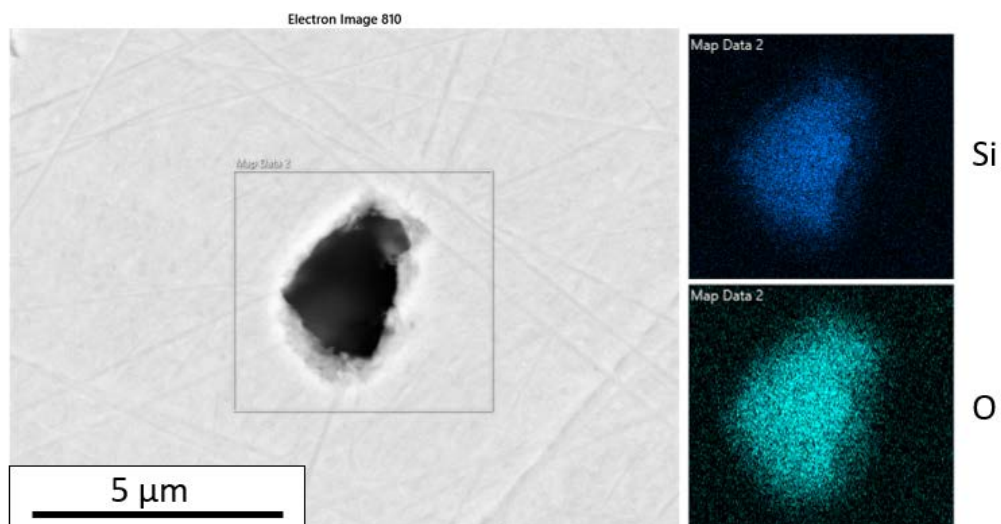


**Figure 5-11:**  $\text{SiO}_2$  inclusion detected in cast and hot-rolled spring steel sample.

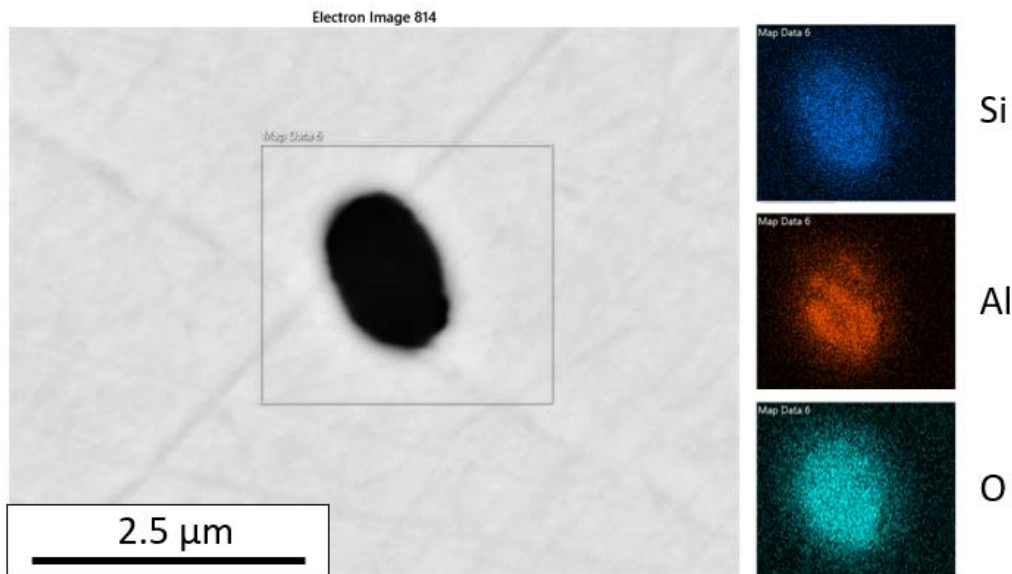


**Figure 5-12:**  $\text{SiO}_2\text{-Al}_2\text{O}_3$  inclusion detected in cast and hot-rolled spring steel sample.

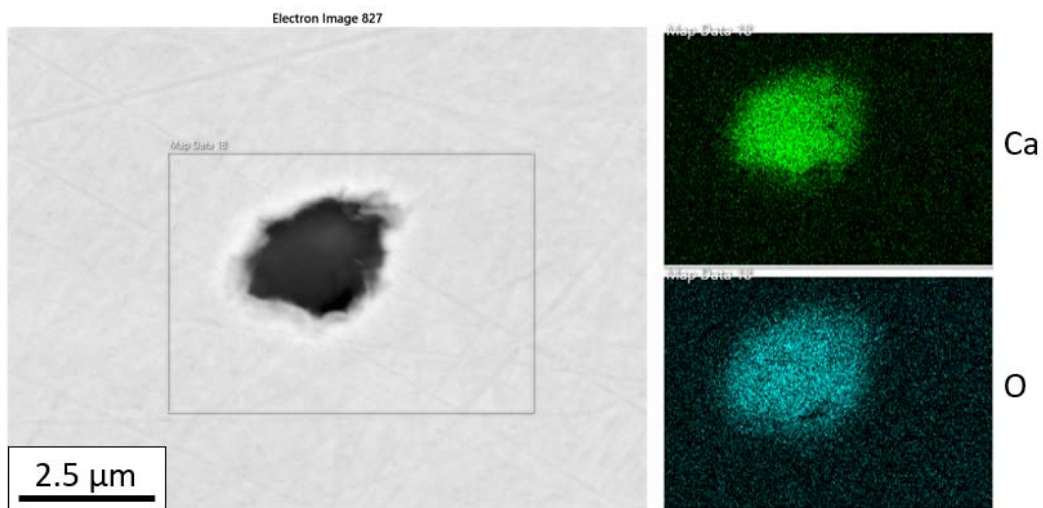


**Figure 5-13:** CaO inclusion detected in cast and hot-rolled spring steel sample.

Furthermore, heterogeneous inclusions consisting of the above mentioned MnS and particles of the oxidic system could be detected in various combinations. **Figure 5-14** shows an alumina rich oxide surrounded by MnS. Very few observed inclusions show contents of MgO. In **Figure 5-15** a complex heterogeneous particle is shown consisting of a large complex Si-Ca-Al-Mg-Oxide together with small MnS particles at the edges.

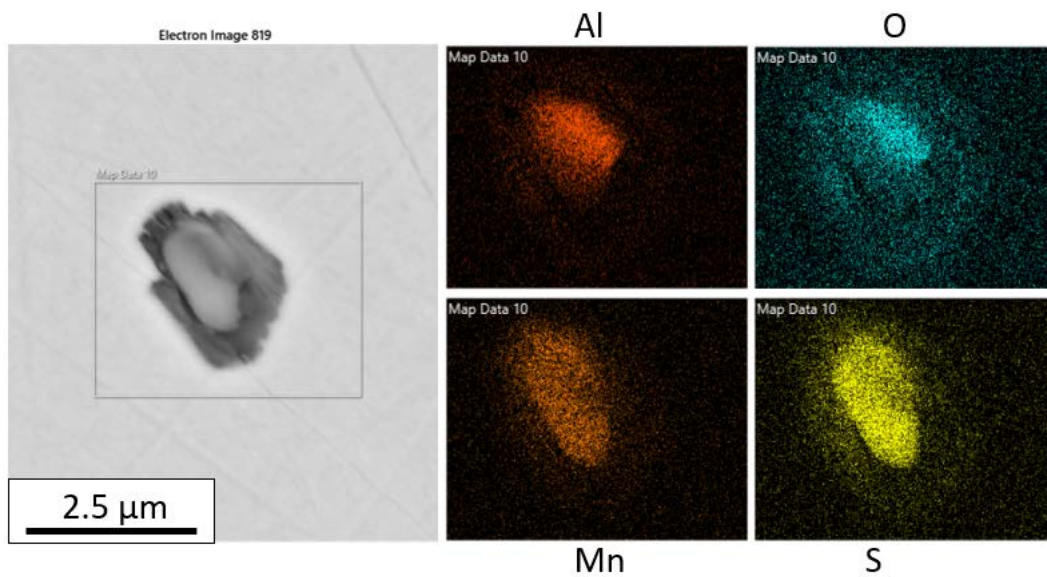


**Figure 5-14:** Alumina oxide surrounded by MnS inclusion detected in cast and hot-rolled spring steel sample.

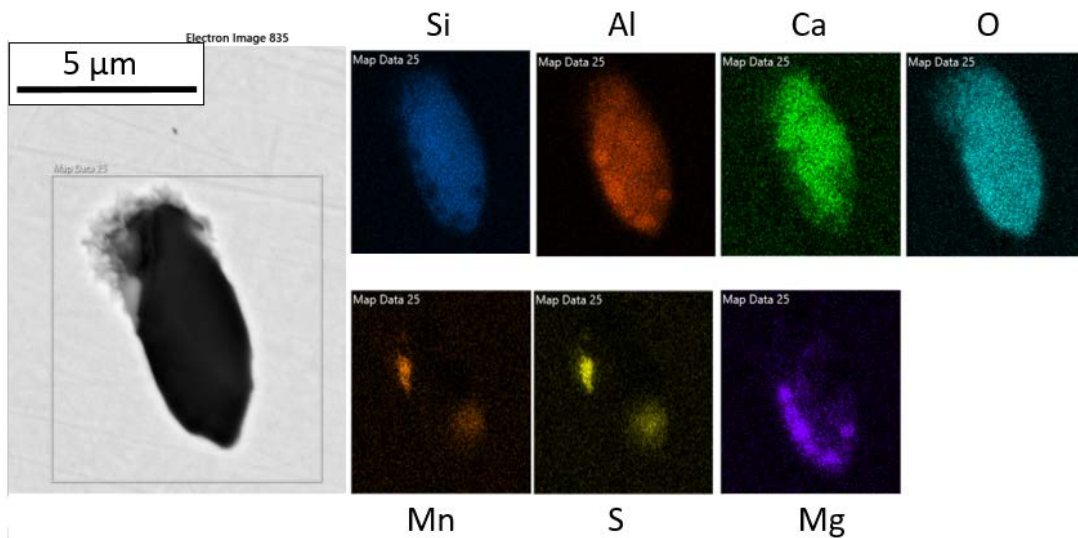


**Figure 5-15:** Complex heterogeneous oxide inclusion accompanied by MnS detected in cast and hot-rolled spring steel sample.

Particles measured after treatment with experimental slags showed similar morphology and chemical compositions, but some detected particles showed contents of the respective alkali elements as shown in **Figure 5-16** where a round homogeneous oxide particle containing Si, Al, Ca, and Na was detected after contact with slag N3 for 30 min. The existence of such particles proof the concept of modifying the chemical composition of NMI using alkali metal oxides and shifting their melting temperatures to lower values thus decreasing the risk of negative influence on the mechanical properties of the steel.

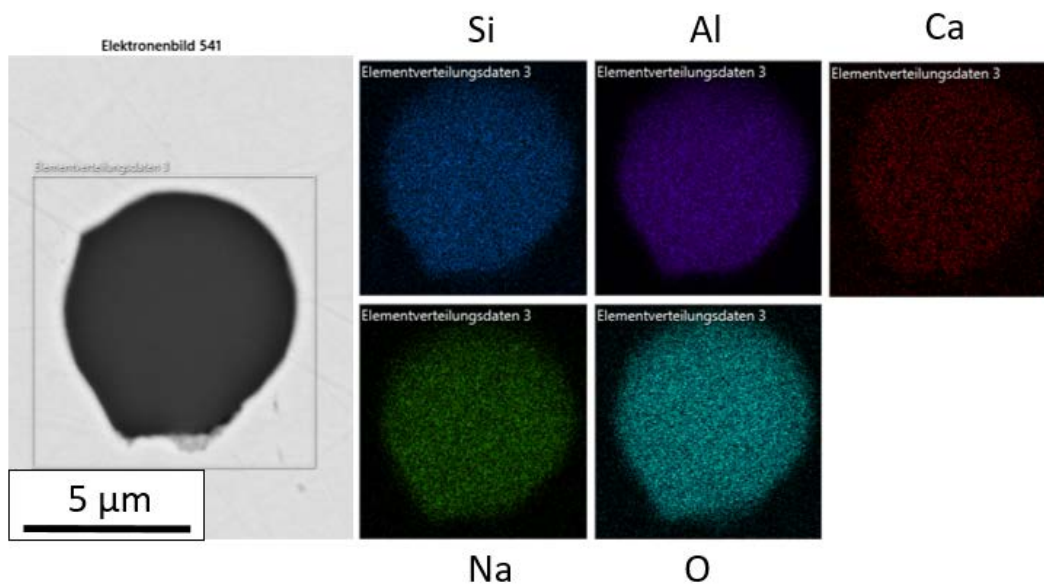


**Figure 5-16:** Homogeneous complex oxide inclusion containing Na detected in steel sample after contact with slag N3 for 30 min.

A similar particle could be found also in samples refined with  $K_2O$  containing slags, where again round complex oxides could be detected as shown in **Figure 5-17**. Again the existence of such particles indicates that inclusion modification using  $K_2O$  containing slag is possible and could lead to overall increased mechanical properties of the steel. As lithium cannot be detected using the available SEM/EDS-equipment it is not possible to observe if lithium can modify NMI in the refined steel samples.

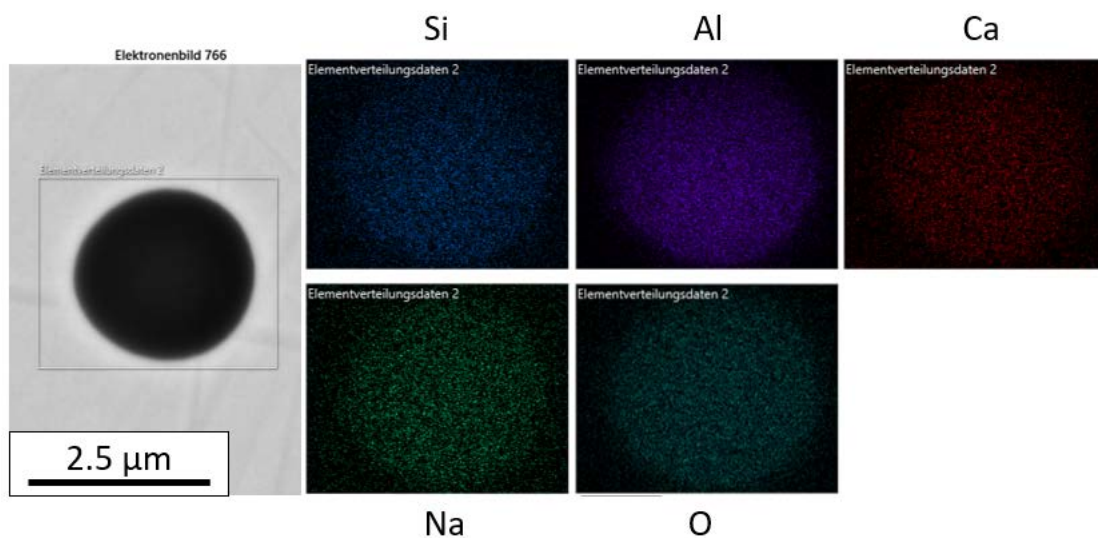


**Figure 5-17:** Homogeneous complex oxide inclusion containing K detected in steel sample after contact with slag K3 for 30 min.

### 5.3.5 Chemical Composition of Detected O- and OS-Particles

Another very important factor regarding steel cleanliness is the chemical composition of NMI. As stated in **Chapters 2.1** and **2.3** this has a great influence on the mechanical properties of NMI and therefore is of high importance regarding the quality of the product. The chemical composition of all detected NMI is measured by EDS during SEM analysis. As shown in **Chapter 5.3.1** most of the detected NMI are classified as oxides or particles containing oxygen as well as sulphur. As particles containing oxides (especially  $\text{Al}_2\text{O}_3$ ) tend to be the most detrimental to the products quality due to their mechanical properties, and purely sulfidic particles are rare in the analyzed samples, only the composition of O and OS particles is further discussed. The composition of NMI typically resembles the composition of the refining slag due to thermodynamic reactions, therefore most NMI should be located in the ternary range of  $\text{Al}_2\text{O}_3$ -CaO-SiO<sub>2</sub>. By plotting the composition of detected O- and OS-particles in this ternary range differences in inclusion population between samples can be shown effectively. In **Figure 5-18** the chemical composition of O- and OS-particles after treatment with reference slag for 30 min is shown. Darker areas in the ternary range indicate multiple measured NMI at that composition. It can be seen that most analyzed NMI are near the binary edges of the diagram, mainly in the areas of pseudo-wollastonite, tridemite, and mullite. A majority of detected particles concentrates at the corner representing pure silica particles. Only few particles contain all three species alumina, silica and lime. Particles in the low-melting area of the calculated ternary phase diagram (**Chapter 3**) are hardly found.

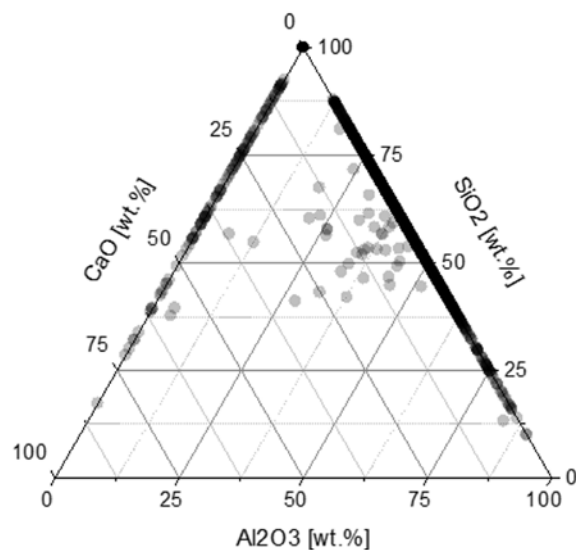


**Figure 5-18:** Chemical composition of NMI after contact with reference slag for 30 min.

As indicated in **Figure 5-19** the composition of NMI does not change significantly over the duration of the experiment. Subfigures a) – d) show the composition of detected particles after 10, 20, 25, and 30 min of experimental time respectively. In **Figure 5-20** the same results are shown for samples which have been in contact with slag N3. Samples were taken again at 10, 20, 25, and 30 min refining time. There is a clear difference to the samples which have been in contact with the reference slag as much more particles show contents of all three components of the ternary range. Most particles are located near the  $\text{SiO}_2$ -rich corner in the range of cristobalite or along the binary edge between  $\text{SiO}_2$  and  $\text{Al}_2\text{O}_3$  in the range of mullite. The same is true for samples treated with slag K3. Results for this are shown in **Figure 5-21**. Again most particles are located in the range of cristobalite and mullite, but with increasing contact time, there seems to be a trend toward more  $\text{Al}_2\text{O}_3$ -rich inclusions in the corundum/ $\text{CA}_6$ / $\text{CA}_2$ -range. Additionally, there are some NMI located in the range of pseudo-wollastonite which was not the case for samples refined with  $\text{Na}_2\text{O}$ -containing slags. Analyzed  $\text{Li}_2\text{O}$ -treated samples show similar compositions with most of the inclusions oriented toward the  $\text{SiO}_2$ -corner and alongside the mullite edge. At 10 min experimental time there are also some  $\text{CaO}$ -rich particles, which seem to dissolve with further duration of the experiment. Additionally, some inclusions show compositions located in the corundum area especially after 30 min of experimental time. This trend seems to be strongest with the addition of  $\text{Li}_2\text{O}$ . The resulting ternary diagrams for samples which have been in contact with slag L2 are shown in **Figure 5-22**. Due to problems with sampling only results for experimental times of 10, 25, and 30 min are available. Overall, there seem to be similar trends regarding the chemical composition with additions of all three alkali metal oxides to the experimental slags and a clear difference in comparison to samples treated with the reference slag can be shown. The analyzed experimental slags tend to decrease the amount of particles with high contents of  $\text{CaO}$ , form complex particles in the ternary range and show a trend to formation of some alumina-rich particles alongside the bulk of silica-dominated NMI.

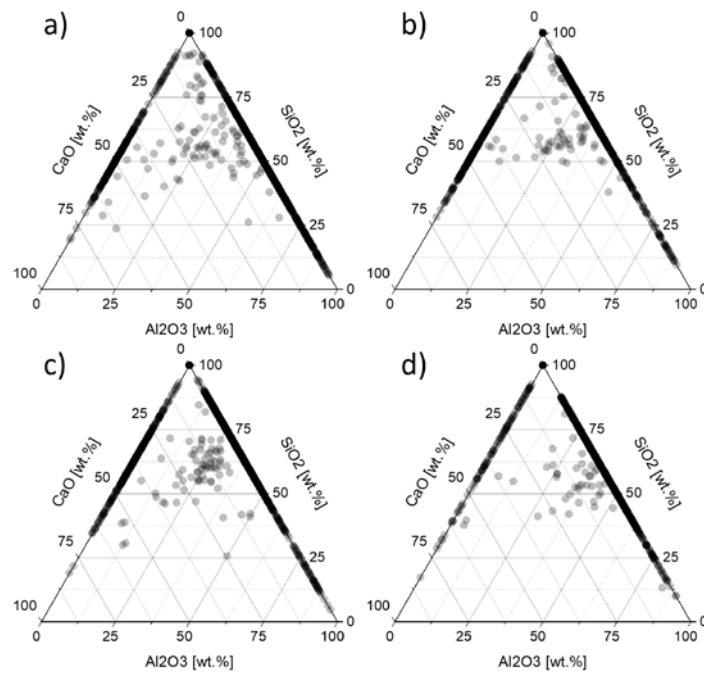


**Figure 5-19:** Chemical composition of NMI after contact with reference slag for a) 10 min, b) 20 min, c) 25 min and d) 30 min.

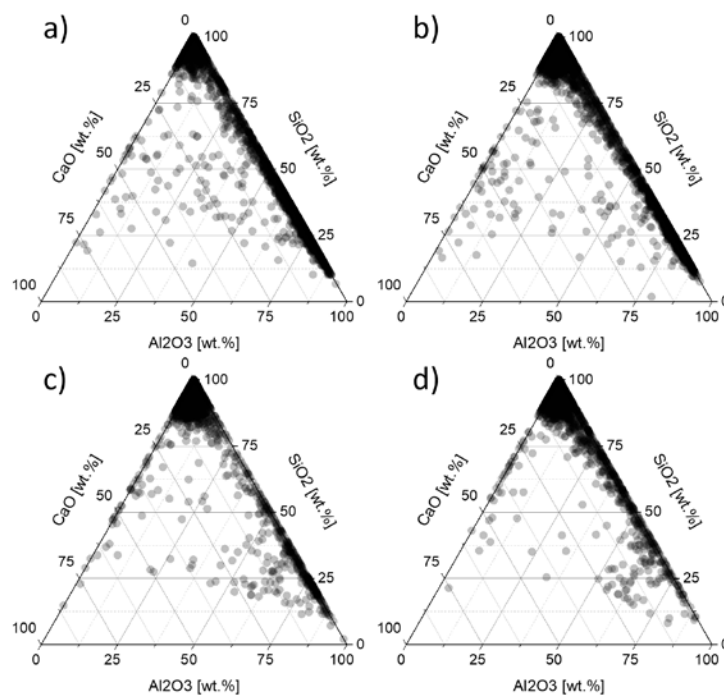


**Figure 5-20:** Chemical composition of NMI after contact with slag N3 for a) 10 min, b) 20 min, c) 25 min and d) 30 min.

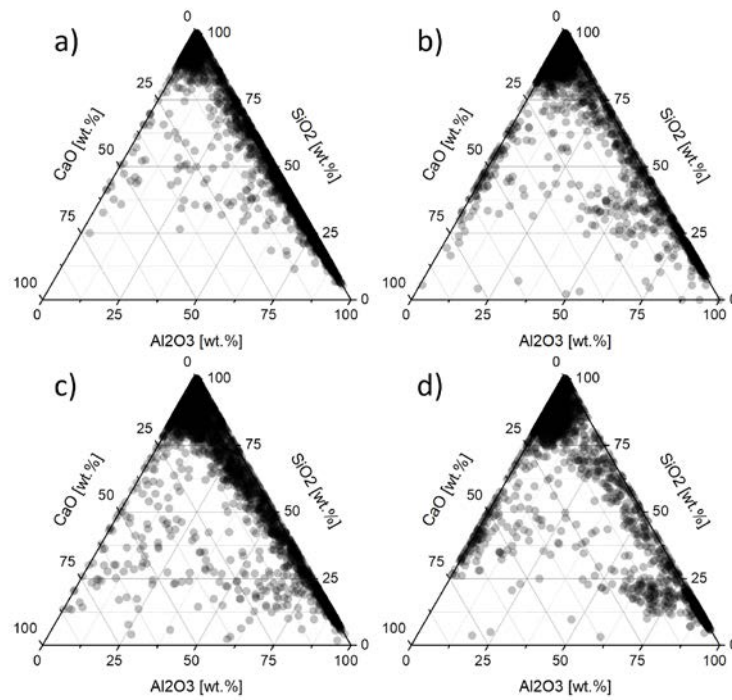


**Figure 5-21:** Chemical composition of NMI after contact with slag K3 for a) 10 min, b) 20 min, c) 25 min and d) 30 min.

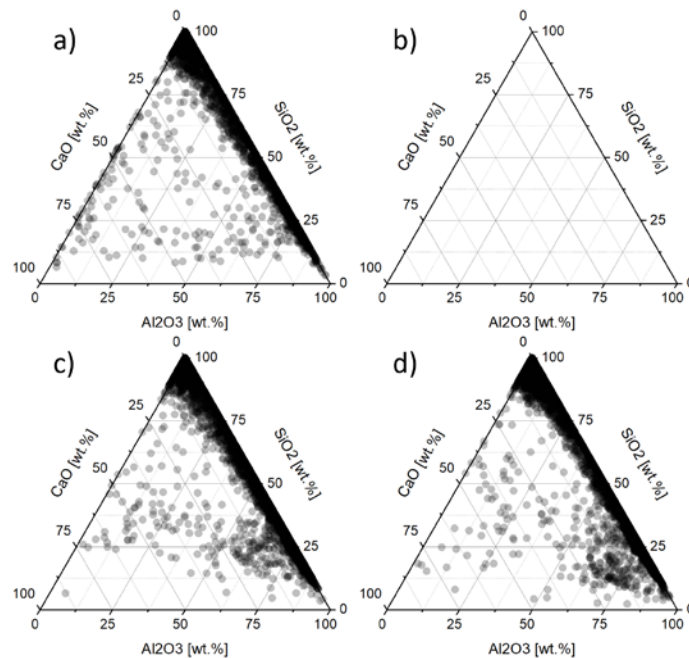


**Figure 5-22:** Chemical composition of NMI after contact with slag L2 for a) 10 min, c) 25 min and d) 30 min.



To gain insight into the influence of the added alkali metal oxides on these shifts in chemical composition the measured NMI can be sorted according to their content of respective alkali element. Data after 30 min of contact with the experimental slags has been used for this. Thresholds of measured alkali element contents were chosen with 0.2 wt% and 1.0 wt%. This leads to three different classes of O and OS-particles. NMI where automated feature analysis measured less than 0.2 wt% of alkali elements, particles with measured contents over 0.2 wt% of alkali elements and lastly inclusions with measured contents of 1.0 wt% of the respective alkali elements and above. As lithium content cannot be measured with the available EDS-detectors this is only done for experimental slags containing sodium- or potassium oxide. For samples in contact with slags N1, N2, and N3 it is shown that particles with higher contents of Na<sub>2</sub>O tend towards higher concentrations of Al<sub>2</sub>O<sub>3</sub>. Slags N1 and N2 show very similar results, where particles with contents of sodium above 0.2 or even 1.0 wt% tend to lowest contents of CaO and appear to favor higher contents of Al<sub>2</sub>O<sub>3</sub>, while the amount of pure SiO<sub>2</sub> particles drops drastically. Examining the sample treated with slag N3 regarding sodium-content in the particles this effect shows even more, where almost all particles with contents of 1.0 wt% sodium or more are located near the Al<sub>2</sub>O<sub>3</sub> rich corner of the ternary system. These trends are also shown in **Figure 5-23** where subfigures a), d), and g) show particles with Na-contents below 0.2 wt%, subfigures b), e), and h) show particles with Na-contents above 0.2 wt%, and subfigures c), f), and i) show O and OS particles with Na-contents above 1.0 wt%.

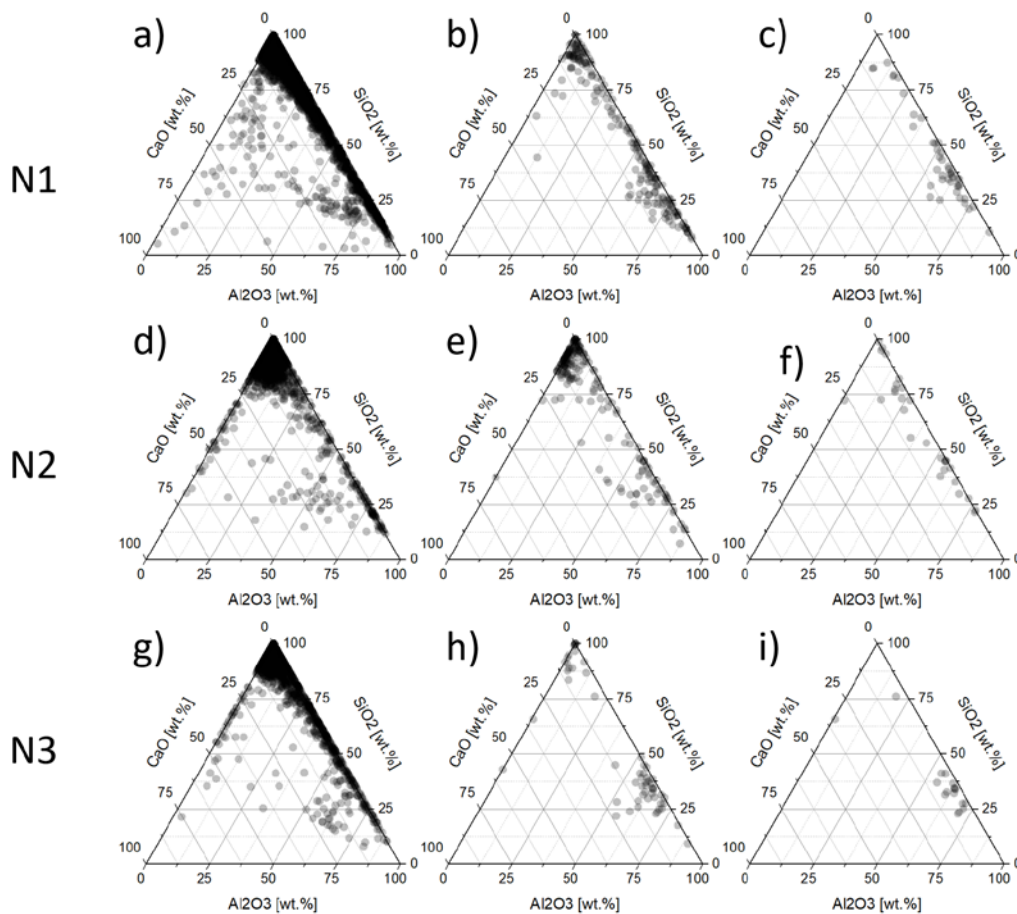


**Figure 5-23:** Chemical composition of O and OS particles after contact for 30 min with slags a) – c) N1, d) – f) N2, and g) – i) N3.

Similar analysis was done for samples which have been in contact with  $K_2O$ -containing experimental slags. Here particles were divided regarding their measured contents of potassium, again with thresholds of 0.2 and 1.0 wt%. The results are shown in **Figure 5-24**. For the steel sample treated with slag K1 there is also a trend towards  $Al_2O_3$ -rich inclusions with higher contents of potassium in the analyzed particles. But even with contents above 1.0 wt% potassium there are still many particles with chemical compositions near the  $SiO_2$  corner of the ternary diagram, as opposed to the sample which has been in contact with slag N1, where most of the particles with high alkali element concentrations were in the area of mullite and corundum. The sample treated with slag K2 shows a different inclusion population regarding the particles with amounts of potassium below 0.2 wt%, as there were high numbers of CaO-rich particles. Additionally, particles in the binary range of CaO- $Al_2O_3$  are measured. This is true only for the sample treated with slag K2 after 30 min of experimental time. When analyzed, the same sample after only 20 min of contact time, the inclusion landscape resembles more closely all other measured results as shown in **Figure 5-25**.

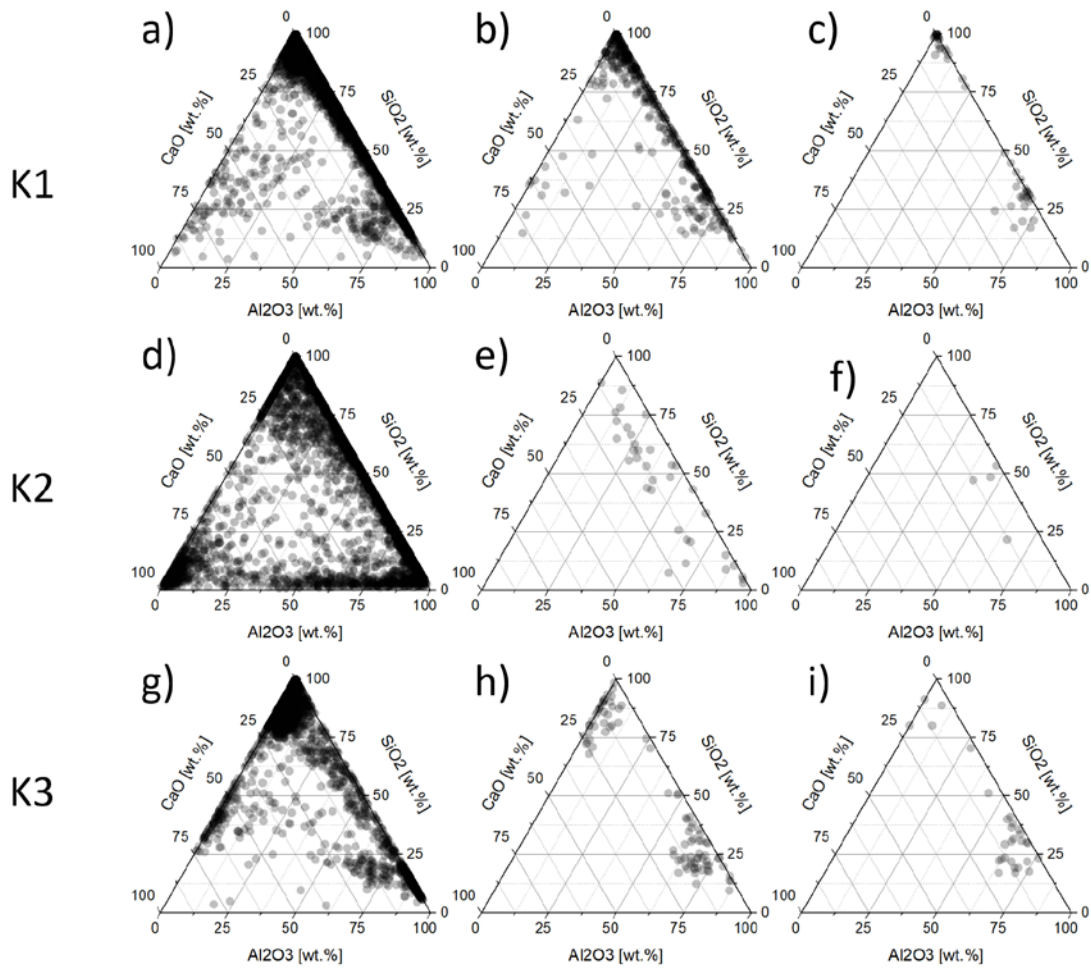


**Figure 5-24:** Chemical composition of O and OS particles after contact for 30 min with slags  
a) – c) K1, d) – f) K2, and g) – i) K3.

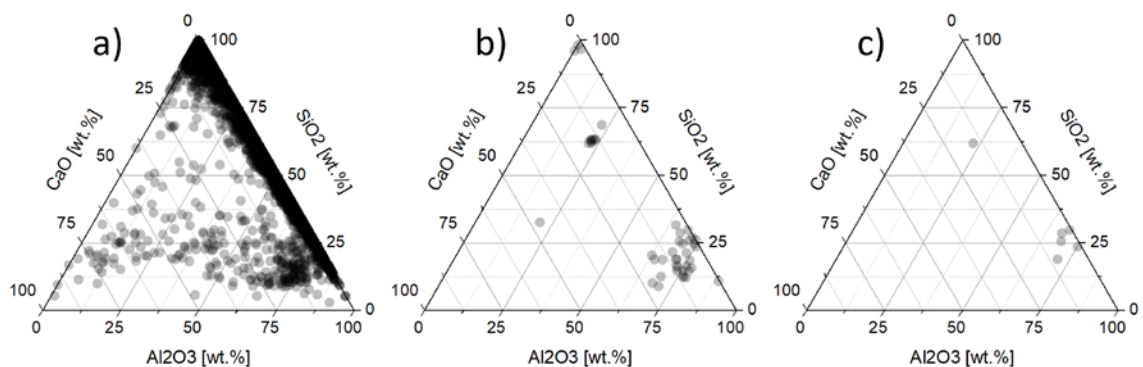


**Figure 5-25:** Chemical composition of O and OS particles after contact for 20 min with slag K2,  
Particles contain a) below 0.2 wt%, b) above 0.2 wt%, c) above 1.0 wt% of potassium.

In samples which have been in contact with slag K3 similar trends as samples treated with Na<sub>2</sub>O-containing slags can be shown, where the CaO content of particles decreases, and with higher contents of potassium in the inclusions the composition shifts towards the Al<sub>2</sub>O<sub>3</sub>-rich corner. Barely any SiO<sub>2</sub>-rich particles were found with contents of 1.0 wt% of potassium or above. The population of particles with no significant amounts of potassium includes additionally relatively high amounts of particles in the range of pseudo-wollastonite. These compositions were not observed for inclusions containing more than 0.2 wt% of potassium.

**Table 5-IV** shows the composition of selected particles detected in the steel sample after interaction with slag N3 in the quaternary range of SiO<sub>2</sub>-CaO-Al<sub>2</sub>O<sub>3</sub>-Na<sub>2</sub>O. Liquidus temperatures have been calculated for these particles using FactSage. Calculations of the composition of these particles were done with no regard concerning other measured components (Fe, Mn, Mg, S). It is assumed these particles are purely oxidic and of homogeneous composition as presented in **Chapter 5.3.4**. A broad range of liquidus temperatures can be observed, which is highly dependent not only on the content of Al<sub>2</sub>O<sub>3</sub> but also on the ratio of Na<sub>2</sub>O/SiO<sub>2</sub> and Na<sub>2</sub>O/Al<sub>2</sub>O<sub>3</sub>.

**Table 5-IV:** Calculated liquidus temperatures of particles containing high amounts of Na<sub>2</sub>O.

Liq. Temp [°C]	Na <sub>2</sub> O [wt%]	SiO <sub>2</sub> [wt%]	CaO [wt%]	Al <sub>2</sub> O <sub>3</sub> [wt%]	Na <sub>2</sub> O/SiO <sub>2</sub> [-]	Na <sub>2</sub> O/Al <sub>2</sub> O <sub>3</sub> [-]
549	35	60	0	5	0.6	7.0
845	35	62	3	0	0.6	/
955	39	55	2	4	0.7	14.7
1065	41	52	5	2	0.8	22.6
1395	66	23	11	0	2.9	/
1457	53	17	0	29	3.0	1.8
1517	47	20	4	29	2.4	1.6
1578	50	17	1	32	2.9	1.6
1680	43	13	4	40	3.2	1.1
1719	43	14	2	41	3.0	1.1

## 6 Discussion

### 6.1 Influence on the Liquidus Temperature and Viscosity of the Slag

Liquidus temperatures of the ternary system of  $\text{SiO}_2\text{-CaO-Al}_2\text{O}_3$  have been calculated by FactSage:

- a) All investigated alkali metal oxides lead to an increase in area of low melting composition. The liquidus temperature reducing effect is strongest with addition of  $\text{Li}_2\text{O}$  and decreases with higher atomic number of the alkali elements. This is in good agreement with reports from literature. [9,10,14,46,50] Calculated liquidus temperatures should be verified by experimental study in future work as not much has been reported in this regard.
- b) Measurements and thermodynamic calculations of slag viscosities do not fully agree with theoretical considerations regarding the slag structure and impact of the alkali metal oxides on slag viscosity. Addition of  $\text{Li}_2\text{O}$  leads to the predicted strong decrease in viscosity as well as observed for  $\text{Na}_2\text{O}$ . With additions of  $\text{K}_2\text{O}$  the measured and calculated viscosity did in fact increase slightly when calculated by FactSage as reported in literature [9,10,14,46,50], but decreased according to Riboud-model calculations and measurements. This cannot be explained by theoretical slag models regarding the charge compensation effect. As reported in research this should have more influence as viscosity decreasing depolymerization of silicate structures through provided single  $\text{O}^{2-}$  anions, thus increase in content of  $\text{K}_2\text{O}$  should also increase slag viscosity.

- c) Further investigation on the influence of alkali metal oxides on the viscosity and structure of the slag should be conducted not only by thermodynamic calculation but also by measurement, as thermodynamic databases for calculation could be insufficient for detailed investigation.

## 6.2 Influence on the Dissolution of Non-Metallic Inclusions

Extensive observations of particle dissolution in experimental slags containing alkali metal oxides have been performed using HT-CSLM.

- a) Dissolution of alumina, spinel and silica type particles was significantly influenced by the addition of  $\text{Li}_2\text{O}$ ,  $\text{Na}_2\text{O}$ , and  $\text{K}_2\text{O}$ . Strongest impact was found with  $\text{Li}_2\text{O}$  containing slags, as dissolution of every observed type of particle was enhanced drastically.
- b) Higher contents of  $\text{Li}_2\text{O}$  lead to faster dissolution, where dissolution of alumina particles was about 8-times faster with contents of about 5 wt% of  $\text{Li}_2\text{O}$ . Effect on dissolution of spinel and silica particles was not as profound but still dissolution-rates could be doubled with higher additions of  $\text{Li}_2\text{O}$  to the slag. This effect is in strong contrast with predictions found in literature [11,13,14], where  $\text{Li}_2\text{O}$  is reported to hinder dissolution of NMI as described in **Chapter 2.5**. Addition of  $\text{Li}_2\text{O}$  decreases slag viscosity as discussed in **Chapters 3** and **6.1** and therefore benefits the mechanism of inclusion separation as presented in **Chapter 2.2**. This leads to the suggestion that  $\text{Li}_2\text{O}$  in low basicity refining slags should theoretically have a beneficial effect on overall steel cleanness, due to enhanced inclusion removal. The effect of increased slag entrapment could not be analyzed sufficiently with the chosen presented experimental setup.
- c)  $\text{Na}_2\text{O}$  leads in conducted experiments to about twice as fast dissolution of alumina particles compared to dissolution in slag without contents of alkali metal oxides. However, higher contents of  $\text{Na}_2\text{O}$  do not seem to improve dissolution of alumina particles further. Dissolution of spinel particles could be enhanced with all contents of  $\text{Na}_2\text{O}$ , where higher contents lead to faster dissolution. With addition of 7.4 wt% of  $\text{Na}_2\text{O}$  dissolution of spinel was about twice as fast compared to dissolution in reference slag. Effect of  $\text{Na}_2\text{O}$  on silica dissolution is unclear as results show no distinct trend. Again these observations do not agree with other research, as  $\text{Na}_2\text{O}$  is reported to hinder inclusion dissolution. Due to the same reason as stated above

---

for  $\text{Li}_2\text{O}$ , the addition of  $\text{Na}_2\text{O}$  seems beneficial to the removal of alumina- and alumina rich spinel type particles.

- d) With addition of  $\text{K}_2\text{O}$  up to a content of 5.6 wt% the dissolution of alumina particles could be enhanced, but with higher contents the dissolution was hindered. Spinel particles dissolved nearly twice as fast with all additions of  $\text{K}_2\text{O}$  with effects slightly decreasing with higher contents. Dissolution of  $\text{SiO}_2$  could not be improved with addition of  $\text{K}_2\text{O}$ . There is no clear trend on the influence of increasing contents of  $\text{K}_2\text{O}$  on  $\text{SiO}_2$  dissolution. Therefore, small additions up to a content of 5.6 wt% of  $\text{K}_2\text{O}$  to low basicity refining slags seem to enhance dissolution of alumina and alumina rich spinel type particles.
- e) Regarding the dissolution mechanism, addition of  $\text{Li}_2\text{O}$  seems to promote diffusivity of particle species in the slag as dissolution curves show a parabolic form with higher contents of  $\text{Li}_2\text{O}$ . Especially for dissolution of alumina, a clear shift from a S-type dissolution curve to very fast parabolic dissolution can be observed. Dissolution of spinel particles in reference slag and slags containing alkali metal oxides, especially  $\text{K}_2\text{O}$ , appears nearly linear. This is typical for dissolution controlled by the speed of a chemical reaction as opposed to diffusion in the stagnant fluid or mass transport in the boundary layer. Due to this the combined dissolution model presented in **Chapter 2.2** is probably not applicable on the dissolution of these spinel particles. Further investigation regarding the dissolution mechanism of this type of particle has to be conducted. Experiments stopping dissolution of spinel particles in slag could be performed to analyze the boundary layer and investigate if intermediate phases are formed during dissolution.
- f) Dissolution times of the same types of particles in the same slag composition can vary drastically in specific cases, as mentioned in **Chapter 5.2.2** and shown in **Figure 5-2**. In this work the mean value of dissolution times and curves has been used for analysis of the influence of addition of alkali metal oxides. This could lead to some uncertainties in identifying the underlying dissolution mechanism for some experiments. For the sake of analyzing the influence on dissolution capability of experimental slags this should not influence the presented results significantly. To improve insight in dissolution mechanisms of NMI in alkali metal oxide containing slags further experiments have to be conducted.

### 6.3 Influence on the Inclusion Population

The amount of detected NMI in steel samples before and after interaction with experimental slags has been presented in **Chapter 5.3.1**. Comparing the count of total inclusions per mm<sup>2</sup> of the original sample with the amount of inclusions after contact with experimental slags, it appears that the slag treatment had detrimental effects on the steel cleanliness. These results could be influenced due to several reasons:

- a) Great differences in measured area of samples before and after slag treatment. This could lead to statistical error, if the measured sample area is not representative of the whole melt.
- b) Slag entrapment due to the sampling procedure via sampling rod.
- c) Introduction of exogeneous particles due to melting of the sampling rod.
- d) The focus of the conducted experiments was on the modification of inclusions, so changes in the amount of detected inclusions have to be interpreted very carefully, considering the used experimental set-up.

Inclusion types commonly present in steels of the analyzed grade are oxidic particles in the range of the SiO<sub>2</sub>-CaO-Al<sub>2</sub>O<sub>3</sub>-MgO quaternary system as well as MnS particles. [19,20,45,55] During analysis of steel samples after contact with experimental slags the following can be concluded:

- a) Relatively large quantities of complex heterogeneous particles consisting of oxidic parts from the SiO<sub>2</sub>-CaO-Al<sub>2</sub>O<sub>3</sub> ternary system with surrounding MnS are observed.
- b) Only very small amounts of particles containing MgO can be detected. Instead the vast majority of NMI concentrates in the SiO<sub>2</sub>-rich area of the ternary system SiO<sub>2</sub>-CaO-Al<sub>2</sub>O<sub>3</sub>.
- c) It has been shown that the addition of alkali metal oxides to refining slags can modify the chemical composition of NMI in a way that the liquidus temperature decreases. This is due to homogeneous contents of respective alkali elements in the observed particles.
- d) Only very little amounts of analyzed particles showed significant amounts of respective alkali elements. This could be caused by too little interaction of steel and slag during the experiment due to the lack of stirring or bubbling with the chosen experimental setup.



- e) Particles containing higher amounts of respective alkali element show a tendency to alumina-rich compositions. This trend would be detrimental as alumina-rich hard non-deformable particles should be avoided and particle compositions should ideally concentrate in low melting areas of the ternary system  $\text{SiO}_2\text{-CaO-Al}_2\text{O}_3$ .
- f) By analyzing  $\text{Na}_2\text{O}$  containing slag after steel-slag interaction experiments increased amounts of  $\text{Al}_2\text{O}_3$  in the slag could be observed. Dissolution experiments showed increased dissolution of alumina particles in the experimental slags and the alumina-crucibles showed visible attack after contact with the slag at elevated temperatures. Therefore, the increase in alumina content of the slag over the duration of the steel-slag interaction experiments is probably due to the dissolution of the alumina crucible. For clarification slags REF and N3 were heated to  $1600^\circ\text{C}$  in crucibles made of  $\text{Al}_2\text{O}_3$ ,  $\text{MgO}$ , and  $\text{ZrO}_2$ . The slags were analyzed at the industry partner. Chemical compositions of the slags are shown in **Table 6-I**. The  $\text{MgO}$ -crucibles were damaged beyond repair by slag infiltration. This is also represented by the massive increase in  $\text{MgO}$  content of these slags. Compared to the initial chemical composition of the slags the samples in contact with  $\text{Al}_2\text{O}_3$  crucibles show a significant increase in  $\text{Al}_2\text{O}_3$ , while slags in contact with the  $\text{ZrO}_2$  crucibles show rather low changes. In **Figure 6-1** the attack on the  $\text{Al}_2\text{O}_3$  crucible is shown, where the wall of the crucible is visibly dissolved, especially at the interface slag-crucible-atmosphere.

**Table 6-I:** Chemical compositions of experimental slags after interaction with crucibles.

Crucible	$\text{Al}_2\text{O}_3$	$\text{Al}_2\text{O}_3$	$\text{MgO}$	$\text{MgO}$	$\text{ZrO}_2$	$\text{ZrO}_2$
Slag	REF	N3	REF	N3	REF	N3
CaO	39.9	37.4	26.3	13.0	41.3	38.4
$\text{SiO}_2$	46.5	43.4	30.7	13.7	48.5	45.1
$\text{Al}_2\text{O}_3$	10.9	10.2	9.2	5.3	6.4	5.8
$\text{Na}_2\text{O}$	0.3	5.4	0.1	1.5	0.3	5.8
$\text{MgO}$	0.7	0.8	22.6	63.3	0.7	0.7
$\text{ZrO}_2$	/	/	6.6	1.4	1.1	1.2



**Figure 6-1:** Attack on Al<sub>2</sub>O<sub>3</sub> crucible (white) from interaction with slag N3.

Regarding the effect on the size of NMI in steel samples in contact with experimental slags all slags could reduce the ECD of detected particles effectively. As there is no clear trend in size, neither regarding the amount nor the kind of added alkali metal oxide, and reference slag led to similar results, this effect is probably more correlated to the experimental setup and procedure as to the chemical composition of the slag. The same is true for the measured amount of NMI in the steel. It is advised that steel-slag interaction experiments are repeated with the following modifications to the experimental procedure:

- a) No sampling or stirring of the slag or the melt during the interaction time to avoid slag entrapment or introduction of exogeneous particles from the sampling rod.
- b) Analysis of larger sample (acquired from solidified melt after steel-slag interaction).
- c) Use of ZrO<sub>2</sub> crucible to avoid dissolution and therefore change of the slag composition to higher contents of Al<sub>2</sub>O<sub>3</sub>. Additionally, ZrO<sub>2</sub> containing particles could easily be identified as exogeneous particles if the crucible is dissolved nonetheless.

## 7 Summary

The influence of addition of selected alkali metal oxides to low basicity refining slags for Si/Mn-deoxidized steels was observed. Alkali metal oxides should in theory impact the viscosity and the liquidus temperature of  $\text{SiO}_2\text{-CaO-Al}_2\text{O}_3$  slag systems. These parameters are of great importance regarding inclusion removal mechanisms and impact of NMI on the mechanical properties of the steel. A literature screening regarding the impact of different alkali metal oxides to different slag systems, mainly high basicity tundish slags as well as low basicity refining slags, led to following conclusions:

- a)  $\text{Li}_2\text{O}$  and  $\text{Na}_2\text{O}$  should decrease viscosity due to depolymerization of silicate structures and networks. This enhances the mechanism of separation of NMI from the steel melt to the liquid slag but does not lead to an improvement in steel cleanliness as excessive reduction of viscosity lead reportedly to increased slag entrapment and NMI were able to leave the slag phase and return to the melt.
- b) Addition of  $\text{K}_2\text{O}$  however is reported to increase steel cleanliness regarding both number as well as size of remaining inclusions after refining. Investigation on the slag structure showed that this is because  $\text{K}_2\text{O}$  increases the slag viscosity, thus avoiding slag entrapment, due to promotion of the formation of complex aluminosilicate networks which additionally reduce the risk of NMI (especially NMI containing  $\text{SiO}_2$  or  $\text{Al}_2\text{O}_3$ ) returning from the slag phase to the melt.
- c)  $\text{Rb}_2\text{O}$  and  $\text{Cs}_2\text{O}$  are reported to influence the slag properties in a similar way as  $\text{K}_2\text{O}$  but their use is deemed economically not feasible for industrial scale production.

Ten experimental low basicity refining slags were produced containing amounts of  $\text{Li}_2\text{O}$ ,  $\text{Na}_2\text{O}$ , and  $\text{K}_2\text{O}$  respectively as well as a slag without contents of alkali metal oxides for comparison of the results. The dissolution of synthetic particles with different chemical

compositions in the produced experimental slags was observed by HT-CSLM. Dissolution of alumina, spinel, and silica particles was drastically enhanced with increasing additions of  $\text{Li}_2\text{O}$ . Dissolution of alumina and spinel particles was enhanced with the addition of  $\text{Na}_2\text{O}$  but the effect was not as pronounced as with the addition of  $\text{Li}_2\text{O}$ . Dissolution of alumina and spinel was enhanced with the addition of  $\text{K}_2\text{O}$ , but increasing amounts of  $\text{K}_2\text{O}$  decreased the effectiveness.

Steel-slag interaction experiments were conducted using an argon flushed laboratory scale furnace. Sampling over 30 min of interaction time of a steel sample from industry partners with all experimental slags was performed and samples were analyzed by manual and automated evaluation using SEM/EDS. Steel cleanliness regarding the amounts of NMI per measured sample area could not be increased regardless of used experimental slag. On the other hand, the average ECD of remaining inclusions could be decreased during all steel-slag interaction experiments. However, both of these effects are most likely linked with the experimental setup and sampling procedure and are not a direct result of the used composition of slags.

Amounts of Na and K could be detected after steel-slag interaction with respective slags in some of the detected NMI. This allows the assumption that modification of NMI using  $\text{Na}_2\text{O}$  or  $\text{K}_2\text{O}$  containing experimental slags is possible. However, the ratio of modified particles to ones containing little to no alkali elements suggest longer interaction times or enhanced contact of the liquid steel with the slag is needed. Chemical composition of particles containing higher amounts of alkali elements concentrate towards the alumina rich area of the ternary system  $\text{SiO}_2\text{-CaO-Al}_2\text{O}_3$ . This effect is opposed to the assumption that addition of alkali metal oxides would lead to a concentration of remaining NMI to low melting compositions. As slag composition after steel-slag interaction was found to have shifted drastically to higher alumina contents, the shift in NMI composition could be explained. Additional alumina content of the slag is likely from dissolution of the alumina crucible used in steel-slag interaction experiments.

It is proposed that steel-slag interaction experiments are repeated with following adaptations to the experimental setup and procedure:

- a) Crucible material should be changed to zirconia to avoid dissolution and  $\text{Al}_2\text{O}_3$  enrichment of the slag
- b) Sampling should be avoided during the treatment to reduce the risk of slag entrapment or melting of the sampling rod, thus minimizing additionally introduced impurities
- c) Analysis of steel samples after contact with  $\text{Li}_2\text{O}$  containing slag needs to be repeated with SEM/EDS detectors capable of detecting Li.

## Bibliography

- [1] Austrian Standards, Warmgewalzte Stähle für vergütbare Federn: Technische Lieferbedingungen. ÖNORM EN 10089 77.140.25, Wien (01.06.2003), Österreichisches Normungsinstitut.
- [2] Austrian Standards, Chirurgische Implantate — Metallische Werkstoffe: Teil 7: Schmiedbare und kaltumformbare Cobalt-Chrom-Nickel-Molybdän-Eisenlegierung. ÖNORM EN ISO 5832-7 11.040.40, Wien (15.11.2019), Austrian Standards International.
- [3] X.F. He, X.H. Wang, S.H. Chen, M. Jiang, F.X. Huang and W.J. Wang, Inclusion composition control in tyre cord steel by top slag refining. *Ironmaking and Steelmaking*. Vol.32 41 (2014), 9, pp. 676–684. doi:10.1179/1743281214Y.0000000182
- [4] C. Chen, M. Sun, X. Chen, B. Wang, J. Zhou and Z. Jiang, State of the Art in Control of Inclusions and Microalloying Elements in Tire Cord Steel and Saw Wire Steel. *STEEL RES INT* 93 (2022), 4, pp. 2100507. doi:10.1002/srin.202100507
- [5] A.L.V.d. Costa e Silva, The effects of non-metallic inclusions on properties relevant to the performance of steel in structural and mechanical applications. *Journal of Materials Research and Technology* 8 (2019), 2, pp. 2408–2422. doi:10.1016/j.jmrt.2019.01.009
- [6] T.V. Shibaeva, V.K. Laurinavichyute, G.A. Tsirlina, A.M. Arsenkin and K.V. Grigorovich, The effect of microstructure and non-metallic inclusions on corrosion behavior of low carbon steel in chloride containing solutions. *Corrosion Science* 80 (2014), pp. 299–308. doi:10.1016/j.corsci.2013.11.038
- [7] Lifeng Zhang, Brian G Thomas, Xinhua Wang and Kaike Cai, Evaluation and control of steel cleanliness - Review (2002).

- [8] A. Mayerhofer, Enhanced characterization of non-metallic inclusions for (sub) micro steel cleanliness evaluations. Ph.D, Leoben, Austria (2021).
- [9] C. Chen, Z. Jiang, Y. Li, M. Sun, K. Chen, Q. Wang and H. Li, Effect of Na<sub>2</sub>O and Rb<sub>2</sub>O on Inclusion Removal in C96V Saw Wire Steels Using Low-Basicity LF (Ladle Furnace) Refining Slags. *Metals* 8 (2018), 9, pp. 691. doi:10.3390/met8090691
- [10] C. Chen, Z. Jiang, Y. Li, M. Sun, G. Qin, C. Yao, Q. Wang and H. Li, Effect of Rb<sub>2</sub>O on Inclusion Removal in C96V Saw Wire Steels Using Low-Basicity LF Refining Slag. *ISIJ International [ISIJ Int.]* 58 (2018), 11, pp. 2032–2041. doi:10.2355/isijinternational.ISIJINT-2018-385
- [11] C. Chen, Z. Jiang, Y. Li, L. Zheng, X. Huang, G. Yang, M. Sun, K. Chen, H. Yang, H. Hu and H. Li, State of the Art in the Control of Inclusions in Tire Cord Steels and Saw Wire Steels – A Review. *STEEL RES INT* 90 (2019), 8, pp. 1800547. doi:10.1002/srin.201800547
- [12] K. Choi, Y. Kang and I. Sohn, Effect of Rb<sub>2</sub>O and Cs<sub>2</sub>O on Inclusion Removal in 321 Stainless Steels Using Novel Basic Tundish Fluxes. *Metallurgical and Materials Transactions B, Process Metallurgy and Materials Processing Science* 47 (2016), 3, pp. 1520–1526. doi:10.1007/s11663-016-0604-2
- [13] Y. Li, C. Chen, Z. Jiang, M. Sun, H. Hu and H. Li, Application of Alkali Oxides in LF Refining Slag for Enhancing Inclusion Removal in C96V Saw Wire Steel. *ISIJ International [ISIJ Int.]* 58 (2018), 7, pp. 1232–1241. doi:10.2355/isijinternational.ISIJINT-2018-048
- [14] J.Y. Yu, Y. Kang and I. Sohn, Novel Application of Alkali Oxides in Basic Tundish Fluxes for Enhancing Inclusion Removal in 321 Stainless Steels. *Metallurgical and Materials Transactions B, Process Metallurgy and Materials Processing Science* 45 (2014), 1, pp. 113–122. doi:10.1007/s11663-013-0013-8
- [15] J. Zhouhua, C. Changyong, L. Yang, S. Meng and Q. Guoqing, Effect of K<sub>2</sub>O on inclusion removal in C96V saw wire steels using LF refining slags (2018), AIM Associazione italiana di metallurgia.
- [16] Reis B. H. and Bielefeldt W. V. and Vilela A. C. F., Absorption of non-metallic inclusions by steelmaking slags—a review. *J of Mater. Research and Technology* 3 (2014), 2, pp. 179–185. doi:10.1016/j.jmrt.2014.03.011
- [17] Y. Hu, W. Chen, C. Wan, F. Wang and H. Han, Effect of Deoxidation Process on Inclusion and Fatigue Performance of Spring Steel for Automobile Suspension. *Metall and Materi Trans B* 49 (2018), 2, pp. 569–580. doi:10.1007/s11663-018-1187-x

- [18] L. Chen, W. Chen, Y. Hu, Z. Chen, Y. Xu and W. Yan, Investigation on the Origin of Al<sub>2</sub>O<sub>3</sub>-Rich Inclusions in Valve Spring Steel under Vacuum Condition. *Steel Research International*. Vol.76 88 (2017), 7, pp. 1600376. doi:10.1002/srin.201600376
- [19] H.L. Yang, J.S. Ye, X.L. Wu, Y.S. Peng, Y. Fang and X.B. Zhao, Effect of Top Slag with Low Basicity on Transformation Control of Inclusions in Spring Steel Deoxidized by Si and Mn. *ISIJ International [ISIJ Int.]* 56 (2016), 1, pp. 108–115. doi:10.2355/isijinternational.ISIJINT-2015-468
- [20] H. Yang, J. Ye, X. Wu, Y. Peng, Y. Fang and X. Zhao, Optimum Composition of CaO-SiO<sub>2</sub>-Al<sub>2</sub>O<sub>3</sub>-MgO Slag for Spring Steel Deoxidized by Si and Mn in Production. *Metallurgical and Materials Transactions B, Process Metallurgy and Materials Processing Science* 47 (2016), 2, pp. 1435–1444. doi:10.1007/s11663-015-0581-x
- [21] C. Chen, Z. Jiang, Y. Li, M. Sun, Q. Wang, K. Chen and H. Li, State of the Art in the Control of Inclusions in Spring Steel for Automobile - a Review. *ISIJ International [ISIJ Int.]* 60 (2020), 4, pp. 617–627. doi:10.2355/isijinternational.ISIJINT-2019-513
- [22] D. Kalisz, P. Migas, M. Karbowiczek, M. Moskal and A. Hornik, Influence of Selected Deoxidizers on Chemical Composition of Molten Inclusions in Liquid Steel. *J. of Materi Eng and Perform* 29 (2020), 3, pp. 1479–1487. doi:10.1007/s11665-019-04493-2
- [23] C. Mapelli, Non-metallic inclusions and clean steel. *la metallurgia italiana* 100 (2008), 6, pp. 43–52.
- [24] L. Zhang, C. Guo, W. Yang, Y. Ren and H. Ling, Deformability of Oxide Inclusions in Tire Cord Steels. *Metallurgical and Materials Transactions B, Process Metallurgy and Materials Processing Science* 49 (2018), 2, pp. 803–811. doi:10.1007/s11663-017-1134-2
- [25] H. Wang, F. Wang, N. Hao, Z. Xu and L. Jin, Thermodynamics of Composition Control of CaO-MnO-Al<sub>2</sub>O<sub>3</sub>-SiO<sub>2</sub> Inclusions in Tire Cord Steel. *Steel Research International*. Vol.76 78 (2007), 4, pp. 299–304. doi:10.1002/srin.200705895
- [26] G.D. EDWARDS, VALVE-SPRING MATERIALS AND DESIGN. *Industrial Lubrication and Tribology* 35 (1983), 2, pp. 44–51. doi:10.1108/eb053262
- [27] S. Suda and N. Iwakari, The Past and Future of High-strength Steel for Valve Springs. *Kobelco Technology Review* No.26 (2005), pp. 21–25.
- [28] N. Yoshihara, Development History of Wire Rods for Valve Springs. *Kobelco Technology Review* No.30 (2011), pp. 41–45.

- [29] Y. FURUYA, T. Abe and S. MATSUOKA, 1010-cycle fatigue properties of 1800 MPa-class JIS-SUP7 spring steel. *Fatigue & Fracture of Engineering Materials & Structures* 26 (2003), 7, pp. 641–645. doi:10.1046/j.1460-2695.2003.00661.x
- [30] L. Zhang and B.G. Thomas, State of the art in evaluation and control of steel cleanliness, *Review. ISIJ International* 43 (2003), 3, pp. 271–291.
- [31] P. Cunha Alves, V. Da Cardoso Rocha, J.A. Morales Pereira, W.V. Bielefeldt and Vilela, Antônio Cezar Faria, Evaluation of Thermodynamic Driving Force and Effective Viscosity of Secondary Steelmaking Slags on the Dissolution of Al<sub>2</sub>O<sub>3</sub>-Based Inclusions from Liquid Steel. *ISIJ International [ISIJ Int.]* 61 (2021), 7, pp. 2092–2099. doi:10.2355/isijinternational.ISIJINT-2021-037
- [32] Y. Zhou, Z. DENG and M. ZHU, Study on the separation process of non-metallic inclusions at the steel–slag interface using water modeling. *Int J Miner Metall Mater* 24 (2017), 6, pp. 627–637. doi:10.1007/s12613-017-1445-y
- [33] M. Valdez, G.S. Shannon and S. Sridhar, The Ability of Slags to Absorb Solid Oxide Inclusions. *ISIJ International [ISIJ Int.]* 46 (2006), 3, pp. 450–457. doi:10.2355/isijinternational.46.450
- [34] L. Wang, H.-G. LEE and P. Hayes, A New Approach to Molten Steel Refining Using Fine Gas Bubbles. *ISIJ Int.* 36 (1996), 1, pp. 17–24. doi:10.2355/isijinternational.36.17
- [35] D. Satish Kumar, T. Rajendra, R. Prasad, A. Sarkar and M. Ranjan, Forced flotation of inclusions in tundish. *Ironmaking & Steelmaking: Processes, Products and Applications* 36 (2009), 6, pp. 470–475. doi:10.1179/174328108X393849
- [36] L. Zhang, S. Taniguchi and K. Matsumoto, Watermodel study on inclusion removal from liquid steel by bubble flotation under turbulent conditions. *Ironmaking and Steelmaking* 29 (2002), 5, pp. 326–336.
- [37] H. Tozawa, Y. Kato, K. Sorimachi and T. Nakanishi, Agglomeration and Flotation of Alumina Clusters in Molten Steel. *ISIJ International* 39 (1999), 5, pp. 426–434. doi:10.2355/isijinternational.39.426
- [38] J. Strandh, K. Nakajima, R. Eriksson, J. Öuml and P. NISSON, Solid Inclusion Transfer at a Steel-Slag Interface with Focus on Tundish Conditions. *ISIJ International [ISIJ Int.]* 45 (2005), 11, pp. 1597–1606. doi:10.2355/isijinternational.45.1597
- [39] Y.J. Choi, H.G. Lee and J.S. Kim, Dissolution Rate of Al<sub>2</sub>O<sub>3</sub> into Molten CaO-SiO<sub>2</sub>-Al<sub>2</sub>O<sub>3</sub> Slags. Department of Materials Science and Engineering, Pohang University of Science and Technology, Pohang (2002)



- [40] S. Feichtinger, In-situ study of the dissolution of SiO<sub>2</sub> inclusions in secondary steelmaking slags for the production of steel wire. Masterarbeit, Leoben (2013).
- [41] S. Feichtinger, S.K. Michelic, Y.-B. Kang and C. Bernhard, In-situ observation of the dissolution of SiO<sub>2</sub> particles in CaO–Al<sub>2</sub>O<sub>3</sub>–SiO<sub>2</sub> slags and mathematical analysis of its dissolution pattern. *Journal of the American Ceramic Society* 97 (2014), 1, pp. 316–325. doi:10.1111/jace.12665
- [42] H. Suito and R. Inoue, Thermodynamics on Control of Inclusions Composition in Ultra-clean Steels. *ISIJ Int.* Vol.35 36 (1996), 5, pp. 528–536. doi:10.2355/isijinternational.36.528
- [43] A. Srivastava, A. Kamaraj, D. Mandal, K. Mondal and G.K. Mandal, Role of Synthetic Slag Treatment on the Morphology of Non-Metallic Inclusions and Subsequent Cold Drawability of the High Carbon Wire Rod Steel. *Met. Mater. Int.* 28 (2022), 7, pp. 1763–1777. doi:10.1007/s12540-021-01060-0
- [44] H. Tang, Y. Wang, G. Wu, P. Lan and J. Zhang, Inclusion evolution in 50CrVA spring steel by optimization of refining slag. *J. Iron Steel Res. Int.* 24 (2017), 9, pp. 879–887. doi:10.1016/S1006-706X(17)30130-9
- [45] Y. Hu and W.Q. Chen, Influence of refining slag composition on cleanliness and fatigue life of 60Si2MnA spring steel. *Ironmaking & Steelmaking: Processes, Products and Applications* 43 (2016), 5, pp. 340–350. doi:10.1179/1743281215Y.0000000045
- [46] Y. Hou, G. Zhang, K. Chou and D. Fan, Mixed Alkali Effect in Viscosity of CaO–SiO<sub>2</sub>–Al<sub>2</sub>O<sub>3</sub>–R<sub>2</sub>O melts. *Metall and Materi Trans B* 51 (2020), 3, pp. 985–1002. doi:10.1007/s11663-020-01830-y
- [47] E. Benavidez, L. Santini, M. Valentini and E. Brandaleze, Influence of Different Oxides on the Viscosity of Fluorine-Free Mold Fluxes. *Procedia Materials Science* 1 (2012), pp. 389–396. doi:10.1016/j.mspro.2012.06.052
- [48] E. Brandaleze, G. Di Gresia, L. Santini, A. Martn and E. Benavidez, Mould Fluxes in the Steel Continuous Casting Process, in: M. Srinivasan (Ed.), *Science and Technology of Casting Processes* (2012), InTech.
- [49] H.Y. CHANG, T.F. LEE and T. EJIMA, Effect of alkali-metal oxide and fluoride on mold flux viscosity. *ISIJ Int.* 27 (1987), 10, pp. 797–804. doi:10.2355/isijinternational1966.27.797
- [50] H. Kim, W.H. Kim, J.H. Park and D.J. Min, A Study on the Effect of Na<sub>2</sub>O on the Viscosity for Ironmaking Slags. *STEEL RES INT* 81 (2010), 1, pp. 17–24. doi:10.1002/srin.200900118

- [51] N. Preisser, J. Cejka, S. Ramesh Babu, G. Klösch and S.K. Michelic, DISSOLUTION OF  $Al_2O_3$ ,  $MgO \cdot Al_2O_3$  AND  $SiO_2$  IN ALKALI OXIDE CONTAINING SECONDARY METALLURGICAL SLAGS. Liquid Metal Processing & Casting Conference 2022, pp. 87–96, Pennsylvania, USA (2022).
- [52] S.K. Michelic, J. Goriupp, S. Feichtinger, Y.-B. Kang, C. Bernhard and J. Schenk, Study on Oxide Inclusion Dissolution in Secondary Steelmaking Slags using High Temperature Confocal Scanning Laser Microscopy. *Steel Research International* 87 (2016), 1, pp. 57–67. doi:10.1002/srin.201500102
- [53] Y. Ren, P. Zhu, C. Ren, N. Liu and L. Zhang, Dissolution of  $SiO_2$  Inclusions in CaO- $SiO_2$ -Based Slags In Situ Observed Using High-Temperature Confocal Scanning Laser Microscopy. *Metallurgical and Materials Transactions B, Process Metallurgy and Materials Processing Science* 53 (2022), 2, pp. 682–692. doi:10.1007/s11663-021-02401-5
- [54] S. Ramesh Babu, N. Preisser and S.K. Michelic, Image Processing Procedure to Evaluate Inclusion Dissolution in a Slag Observed by High-Temperature Confocal Scanning Laser Microscopy. *Metals* 12 (2022), 4, pp. 531. doi:10.3390/met12040531
- [55] X. Cai, Y. Bao, L. Lin and C. Gu, Effect of Al Content on the Evolution of Non-Metallic Inclusions in Si-Mn Deoxidized Steel. *Steel Research International*. Vol.76 87 (2016), 9, pp. 1168–1178. doi:10.1002/srin.201500305

## Appendix A: Synthetic Particles Datasheets



## ALUMINA 99.9%

ROHS & REACH COMPLIANT

---

### Physical properties

<b>DENSITY</b>	3.96 g/cm <sup>3</sup>
<b>COMPOSITION</b>	AL <sub>2</sub> O <sub>3</sub> 99.9%
<b>COLOUR</b>	cream

---

### Thermal properties

<b>SPECIFIC HEAT</b>	900 J/kg K (at 100°C)
<b>CONDUCTIVITY</b>	30 W/m.K (at 20°C)
<b>EXPANSION</b>	7.5 10 <sup>-6</sup> /K <sup>-1</sup>
<b>SHOCK RESISTANCE</b>	200°C
<b>MAX WORKING TEMPERATURE</b>	1500°C

---

### Mechanical properties

<b>HARDNESS</b>	1900 Vickers
<b>MODULUS OF RUPTURE</b>	2500 MPa
<b>POISSON'S RATIO</b>	0.23
<b>YOUNG'S MODULUS</b>	400 GPa
<b>FRACTURE TOUGHNESS</b>	5 MPa.m <sup>1/2</sup>
<b>COMPRESSIVE STRENGTH</b>	4000 MPa
<b>BENDING STRENGTH</b>	500 MPa

---

### Chemical properties

<b>ACID &amp; ALKALI</b>	excellent resistance
--------------------------	----------------------

---

### Electrical properties

<b>DIELECTRIC CONSTANT</b>	9.7 K at 1MHz
<b>RESISTIVITY</b>	5 10 <sup>14</sup> Ohm.cm (at 20°C)

SANDOZ FILS SA - CHEMIN DU SAUGY 18 , CH-1482 CUGY/FR - TEL +41 26 662 45 00 - [WWW.SANDOZ.CH](http://WWW.SANDOZ.CH)

# SPINELLE

ROHS & REACH COMPLIANT

## Physical properties

<b>CRYSTALLINE STRUCTURE</b>	Cubic monocrystal
<b>COMPOSITION</b>	MgAl <sub>2</sub> O <sub>4</sub>
<b>PURITY</b>	99,99%
<b>DENSITY</b>	3.61 g/cm <sup>3</sup>
<b>DISLOCATION DENSITY</b>	10 <sup>7</sup> – 10 <sup>9</sup> /m <sup>2</sup>

## Thermal properties

<b>MELTING POINT</b>	2300-2330 K
<b>SOFTENING POINT</b>	2070 K
<b>SPECIFIC HEAT</b>	7.9 · 10 <sup>2</sup> j/kg · K at 300 K
<b>THERMAL EXPANSION</b>	5.9 · 10 <sup>-4</sup> /K

## Mechanical properties

<b>HARDNESS</b>	Mohs 8 Knoop 1175-1380
<b>YOUNG'S MODULUS</b>	4.4 · 10 <sup>11</sup> Pa at 300 K
<b>MODULUS OF RUPTURE</b>	4.0 · 10 <sup>8</sup> Pa at 300 K
<b>COMPRESSIVE STRENGTH</b>	2.1 · 10 <sup>9</sup> Pa at 300 K
<b>TENSILE STRENGTH</b>	1.9 · 10 <sup>8</sup> Pa at 300 K
<b>POISSON'S CONSTANT</b>	0.30

## Electrical properties

<b>DIELECTRIC CONSTANT</b>	8-9
----------------------------	-----

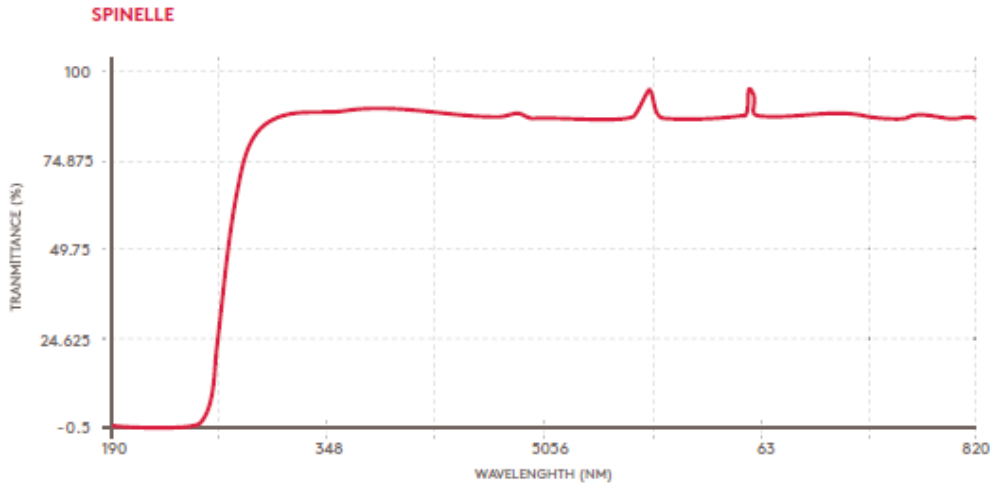
## Optical properties

<b>REFRACTIVE INDEX ND AT 0.5893 μM</b>	1.727
<b>CHROMATIC DISPERSION (N<sub>v</sub> - N<sub>d</sub>) TRANSMISSION, DISC THICKNESS 1 MM :</b>	0.012
<b>- INFRARED</b>	85%      1μm

SANDOZ FILS SA - CHEMIN DU SAUGY 18 , CH-1482 CUGY/FR - TEL +41 26 662 45 00 - [WWW.SANDOZ.CH](http://WWW.SANDOZ.CH)



Transmission



SANDOZ FILS SA - CHEMIN DU SAUGY 18 , CH-1482 CUGY/FR - TEL +41 26 662 45 00 - [WWW.SANDOZ.CH](http://WWW.SANDOZ.CH)



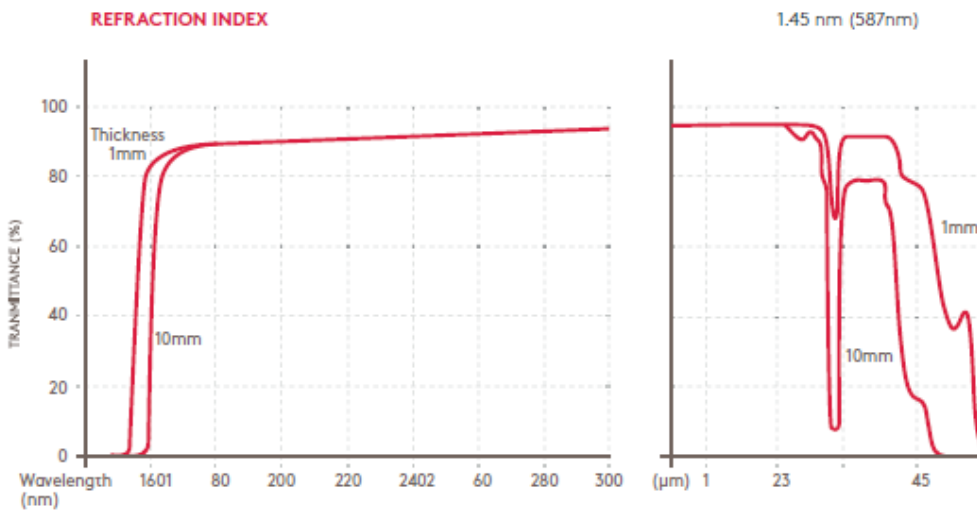
# FUSED SILICA

OHARA SK-1300

## Physical properties

<b>SPECIFIC DENSITY</b>	2,20 g/cm <sup>3</sup>
<b>COMPOSITION</b>	SiO <sub>2</sub>

## Optical properties



## Thermal properties

<b>STRAIN POINT</b>	°C	1060
<b>ANNEALING POINT</b>	°C	1160
<b>SOFTENING POINT</b>	°C	1700
<b>EXPANSION</b>	cm/cm°C	5,5 x 10 <sup>-7</sup>
<b>MAX WORKING TEMPERATURE</b>	°C	1500



---

**Mechanical properties**

<b>HARDNESS (DURETÉ)</b>	vickers	950
<b>POISSON'S RATIO</b>		0,17
<b>YOUNG'S MODULUS</b>	kg/mm <sup>2</sup>	7280
<b>COMPRESSIVE STRENGTH</b>	kg/mm <sup>2</sup>	115
<b>TENSILE STRENGTH</b>	kg/mm <sup>2</sup>	5,6
<b>BENDING STRENGTH</b>	kg/mm <sup>2</sup>	7

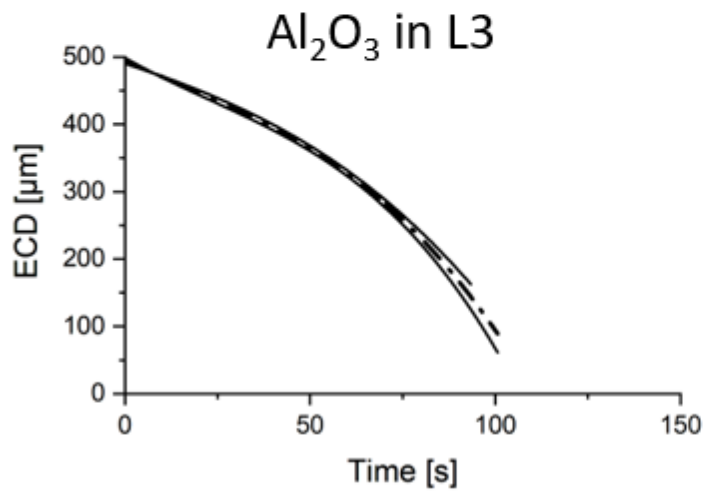
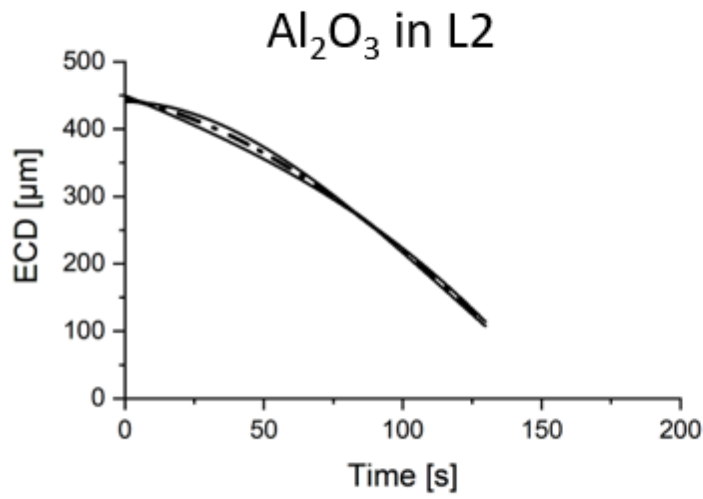
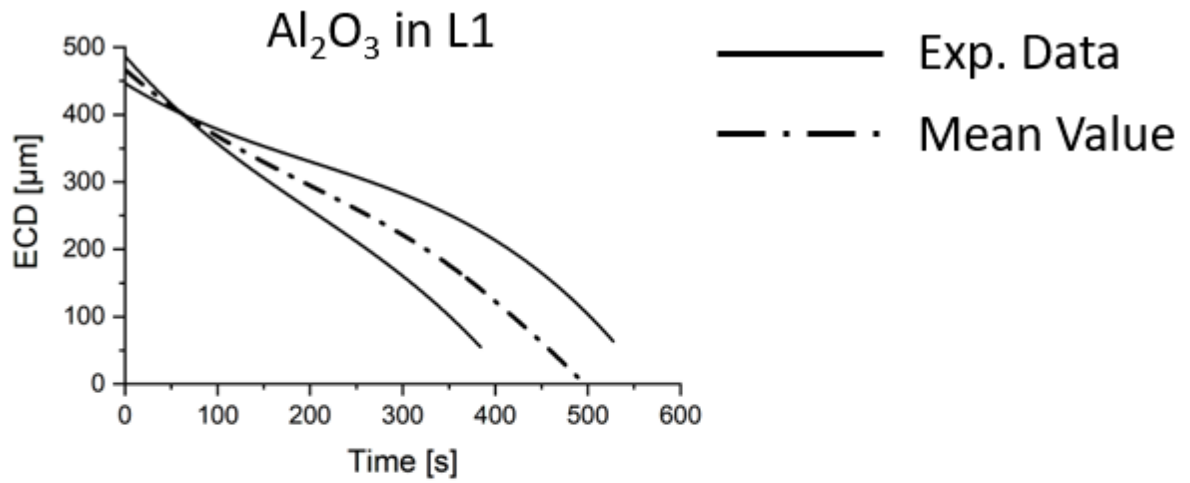
---

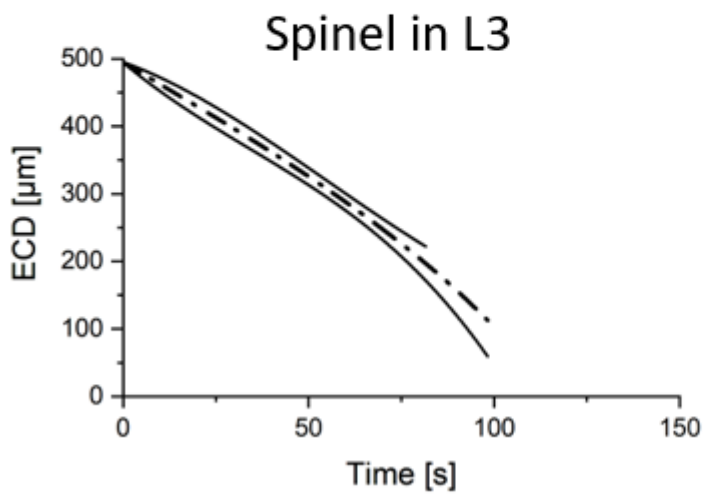
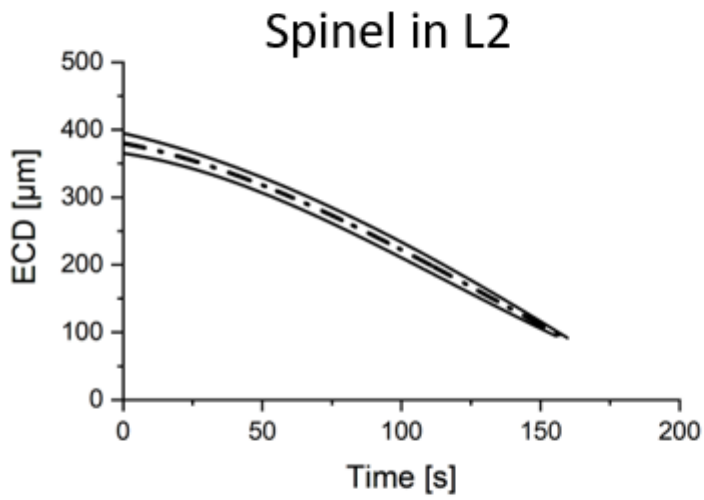
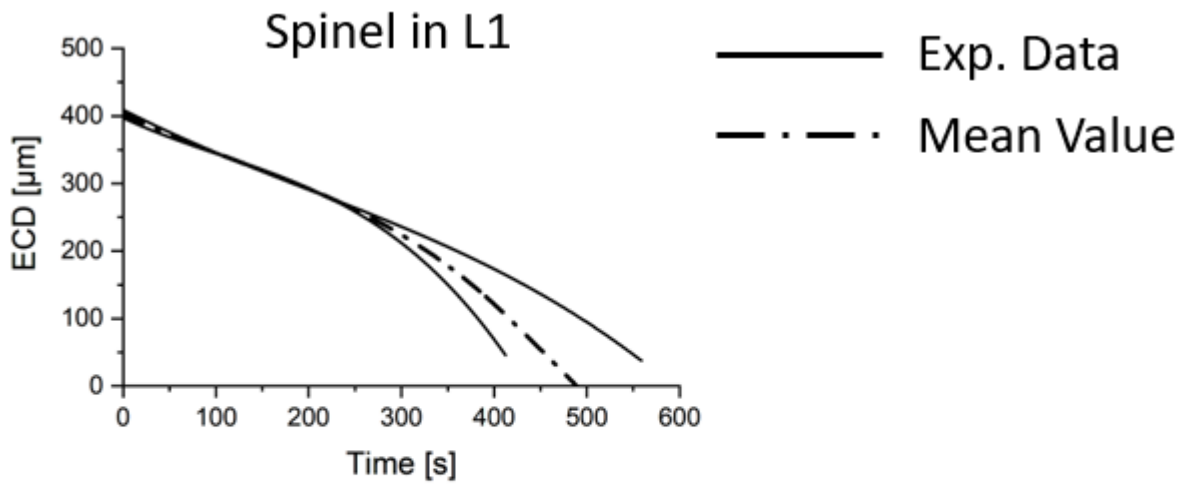
**Chemical properties**

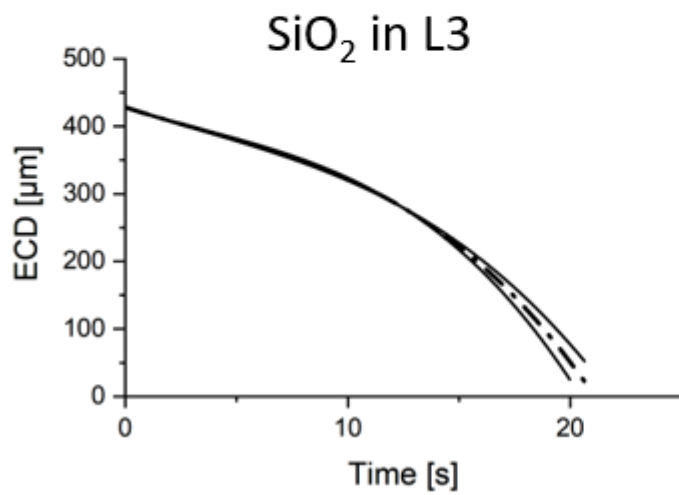
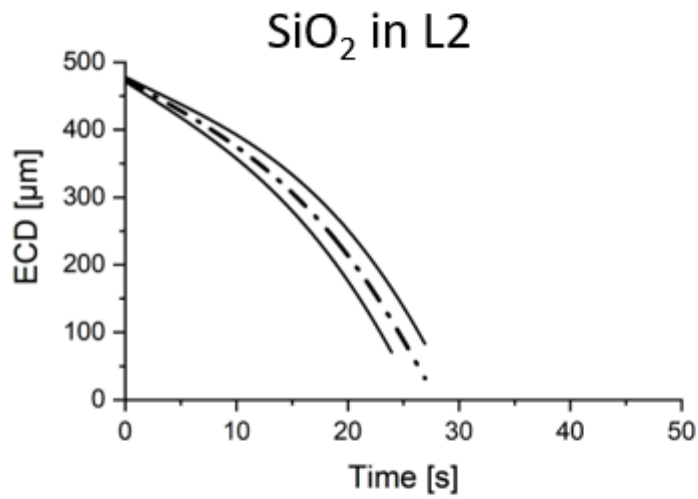
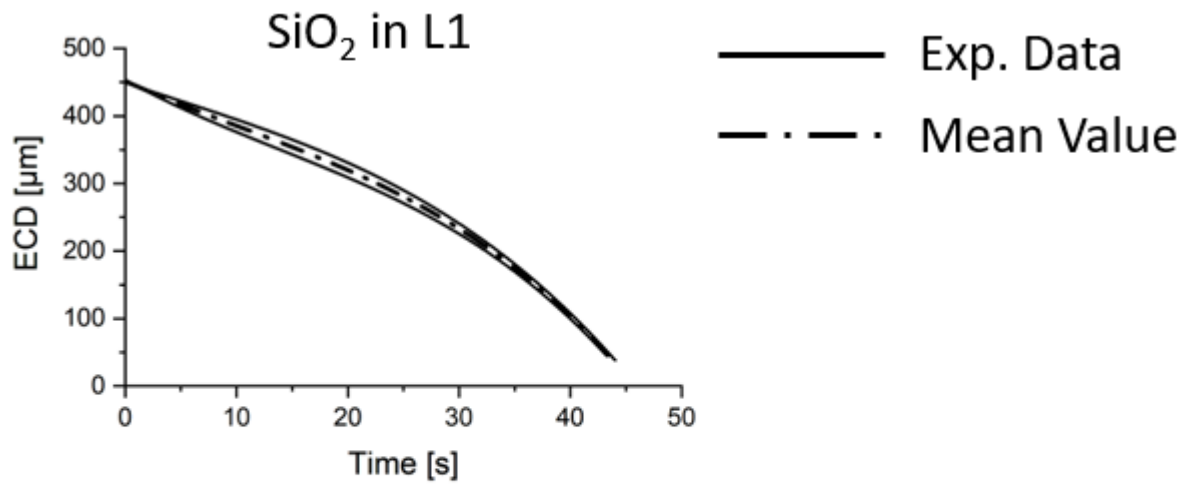
<b>ACID RESISTANCE LOSS</b>	mg/cm <sup>2</sup>	0.01
<b>ALKALI RESISTANCE LOSS</b>	mg/cm <sup>2</sup>	1,35
<b>WATER RESISTANCE LOSS</b>	mg/cm <sup>2</sup>	0,0001

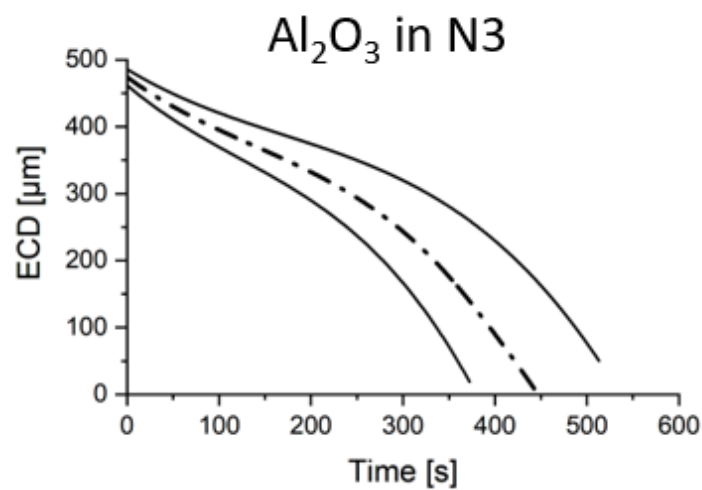
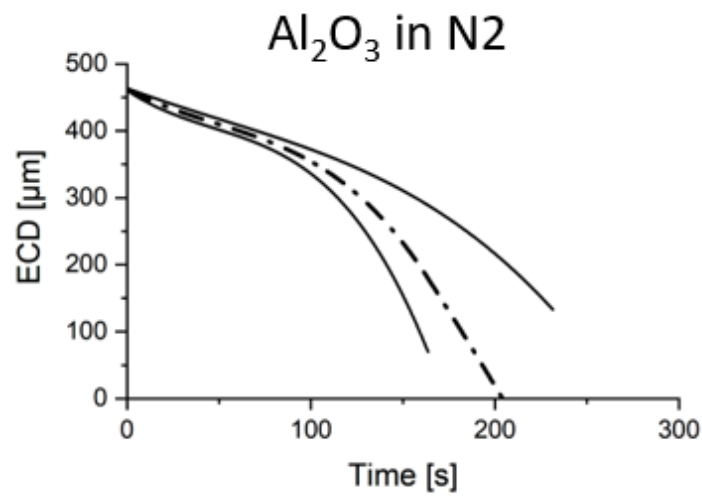
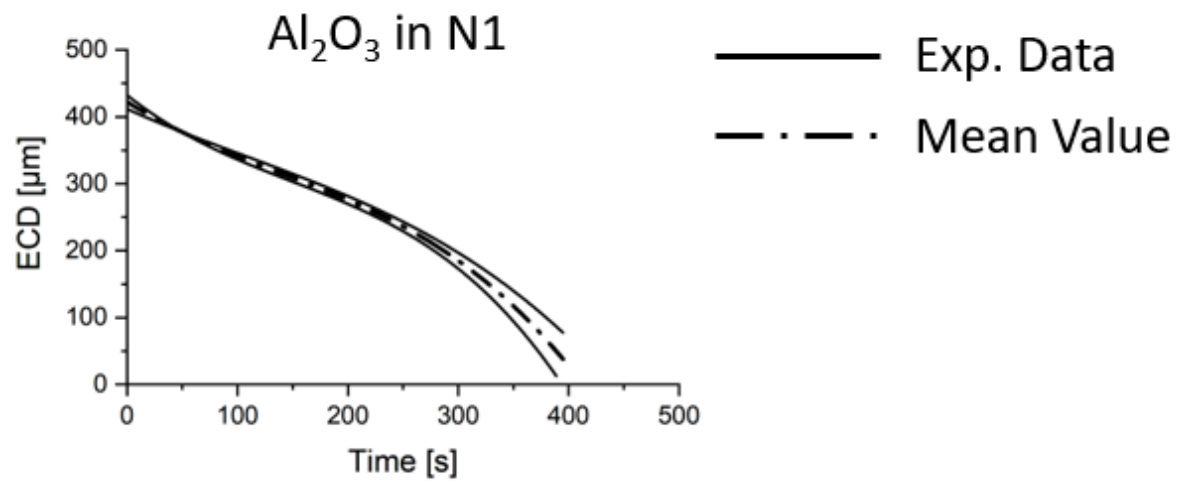


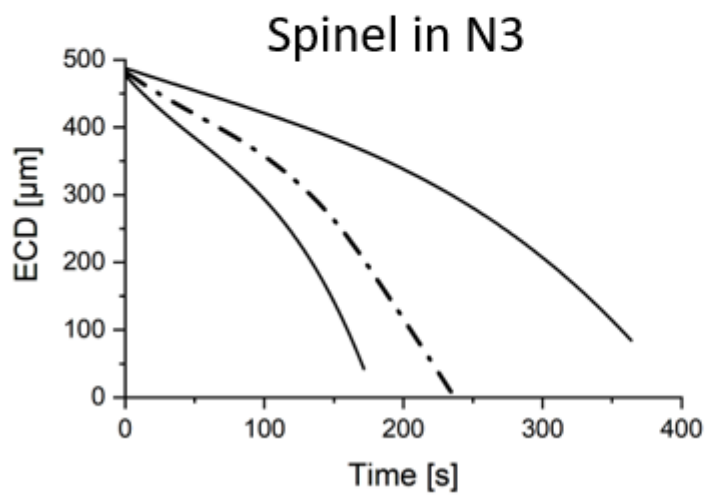
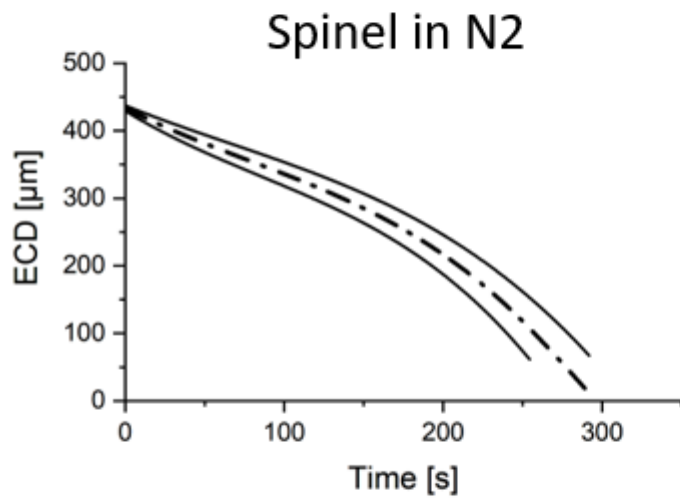
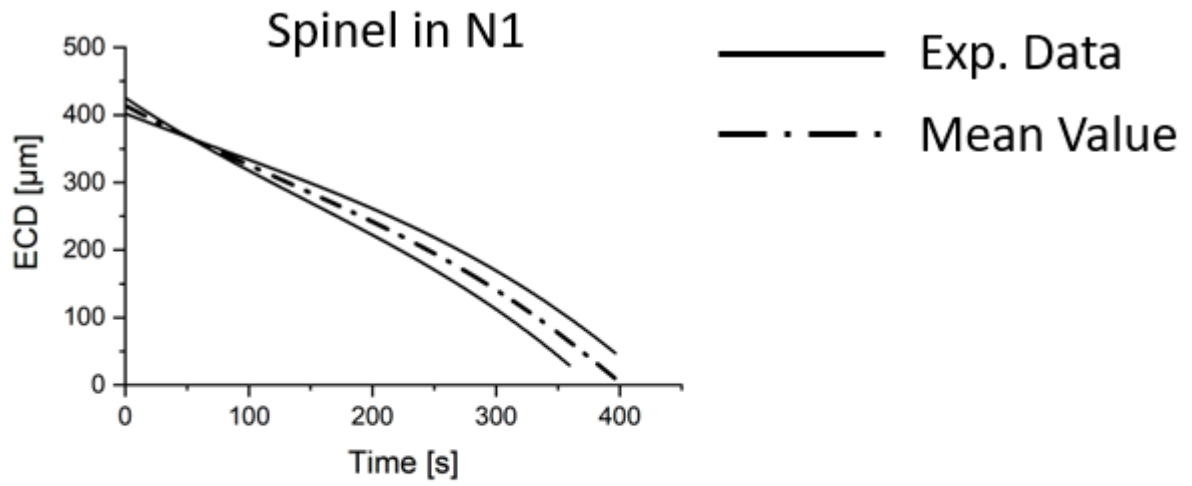
## Appendix B: Dissolution Data

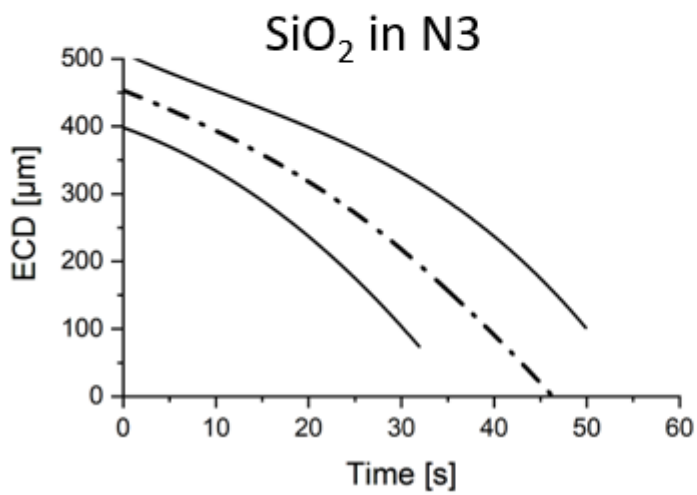
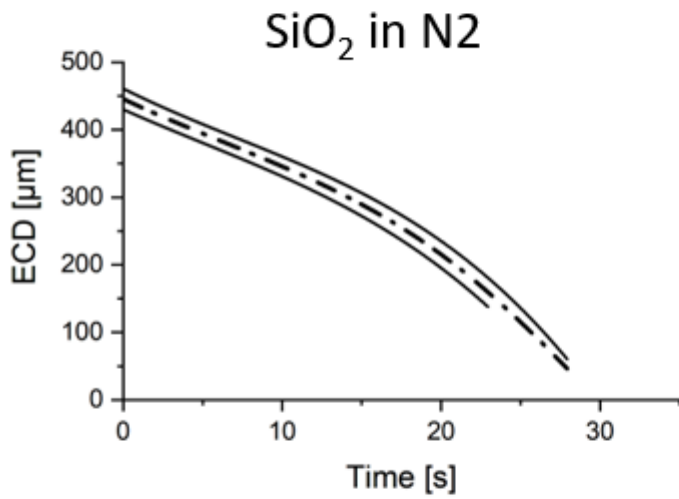
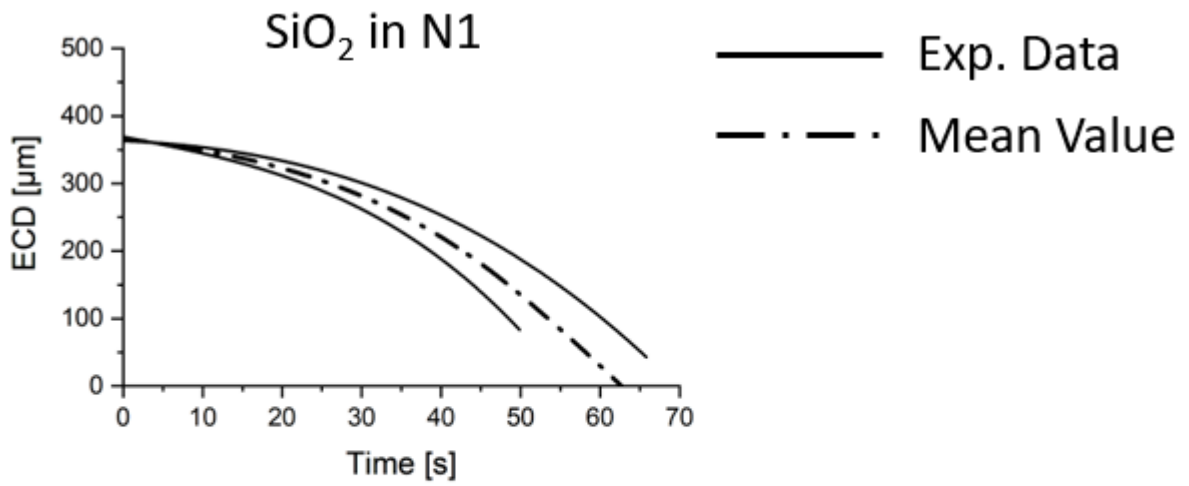


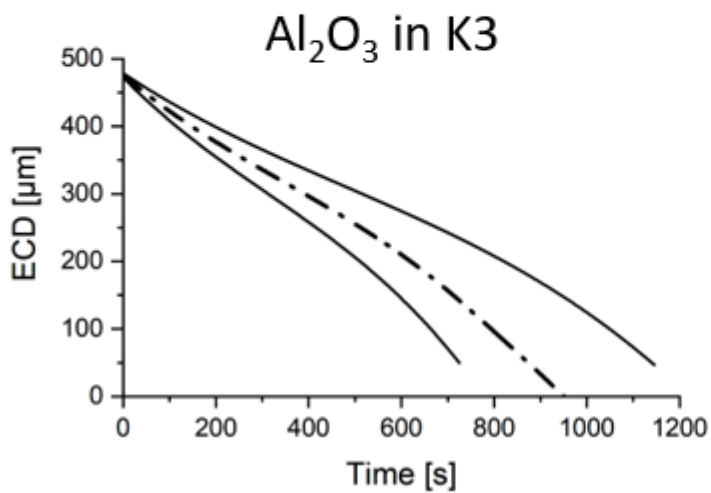
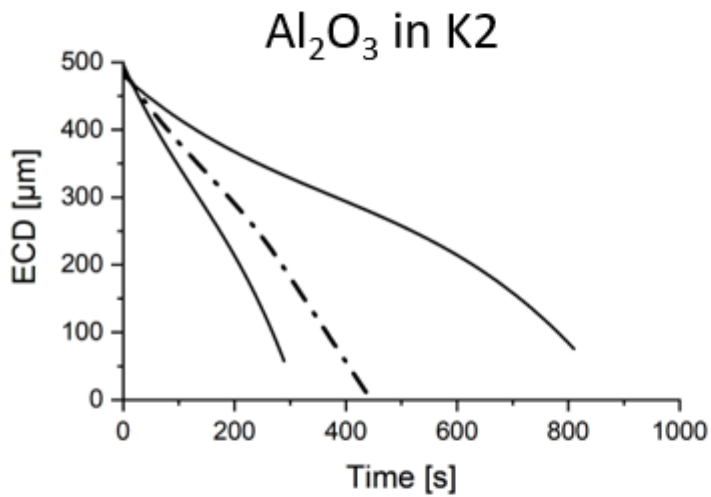
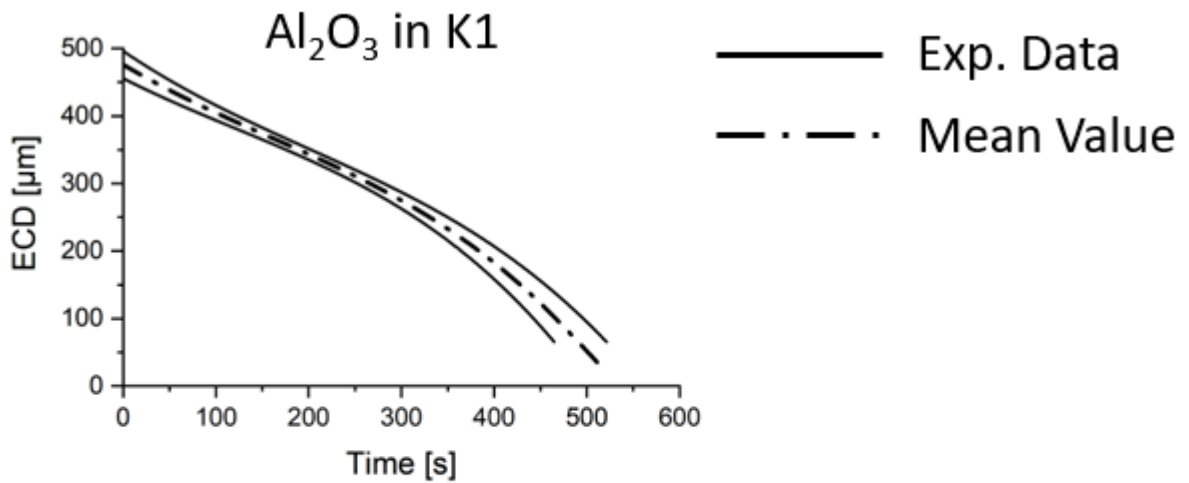




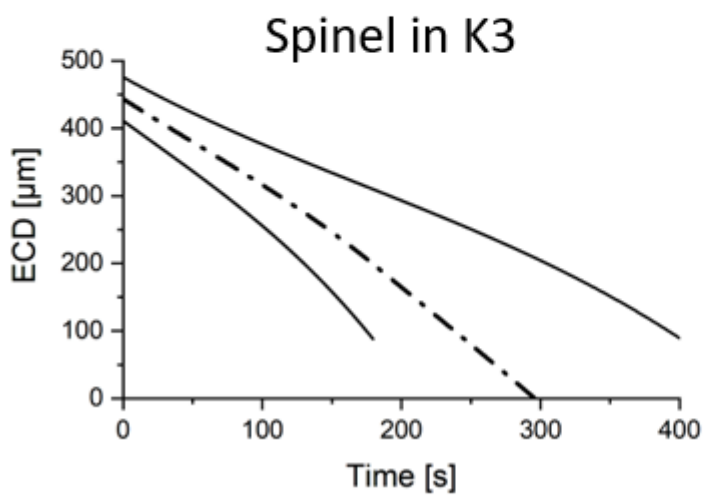
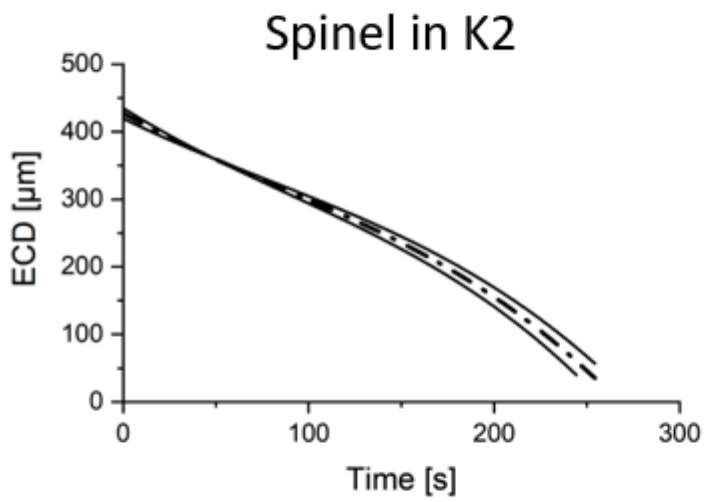
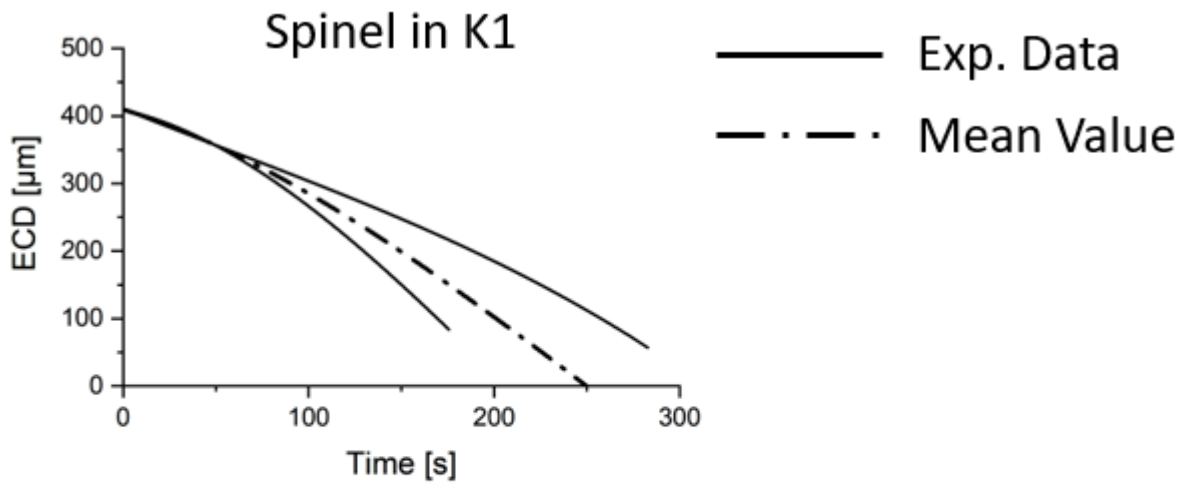


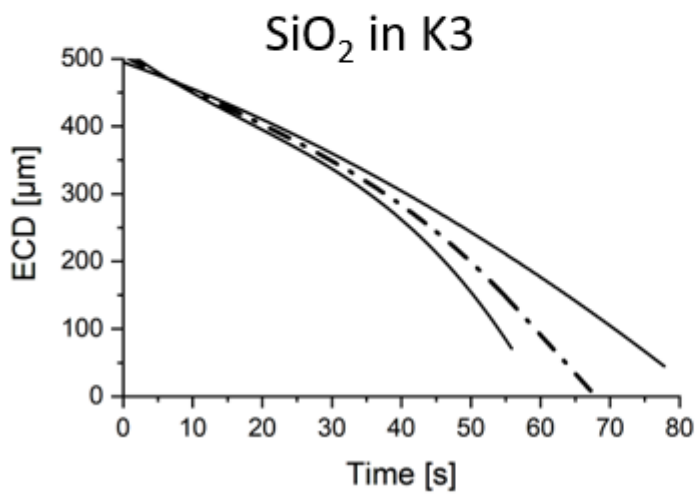
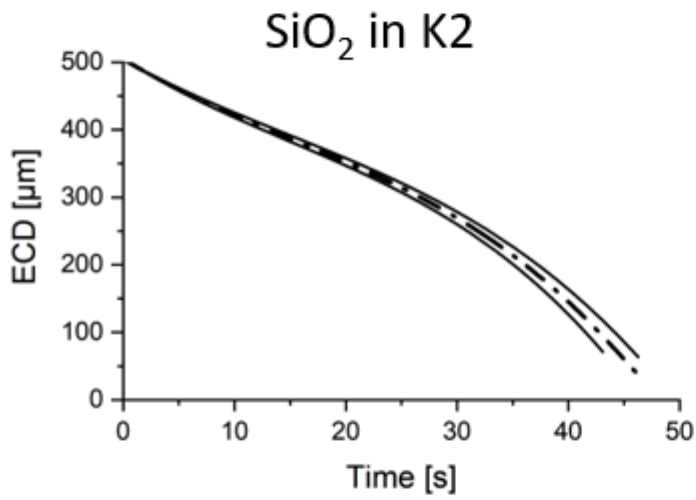
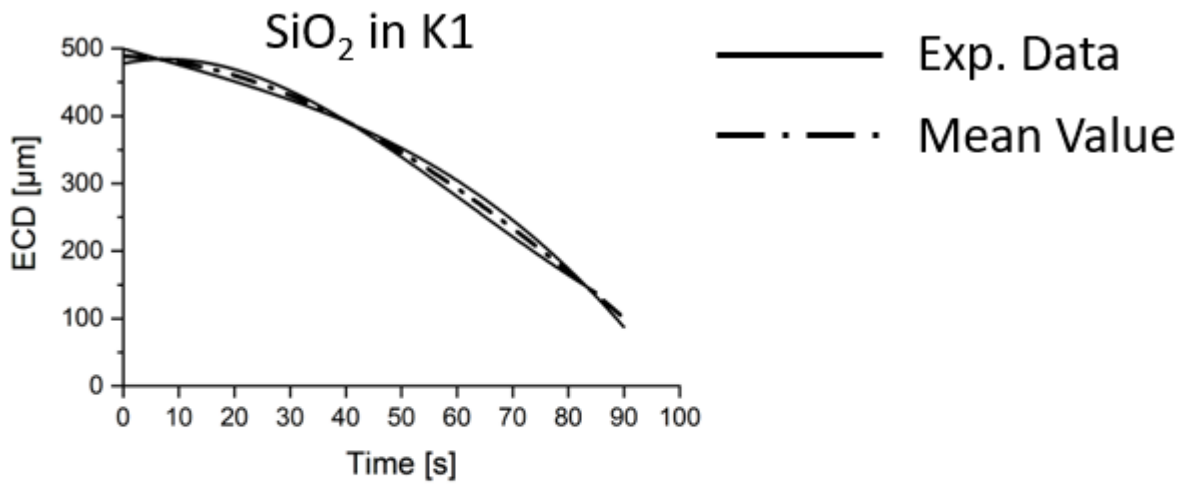


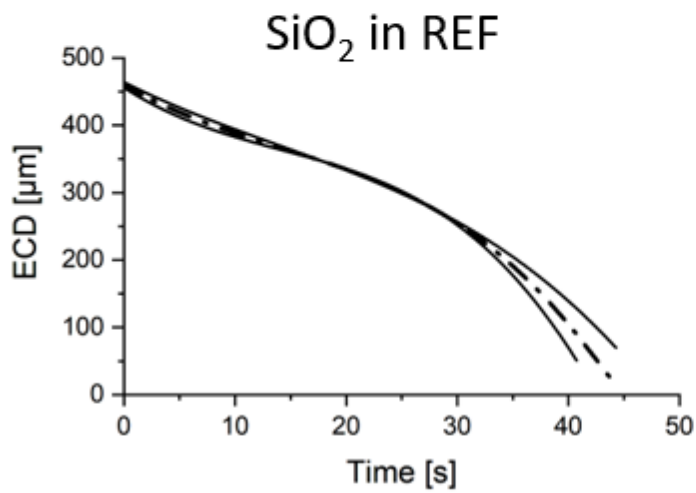
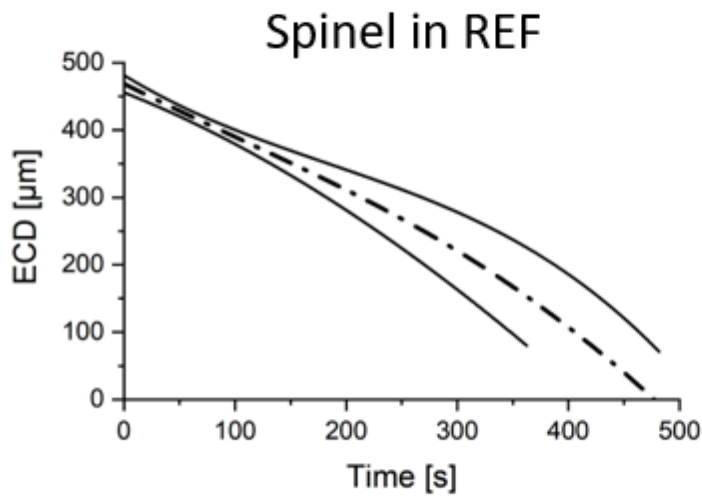
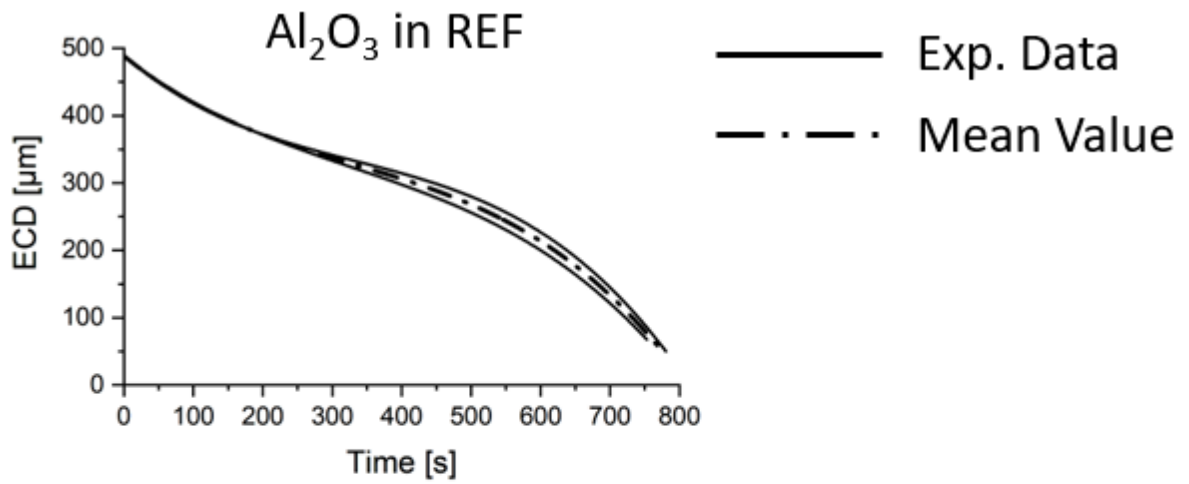












APPENDIX B: DISSOLUTION DATA

Slag	Particle	Name	Ts	Te	Ds	De	Time	Rate	Mean Rate	calc. Max. diss. time
[-]	[-]	[-]	[°C]	[°C]	[μm]	[μm]	[s]	[μm/s]	[μm/s]	[s]
L1	Al2O3	L1A1	1635	1637	512	39	384	1,2	1,0	494
		L1A2	1635	1635	448	30	527	0,8		
	Spinel	L1M1	1635	1634	389	47	412	0,8	0,8	660
		L1M2	1635	1635	410	28	559	0,7		
	SiO2	L1S1	1634	1644	448	32	43	9,6	9,6	52
		L1S2	1635	1643	448	30	44	9,5		
L2	Al2O3	L2A1	1550	1637	448	96	130	2,7	2,7	183
		L2A2	1550	1636	444	87	130	2,7		
	Spinel	L2M1	1635	1638	396	104	160	1,8	1,8	277
		L2M2	1635	1635	371	94	156	1,8		
	SiO2	L2S1	1500	1611	478	82	27	14,7	15,9	32
		L2S2	1502	1609	474	67	24	17,0		
L3	Al2O3	L3A1	1502	1637	485	50	101	4,3	4,0	126
		L3A2	1502	1637	494	156	93	3,6		
	Spinel	L3M1	1498	1636	462	40	98	4,3	4,1	121
		L3M2	1502	1638	486	159	82	4,0		
	SiO2	L3S1	1502	1619	428	28	20	20,0	19,0	26
		L3S2	1501	1620	410	41	21	17,9		
N1	Al2O3	N1A1	1635	1635	429	15	389	1,1	1,0	509
		N1A2	1635	1635	418	61	395	0,9		
	Spinel	N1M1	1635	1635	401	9	359	1,1	1,0	488
		N1M2	1635	1635	402	23	396	1,0		
	SiO2	N1S1	1550	1630	378	72	50	6,1	5,4	93
		N1S2	1549	1637	347	40	66	4,7		
N2	Al2O3	N2A1	1635	1636	463	56	164	2,5	2,0	252
		N2A2	1635	1635	456	113	232	1,5		
	Spinel	N2M1	1635	1636	438	50	292	1,3	1,4	360
		N2M2	1635	1635	423	55	254	1,4		
	SiO2	N2S1	1635	1641	446	59	28	13,9	13,5	37
		N2S2	1635	1641	439	138	23	13,1		
N3	Al2O3	N3A1	1635	1635	439	14	372	1,1	0,9	527
		N3A2	1635	1635	438	49	513	0,8		
	Spinel	N3M1	1635	1635	465	86	364	1,0	1,6	305
		N3M2	1629	1642	414	29	172	2,2		
	SiO2	N3S1	1549	1606	393	68	32	10,2	9,1	55
		N3S2	1506	1635	495	91	50	8,1		

APPENDIX B: DISSOLUTION DATA

Slag	Particle	Name	Ts	Te	Ds	De	Time	Rate	Mean Rate	calc. Max. diss. time
[-]	[-]	[-]	[°C]	[°C]	[μm]	[μm]	[s]	[μm/s]	[μm/s]	[s]
K1	Al <sub>2</sub> O <sub>3</sub>	K1A1	1635	1635	486	52	521	0,8	0,9	583
		K1A2	1636	1635	456	47	465	0,9		
	Spinel	K1M1	1635	1635	412	73	176	1,9	1,6	305
		K1M2	1635	1636	422	43	283	1,3		
	SiO <sub>2</sub>	K1S1	1559	1635	507	76	90	4,8	4,4	114
		K1S2	1551	1637	463	123	85	4,0		
K2	Al <sub>2</sub> O <sub>3</sub>	K2A1	1635	1635	499	48	289	1,6	1,0	486
		K2A2	1635	1635	467	60	810	0,5		
	Spinel	K2M1	1635	1635	437	22	244	1,7	1,6	310
		K2M2	1635	1635	427	39	254	1,5		
	SiO <sub>2</sub>	K2S1	1600	1640	526	61	48	9,7	9,8	51
		K2S2	1601	1641	489	65	43	9,8		
K3	Al <sub>2</sub> O <sub>3</sub>	K3A1	1635	1635	476	27	1146	0,4	0,5	1006
		K3A2	1635	1637	474	38	725	0,6		
	Spinel	K3M1	1635	1634	468	46	424	1,0	1,4	351
		K3M2	1635	1635	398	65	180	1,9		
	SiO <sub>2</sub>	K3S1	1551	1637	489	53	78	5,6	6,6	76
		K3S2	1550	1637	488	61	56	7,6		
REF	Al <sub>2</sub> O <sub>3</sub>	RA1	1635	1638	491	62	753	0,6	0,6	863
		RA2	1633	1634	497	37	781	0,6		
	Spinel	RM1	1621	1624	459	76	363	1,1	1,0	524
		RM2	1636	1637	478	67	482	0,9		
	SiO <sub>2</sub>	RS1	1634	1638	441	31	41	10,1	9,6	52
		RS2	1635	1637	461	56	44	9,1		